GA-A15612
UC-77

PRE- AND POSTIRRADIATION EVALUATION OF TRISO ThO_2 PARTICLES IRRADIATED IN CAPSULE HT-34

by
C. A. YOUNG and C. S. JONES

Prepared under
Contract DE-AT03-76ET35300
for the San Francisco Operations Office
Department of Energy

DATE PUBLISHED: OCTOBER 1980

GENERAL ATOMIC COMPANY

DISCLAIMER

DISCLAIMER

Printed in the United States of America
Available from

National Technical Information Service
U.S. Department of Commerce
5285 Port Royal Road
Springfield, VA 22161
NTIS Price Codes: Printed Copy A07; Microfiche A01

GA-A15612
UC-77

PRE- AND POSTIRRADIATION EVALUATION OF TRISO ThO_2 PARTICLES IRRADIATED IN CAPSULE HT-34

by
C. A. YOUNG and C. S. JONES*

Prepared under
Contract DE-AT03-76ET35300
for the San Francisco Operations Office
Department of Energy

*Present address: Solar Research Institute, Golden, Colorado

GENERAL ATOMIC PROJECT 6400
DATE PUBLISHED: OCTOBER 1980

GENERAL ATOMIC COMPANY

THIS PAGE

WAS INTENTIONALLY

LEFT BLANK

ABSTRACT

Capsule HT-34 was irradiated jointly by General Atomic Company (GA) and Oak Ridge National Laboratory (ORNL). This report presents the pre- and postirradiation evaluation conducted by GA. The purpose of the test was to characterize the mechanical and chemical performance and fission product release of TRISO ThO_2 particles. Sixteen TRISO ThO_2 samples, which had been fabricated in the production-line (240-mm-i.d.) coater, were irradiated at approximately 1200°C and 1450°C to neutron fluences of 5.1 to 10.2 x 10^{25} n/m^2 $(E > 29\ fJ)_{HTGR}$, and burnups of $\geq$5.1 to 12.7% FIMA.

Following are the results of the postirradiation examination:

1. The OPyC coating failure of the 800-μm-diameter particles irradiated at 1200°C was $\leq$1.8%.

2. The pressure-vessel model overpredicted failure up to seven times the observed failure for the samples irradiated at 1200°C.

3. Palladium attack and internal corrosion of the SiC coating was observed in the samples irradiated at 1200°C.

4. Internal corrosion of the SiC coating caused SiC failure up to 100% in the samples irradiated at 1450°C.

5. An average of 16% and 90% of the Cs was released from failed particles irradiated at 1200°C and 1450°C, respectively, after 2686 h of irradiation.

THIS PAGE

WAS INTENTIONALLY

LEFT BLANK

CONTENTS

FIGURES

FIGURES (Continued)

FIGURES (Continued)

FIGURES (Continued)

TABLES

TABLES (Continued)

1. INTRODUCTION

1.1. SCOPE

The irradiation of capsule HT-34 was part of a continuing cooperative effort between GA and ORNL, funded by the Department of Energy-sponsored High-Temperature Gas-Cooled Reactor (HTGR) Fuels and Core Development Program. The irradiation performance of eight TRISO-coated ThO_2 particle batches, fabricated in the 240-mm-i.d. HTGR pilot-plant coater, were characterized in this test. Sixteen samples were irradiated in the uninstrumented capsule in the target facility of the High-Flux Isotope Reactor (HFIR) at ORNL at temperatures of approximately 1200° and 1450°C, over a wide range of fluences and burnups. The HT-capsule experiments provide a rapid means of evaluating and screening fuel materials, since the high-neutron flux in the reactor allows the accumulation of high, fast neutron doses and high thorium burnups in a short time.

The fuel from capsule HT-34 was characterized after irradiation. The postirradiation examinations included a visual examination, metallographic examination, fission gas release (FGR) measurements, and fission product release measurements. The chemical, mechanical, and fission product release performances of the TRISO ThO_2 particles were evaluated.

1.2. OBJECTIVES

The design objectives for testing TRISO-coated ThO_2 particles in capsule HT-34 follow:

1. Test TRISO-coated ThO_2 particles containing 450-μm kernels in an accelerated capsule. The HT-34 particles are representative of

the candidate design for the Fort St. Vrain (FSV) HTGR, and are more retentive of fission products compared to the BISO particle.

2. Evaluate the irradiation performance of unbonded particles fabricated in the 240-mm-i.d. pilot-plant coater, using H_2 for the outer pyrocarbon (OPyC) coating diluent gas; H_2-diluted OPyC coatings were tested in two BISO-particle batches in capsule HT-33 (Ref. 1), but had not been previously tested in TRISO particles. One particle batch with an Ar-diluted OPyC coating was inserted in capsule HT-34 as a comparative sample.

3. Vary the design of the TRISO particle to obtain a range of pressure-vessel failure at 1200° and 1450°C, for correlation with particle stress models.

4. Evaluate the chemical behavior of TRISO ThO_2 particles irradiated at 1200° and 1450°C.

5. Test a range of density, microporosity, coating rate, and anisotropy of the OPyC coating to add to the data base in support of current specifications.

6. Evaluate SiC-coating irradiation performance as a function of the frequency of internal flaws in the SiC coating.

2. CAPSULE DESIGN

2.1. DESCRIPTION

Capsule HT-34 contained four tapered POCO-graphite magazines housed in a primary aluminum container. [See Fig. 2-1* (Ref. 2) for a schematic drawing of a typical HT capsule.] Each magazine held 13 POCO-graphite cylindrical crucibles, which contained unbonded, coated fuel particles. Eight of the 13 crucibles housed fertile particle samples; the other five contained ORNL low-enriched uranium particles to provide an initial fission heat source and to flatten the axial temperature distribution. The magazine-end plugs housed both inert and fertile particles. GA fertile particles occupied the top two magazines in the capsule. After the four magazines were loaded into the primary container, the capsule was sealed with 99.995% pure Ar at a pressure of 0.15 MPa (5 psig). This meant that no in-pile fission gas release could be measured. Capsule temperatures were not monitored during the irradiation, since no thermocouples were in the capsule.

Capsule HT-34 was inserted into the target facility of the HFIR in July 1977 for irradiation for five cycles. It was discharged in late November 1977.

2.2. IRRADIATION CONDITIONS

The design irradiation conditions for the GA samples are given in Table 2-1. The surface temperatures of the graphite crucibles of the two magazines were designed to be 900° and 1250°C. These graphite temperatures correspond to estimated particle surface temperatures of 1200° and 1450°C, respectively. The lower temperature magazine samples reached fluences

*Figures and tables appear at the end of each section.

of approximately 5.3 to 8.3 x 10^{25} n/m^2 (E > 29 fJ)$_{HTGR}$ and burnups of 5.6% to 9.1% FIMA. The fast fluences and burnups for the high temperature magazine were 9.4 to 10.4 x 10^{25} n/m^2 (E > 29 fJ)$_{HTGR}$ and 11.0% to 12.8% FIMA.

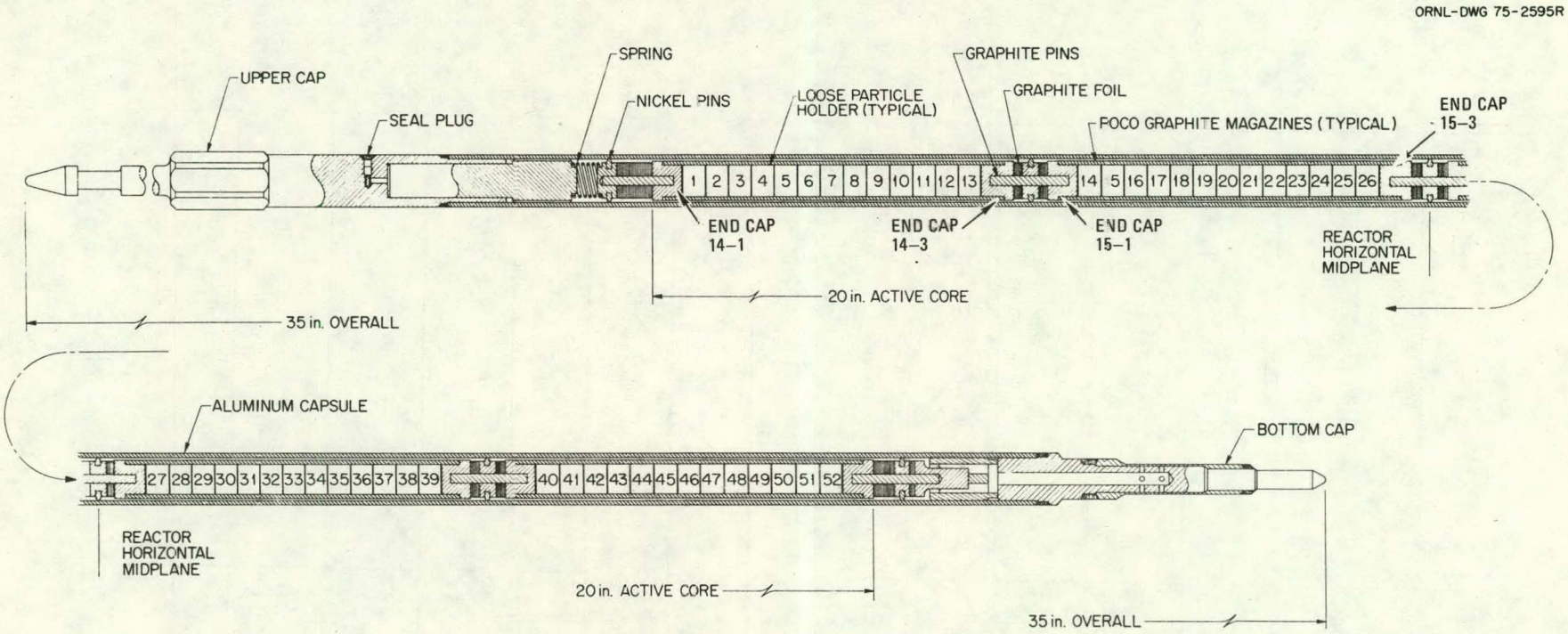

Fig. 2-1. Schematic drawing of a typical HT capsule

TABLE 2-1
DESCRIPTION AND DESIGN IRRADIATION CONDITIONS OF TRISO ThO_2 SAMPLES FOR CAPSULE HT-34

Sample Batch No.	Variables to be Tested						Density-Separated Fraction from Parent Batch	Design Particle Failure after Irradiation[a]		No. Particles	Design Irradiation Condition		
	Buffer Thickness (μm)	SiC Flaw Frequency (%)	OPyC					OPyC	Pressure Vessel		Capsule Position	Fast Fluence [10^{25} n/m^2 (E > 29 fJ)$_{HTGR}$]	Burnup (% FIMA)
			Liquid Gradient Density (Mg/m^3)	Micro-porosity (mℓ/kg)	Coating Rate (μm/min)	Diluent Gas							
Low temp magazine[b]													
6252-20-0161-001	83	6	1.98	59	8.4	H_2	Nominal	Low	0	56	2	5.3	5.6
6252-07-0262-001[c]	60	38	1.80	48	5.0	Ar	Nominal	Low	0	57	4	5.9	6.2
6252-14-0261-001	27	29	1.97	54	7.1	H_2	High	Low	Moderate	56	5	6.2	6.5
6252-14-0171-001	35	9	1.97	57	7.1	H_2	High	Low	Moderate	56	7	6.8	7.1
6252-13-0161-001	57	16	1.79	57	8.3	H_2	Nominal	Low	0	57	8	7.1	7.5
6252-14-0161-001	63	9	1.97	57	7.6	H_2	Nominal	Low	0	57	10	7.6	8.1
6252-15-0161-001	56	12	1.81	21	5.0	H_2	Nominal	Low	0	56	11	7.9	8.5
6252-16-0161-001	57	12	1.96	25	5.3	H_2	Nominal	Low	0	56	13	8.3	9.1
High temp magazine[d]													
6252-20-0161-002	82	6	1.98	59	8.0	H_2	Nominal	Moderate	Moderate	80	15	9.4	11.0
6252-07-0262-002[c]	57	38	1.80	48	5.6	Ar	Nominal	Moderate	High	81	17	9.8	11.5
6252-14-0161-002	62	9	1.97	57	7.6	H_2	Nominal	Moderate	High	81	18	9.9	11.7
6252-14-0271-001	86	29	1.97	54	8.0	H_2	Low	Moderate	Moderate	83	20	10.1	12.1
6252-14-0181-001	91	10	1.97	57	8.1	H_2	Low	Moderate	Moderate	82	21	10.2	12.2
6252-17-0161-001	80	6	1.95	28	5.0	H_2	Nominal	Moderate	Moderate	81	23	10.4	12.5
6252-15-0171-001	84	12	1.81	21	5.6	H_2	Low	Moderate	Moderate	81	24	10.4	12.6
6252-13-0171-001	79	16	1.79	57	8.5	H_2	Low	Moderate	Moderate	85	26	10.4	12.8

[a] Design failure range = low <5%; moderate 20-30%; and high 50-70%

[b] Low temp magazine - 1200°C; 0.0234 g Th-232/position

[c] Sample previously irradiated in capsules HT-31 and HT-33

[d] High temp magazine - 1500°C; 0.0331 g Th-232/position

3. UNIRRADIATED COATED PARTICLE BATCHES

3.1. DESCRIPTION

3.1.1. Parent Batches

Eight TRISO-coated particle batches, containing 450-μm-diam ThO_2 kernels, were tested in capsule HT-34. All batches were made in the 240-mm-i.d. pilot-plant coater. Primary test variables for the parent batches (Table 3-1) included buffer thickness, SiC internal flaw content, and OPyC coating density, microporosity, coating rate, and diluent gas.

The 240-mm-i.d. coater with a cone-shaped gas distributer was selected for the HTGR pilot plant. The TRISO and BISO ThO_2 particles made in this coater were first tested in capsules HT-31 and HT-33 (Ref. 1). The TRISO ThO_2 particles were further tested in HT-34. Since most of the present irradiation data are based on particles made in the 127-mm-i.d. prototype coater, the results of capsules HT-31, HT-33, and HT-34 will aid in assuring that the irradiation performances of particles made in both the small and large coaters are similar.

The parent batches were designed with either a 60- or 85-μm buffer thickness to accommodate a wide range of burnups. The buffer coating provides void volume to accommodate gaseous fission products. More fission gases were generated in coated particles irradiated to high burnups, and thicker buffers were required to limit pressure-vessel failure.

Capsule HT-34 tested TRISO ThO_2 samples having a range of internal flaw fractions in the SiC coating. (See Fig. 3-1 for flaw example.) Internal flaws have been observed on metallographically polished sections in the SiC coating of TRISO particles made at GA. They have been more prevalent in large-diameter particles. The results of previous irradiation capsules,

such as F-30, P13R, and P13S (Refs. 3 and 4), indicated that TRISO particles with these flaws performed satisfactorily. However, the performance of particles might be improved by reducing the SiC internal flaw content, thereby allowing a reduction in coating thickness or an increase in the fuel operating temperature.

GA began to study SiC flaws and observed that large-coater TRISO ThO_2 particles for HT-31 and HT-33 had flaws (Ref. 1). When these batches were burned back to the SiC coating, a visual examination revealed gold spots. Further work showed that each gold spot was a flaw or inclusion in the SiC coating. The fraction of particles with flaws was then determined by counting gold-spotted particles. The flaw counts for capsule HT-34 batches are reported in Table 3-1. Electron microprobe analysis revealed that the flaws were primarily carbon and void.

A short-term experiment was undertaken to reduce the flaw content of SiC coatings made in the large coater for capsule HT-34. Coater batch size was found to be the only significant parameter. As a result, several HT-34 specimens were made using half-size batches (~11 kg) in the SiC-coating run. This reduced the frequency of flawed SiC coatings from 40% to ~10%. It appeared that the ratio of particle-bed height to coater diameter influenced the SiC flaw content (Ref. 5). However, the flaws were never completely eliminated in this experiment. Capsule HT-34 tested a range of flaw frequencies to examine the effect of SiC flaws on irradiation performance.

Two total particle diameters were tested in capsule HT-34, because of the need for two buffer coating thicknesses. The batches having ~60 μm-buffer coatings had a diameter of ~800 μm. These batches are representative of the candidate design for TRISO-coated 450-mm ThO_2 particles for the FSV HTGR reactor (Ref. 6) and the particles tested in the FSV fuel test elements FTE-1 through FTE-8 (Ref. 7). The thick-buffer batches had a diameter of ~870 μm. Higher OPyC coating failures have been observed in large-diameter TRISO ThO_2 particles (Ref. 8). The results of HT-34 were expected to contribute to the data base on the size effect.

Characterizing the outer pyrocarbon coating is part of a continuing effort to ensure adequate irradiation performance of HTGR coated particles. The density, microporosity, coating rate, and anisotropy have been found to affect particle performance significantly (Refs. 4, 8, and 9). The test matrix for the OPyC coating is given in Fig. 3-2. It consisted of two coating rates (5 and 8 μm/min.) and two liquid gradient densities (1.80 and 1.95 Mg/m^3). Microporosity and anisotropy also varied, since they were dependent upon coating rate and density. Particles with the selected coating rates and densities were expected (from previous results) to perform adequately during irradiation at 1200°C.

3.1.2. Capsule Samples

Table 2-1 gives a general description of the 16 TRISO ThO_2-particle samples for capsule HT-34. The samples were selected from the parent batches and prepared for the capsule according to the experiment objectives. The test variables and the corresponding capsule samples are given in Table 3-2. The OPyC coating characteristics were emphasized primarily in the 1200°C magazine; however, all OPyC coating parameters were tested at both temperatures. The 1450°C experiment, since it was a severe test, mainly evaluated mechanical (pressure vessel failure) and chemical behavior. Chemical behavior included kernel migration and attack of the SiC coating. The results were to be correlated with the particle performance models.

One intent of the experiment was to produce a range of pressure-vessel failure by adjusting the buffer thickness over the range of burnups, as shown in Table 2-1. The pressure-vessel failure model was used in the design of the TRISO ThO_2 particles. Low pressure-vessel failure was expected in the low-temperature samples having a 60 μm-thick buffer coating. Two 1200°C samples had 30-μm buffer coatings and were designed to have failure. The high temperature samples were irradiated to very high neutron burnups. Therefore, an 85-μm buffer coating was required for low failure.

Two samples having 60-μm-thick buffer coatings were designed to have high failure at ~1450°C. Also, the different frequencies of internal flaws in the SiC coating were tested at both 1200° and 1450°C to determine their effect on pressure-vessel failure.

The diluent gases used during OPyC coating deposition were either H_2 or Ar. One test objective was to verify that the irradiation performances of the two OPyC coating types are comparable. The reasons for the use of different diluent gases are discussed in Section 3.2. One parent batch (Ar dilution), irradiated in both capsule HT-31 and capsule HT-33, was used as a standard in both magazines of HT-34. Since temperatures were not monitored during the irradiation, the standard was to provide comparative particle performance data and assist in demonstrating that temperatures of these capsules were similar.

Table 2-1 shows that the number of ThO_2 particles in different positions is limited to between 56 and 85 particles. Fuel failure within these limited groups of particles is enough to establish qualitative "gross effects" between different coating attributes. A meaningful quantitative evaluation of low fuel failure fractions versus coating attributes is not possible because of the small size of the samples in each irradiation position; e.g., 330 particles have to be examined with no observed failures to have 95% confidence that the failure fraction in this group is less than 0.01. Thus, the HT-34 capsule was designed to serve as a screening test to determine success or failure between different particle groups and identify mechanisms contributing to particle failure.

3.1.3. End-plug Samples

The four end plugs of the two GA magazines contained two additional coated-particle samples. Batch 7032-149 was BISO ThO_2 with a Si-doped OPyC coating. The developmental Si-doped pyrocarbon exhibits higher strength and improved dimensional stability under irradiation (Ref. 10), when compared

with pure PyC. The HT-34 particle had a 728-μm diam and a 76-μm OPyC thickness. The OPyC coating had a density of 2.22 Mg/m^3 with 34 wt% Si. Batch 6351-04-010 was TRISO inert particles that had been burned back to the SiC coating. This batch was inserted to determine if exposed SiC coating corrodes or volatizes during irradiation. This particle had a substrate diam of 502 mm and a SiC density of 3.22 Mg/m^3. The location, irradiation conditions, Th loading, and number of particles are listed in Table 3-3.

3.2. FABRICATION OF THE PARENT BATCHES

All of the kernels and coatings were manufactured in the HTGR pilot plant in accordance with the specifications in Ref. 11. The 450-μm kernels were made from ThO_2 powder derived from a steam-denitrated Th-nitrate solution. A broth, made from the powder, was then fed into a drop column where it was spheroidized into uniform droplets and gelled into ammonia gas. The gelled spheres were dried in air at 150°C and sintered at $\leq$1300°C.

The coatings were deposited on the kernels in the 240-mm-i.d. pilot-plant dry coater. The fabrication conditions of each batch are given in Table 3-4. The gases entered the coating chamber through a cone-shaped gas distributor with an extension nozzle through the center of the cone. The levitating gas was dispersed at the base of the cone. The deposition and diluent gases were premixed and entered near the top of the extension nozzle.

The diluent gas has an important effect on the pyrocarbon properties. The diluent gases Ar, He, and N_2 have produced acceptable pyrocarbon coatings in smaller (127 mm i.d. or less) coaters. However, pyrocarbon coatings made in the 240-mm-i.d. coater with the cone distributor were frequently sooty and permeable when Ar was the diluent gas. Possibly, this was due to nonhomogeneous dispersion of the coating gases in the large coater bed. Hydrogen dilution reduced soot and permeability (measured by chlorine leach on BISO ThO_2 particles), and produced a more uniform coating. In addition,

the use of H_2 reduced the OPyC coating thickness variability under constant coating conditions. The beneficial effects from H_2 were apparently attributed to the stabilization of the decomposition of the hydrocarbon gas. Two BISO ThO_2 batches in capsule HT-33 (Ref. 1) were deposited with H_2 diluent gas. Seven of the eight TRISO batches in capsule HT-34 had OPyC coatings deposited with the H_2 diluent. Capsule HT-34 was expected to show whether or not this process change affects the irradiation behavior of the pyrocarbon. The OPyC coating was deposited with Ar for the other batch.

The particle batch size in the coater also affects coating properties. The buffer and inner pyrocarbon (IPyC) coatings were deposited in 15 or 17 kg charges. Loads of 10.5 to 22.5 kg were used for the SiC coating. The frequency of flaws in the SiC coating was roughly proportional to the charge size in batches with buffers approximately 60 μm thick. However, the 80-mm-thick buffer batches did not follow this trend, since they had a low frequency of flaws and were coated in large batch sizes. All OPyC-coating load sizes were between 11 and 14 kg.

3.3. PREPARATION OF CAPSULE SAMPLES

The preparation and characterization of the actual capsule specimens from the parent batches, described in Section 3.1 and 3.2, were conducted in accordance with the procedure shown in Fig. 3-3. In the interest of traceability, the numerical changes in sample identification that occurred during these procedures are given in Table 3-5. The various steps in the procedure are described in detail below.

All samples for capsule HT-34 were separated by particle density into a low, mean, or high density from the parent batch. The mean-density fraction was separated out to reduce the variation in all coating attributes but primarily the buffer thickness. This reduction aided in correlating irradiation performance with coating attributes. The buffer thicknesses of the parent batches were nominally 60 or 85 μm. Therefore, the mean-density fractions had 60- or 85-μm-thick buffer coatings.

The design also called for six samples taken from three of the 60-μm-thick buffer parent batches to have 30- and/or 85-μm buffer thicknesses. This meant that the particles with the thinnest and thickest buffer coatings had to be separated from the parent batches. The most practical method for separating them was by total particle density. Calculations were then performed to determine what particle components (kernel and coatings) most influenced the total particle density. The density was calculated for TRISO ThO_2 particles with nominal component dimensions and densities. The dimension of each component was then varied by plus and minus two standard deviations of the nominal value, while the other components were held constant. The results are given in Fig. 3-4. The slope of each line defined how much influence each component had on the total particle density. Fortunately, the buffer thickness had the most effect on the density. This fact made it easier to separate out the particles with thin and thick buffer coatings. However, the figure also shows that the high-density fraction would be expected to have larger kernels and thinner coatings. Conversely, the low-density fraction would have smaller kernels and thicker coatings.

That a particular density may be obtained through a variety of particle designs is illustrated in Fig. 3-5, which shows two different microstructures found in the same low-density fraction of batch 6252-14-0200. One consisted of a nominal OPyC and thin buffer coating, and the other of an even thinner buffer and thick OPyC coating. It is interesting to note the range of OPyC thickness and density occurring within the same batch of particles, deposited over the same period, in the same coater. The thicker OPyC coating obviously has more surface-connected porosity, as the impregnation of Tl indicates, and is probably of lower density.

To prepare the mean-density fractions, the mean total particle density was first measured on ~100 particles from each parent batch; then the mean-density fraction was separated out from a sample of the parent batch in a density-gradient column.

The high- and low-density fractions were separated in a beaker rather than in a density column. For example, 200 low-density particles were separated from a 30-g particle sample using a Tl mallonate solution. All the added particles sank to the bottom. A high-density Tl solution was then added drop-by-drop to the beaker, and stirred thoroughly until approximately 200 of the least-dense particles were floating on the surface. These floating particles were skimmed off and became the low-density fraction. Conversely, the high-density fraction was obtained by preparing a solution in which all particles floated. A low-density Tl solution was then added until the required number of particles sank.

The density-separated samples were then X-radiographed, and the dimensions were measured to determine whether they met their individual buffer-thickness requirements. For those not meeting the requirements, another density separation was made. The high-and low-density tails were radiographed in slotted brass holders, so that defective particles could be located and removed. Defective (per Ref. 11) particles were removed from all high- and low-density fractions, but not from the mean-density fractions, which generally had few, if any, defects.

The density separation was followed by a 1-h, 1400°C, vacuum (5×10^{-4} mm Hg) heat treatment to remove the Tl. All capsule samples and historical specimens were heated together. Following this initial heat treatment, the historical samples were removed and stored. The capsule specimens were then heat treated at 1650°C in Ar for 30 min to simulate the fuel rod heating.

After the final heat treatment, the capsule specimens were radiographed again. The number of particles needed per capsule to meet the specified Th loading (see Table 3-6) was calculated. Then, the excess particles from each capsule specimen were removed and used for OPyC and optical anisotropy (BAF_o) characterization. A final radiograph was taken of the particles to be inserted in the capsule, and measurements were noted on the kernel and coating dimensions for each capsule sample.

Stress calculations were performed with the TRISO MONTE-NOCO computer code, using design irradiation conditions and data on selected capsule samples (see Table 3-7). Predicted failure levels for the HT-34 samples were determined by imposing the calculated stress curves on an apparent failure stress of -3400 psi. This value was based on the stress studies of HT and P13S capsules (Ref. 12). The failure fractions, assuming both zero and 100% OPyC failure, are given in Table 9. The chance of failure was equal to the probability that the apparent failure stress was exceeded for each capsule sample. It is obvious from Table 3-8 that a meaningful test of the particle designs against the models could be realized only if the OPyC remained intact.

3.4. PROPERTIES

All parent batches and capsule samples were extensively characterized prior to irradiation. The results of the quality-control analysis are presented in Tables 3-9 through 3-14. Representative photomicrographs of X-radiograph, stereo view, and metallographic cross sections of coated particles from each parent batch are shown in Figs. 3-6 through 3-21.

Coated-particle properties were measured at different stages of preparation. On the parent batches, items measured included kernel density and impurities, coating densities, IPyC and OPyC BAF_O, SiC flaws, faceting, accessible porosity (measured by mercury intrusion), chemical composition and impurities, defective SiC coatings, contamination, and fission gas release (FGR). The total particle density and some BAF_O values were measured on the density-separated fractions. The particle dimensions, SiC and OPyC coating rates, and Th loadings were measured or calculated on the capsule-particle samples.

3.4.1. Parent Batches

The properties of the parent batches are presented in Tables 3-4 and 3-9 through 3-11. The kernel characteristics are similar for all batches.

The ThO_2 was $\geq$97.8% of theoretical density and its impurity content was low. The average diameter was very close to 450 μm for all batches.

The measured properties of the coatings agreed fairly well with the design properties given in Table 3-1. Buffer thickness ranged from 54 to 63 μm and 86 to 90 μm. The SiC-flaw frequencies were measured after the OPyC coating was burned off, and 6% to 38% of the particles showed flaws. The liquid gradient densities and coating rates of the OPyC ranged from 1.79 to 1.98 Mg/m^3 and 5.3 to 9.0 μm/min. The measured surface-connected porosity (microporosity) was dependent upon the coating rate, except for the Ar-diluted OPyC coating, and varied from 21 to 59 ml Hg/kg of OPyC coating. The Ar-diluted OPyC had a microporosity of 48 ml/kg OPyC, and a coating rate of 5.3 μm/min, while the H_2-diluted batches had values of <28 ml/kg OPyC for the same coating rates. These Hg intrusion values show that H_2 dilution reduced the interconnecting porosity in the OPyC coating. The optical anisotropy ranged from 1.027 to 1.049 BAF_o for the batches. As expected, the anisotropy increased with density and decreased with coating rate (Ref. 8).

The total coated-particle properties include density, impurities, coating defects, and heavy metal contamination. Particle density, measured by mercury porosimetry, is a bulk density, since the mercury does not penetrate the OPyC pores. The liquid gradient density is higher, since the liquid penetrates the larger surface-connected pores of the OPyC coating. The chemical impurities were low for all batches. The SiC-coating had more defects (burn-batch test) than specified ($\leq 1 \times 10^{-3}$) for two of the eight batches. Table 3-11 shows that for five of the parent batches, the SiC-coating defect measurements were higher in the burn-visual examination than they were with the burn-leach technique. It is presumed that the liquid-leach method did not always leach all of the ThO_2 kernel out of cracked SiC-coated particles. Exposed heavy-metal Th contamination, measured by a liquid-leach method, was less than specified ($\leq 1 \times 10^{-4}$) for six of the eight batches. The FGR specification of $\leq 3 \times 10^{-5}$ R/B (release/birth) was met for five of the batches.

An interesting observation was that the FGR appeared to correlate somewhat with the defective SiC-coating fraction. The intact-OPyC coating of the defective SiC-coated particles may be permeable to the fission gases. Further supporting this permeability is the finding that the FGR tends to be higher in defective SiC-coated batches that have an OPyC coating deposited at higher coating rates. Kaae has reported (Ref. 13) that increasing the coating rate increased the surface-connected porosity of the pyrocarbon, which affects the permeability. The high SiC-coating defects in some batches will not affect the results of capsule HT-34, since any defective particles (determined by X-radiography) were removed from the approximately 140 particles of each batch inserted in the capsule.

3.4.2. Capsule Specimens

The capsule specimens for HT-34 were selected from the parent batches described in Section 3.4.1; therefore, they reflect similar general properties. Complete characterization (R/B, chemical analysis, etc.) was done on the parent batches. Many of these tests were not duplicated on the actual capsule specimens, since the only major change was in particle dimensions.

Table 3-12 gives actual HT-34-capsule-specimen density and dimensional measurements. A summary of the properties of the capsule samples is presented in Table 3-13. The properties measured on the capsule samples are compared to the parent batch properties in Table 3-14. As expected, the standard deviation of the buffer thickness and the total particle diameter were significantly reduced in the capsule samples. The table shows how the buffer coating and the other coating thicknesses changed for low-, mean-, and high-density fractions. The dimensions of the mean-density fractions were in good agreement with those of the parent batches.

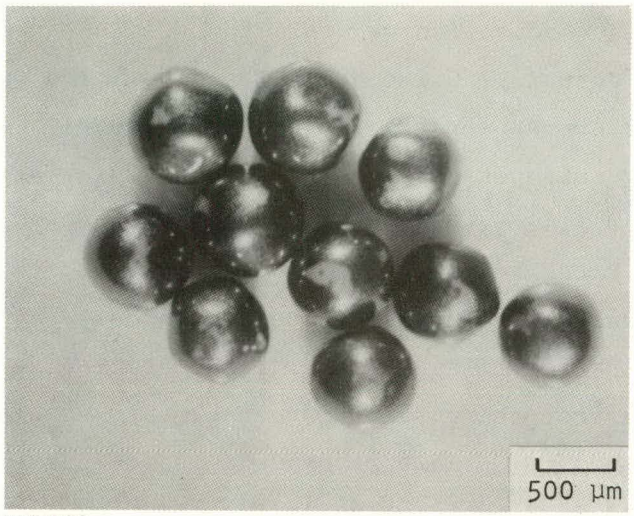

N77003

STEREO VIEW OF SiC-COATED PARTICLES
SHOWING GOLD SPOTS OR FLAWS

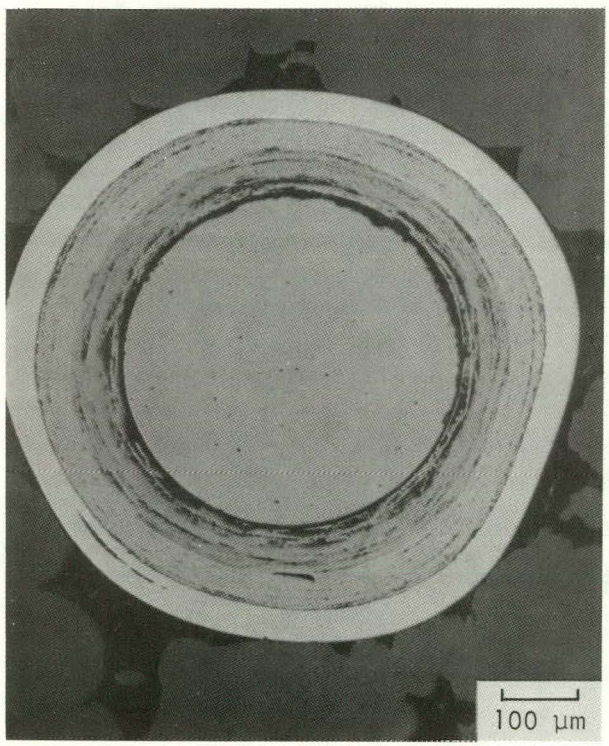

MP77001-11

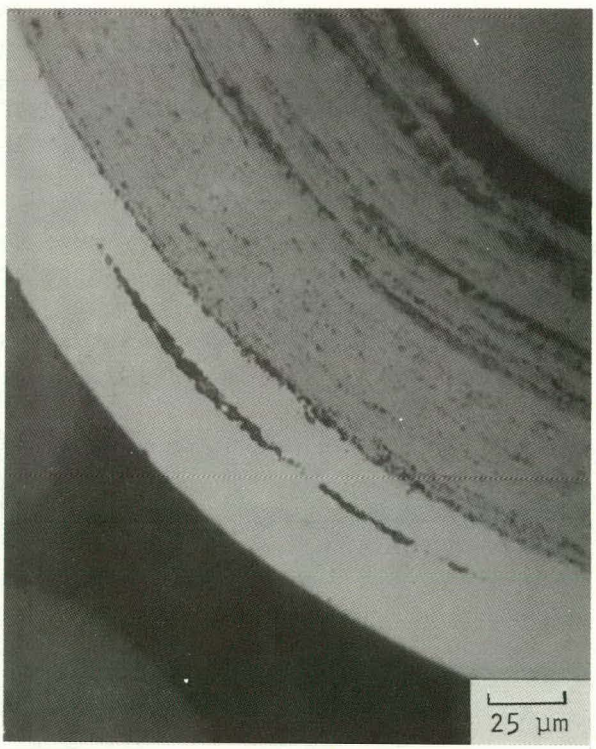

MP77001-10

METALLOGRAPHIC CROSS SECTION

Fig. 3-1. Typical internal flaws in the SiC coating of a TRISO-ThO_2 particle

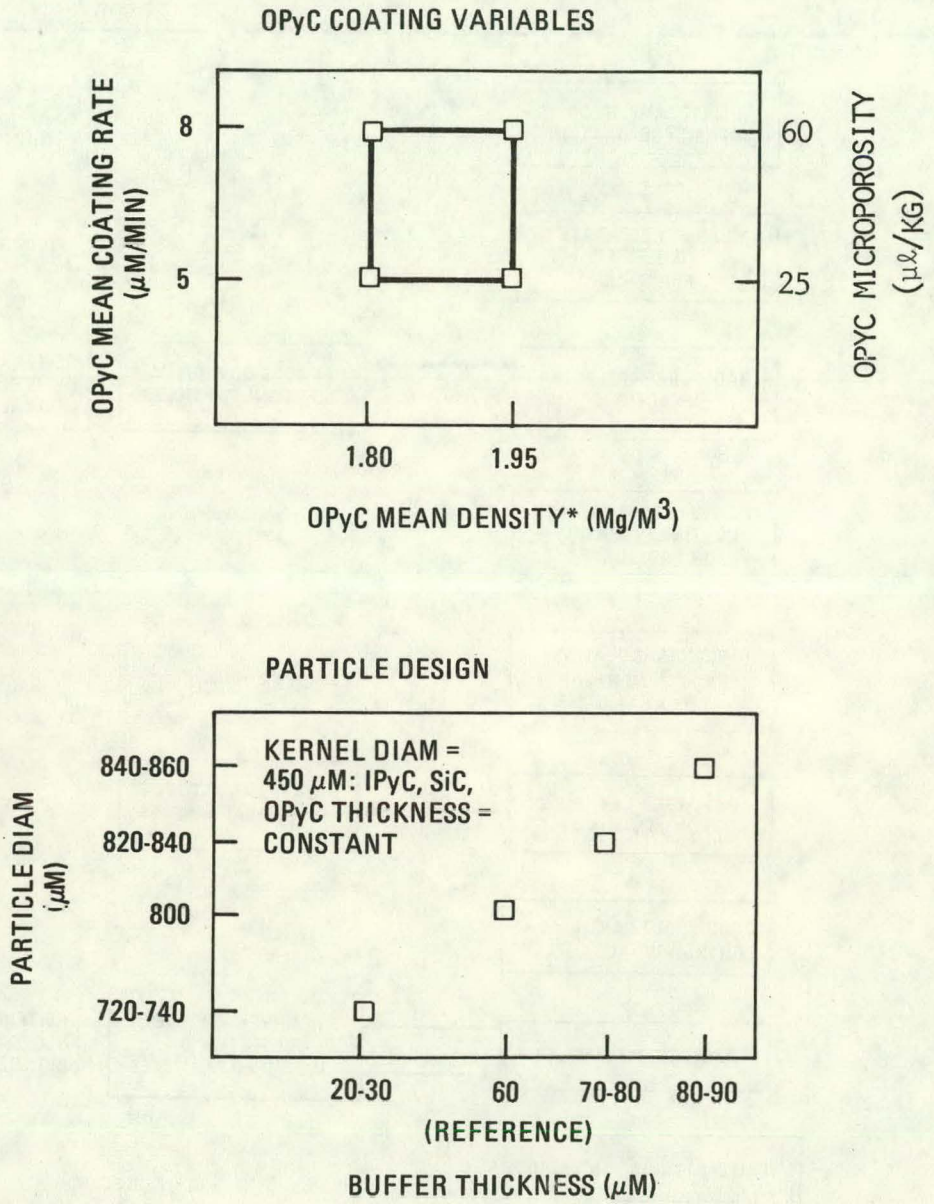

Fig. 3-2. Design test matrix of TRISO ThO_2 particles for capsule HT-34. Particles made in 240-mm-diam coater using H_2 dilution for the OPyC deposition

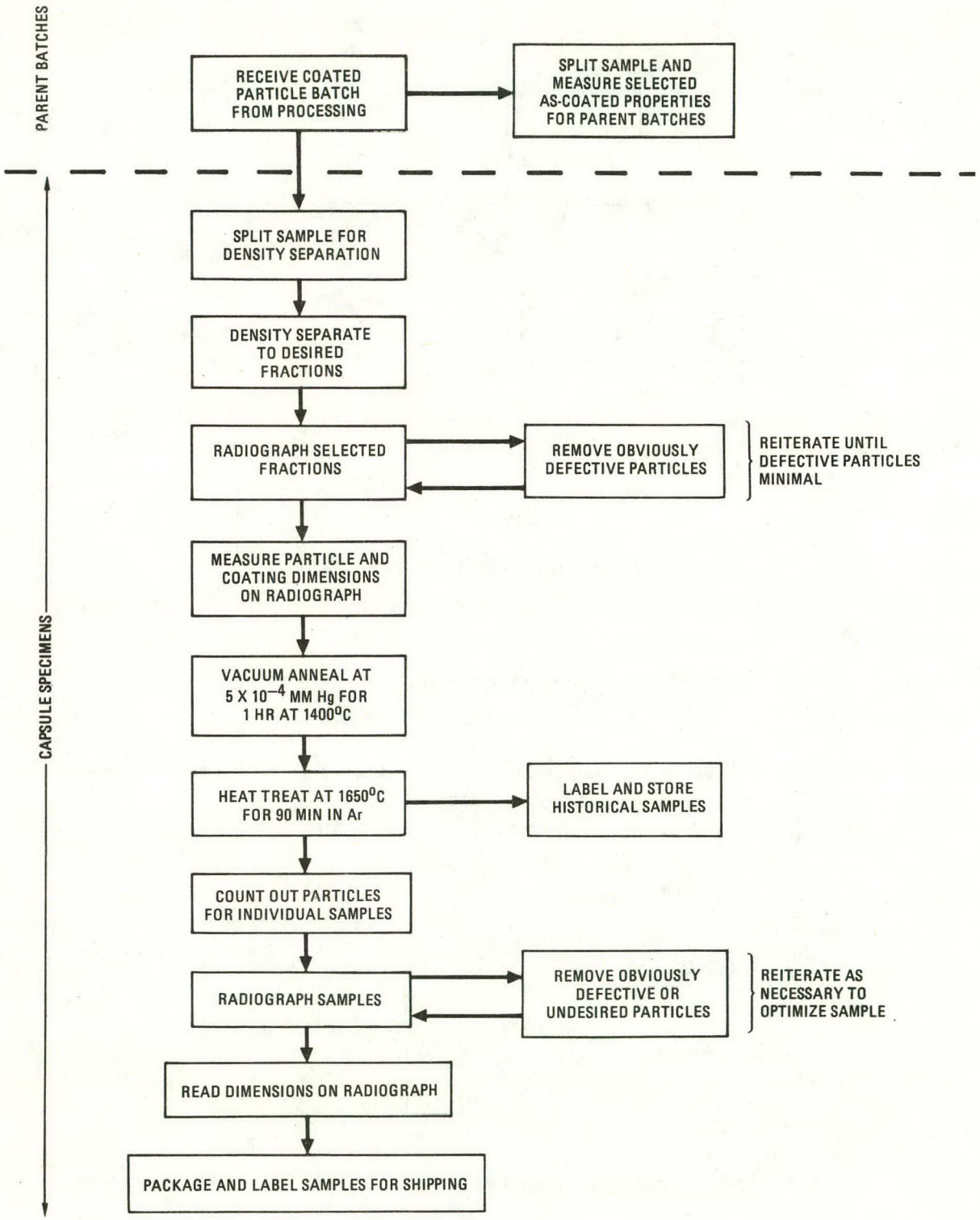

Fig. 3-3. Selection and characterization procedure for HT-34-capsule specimens

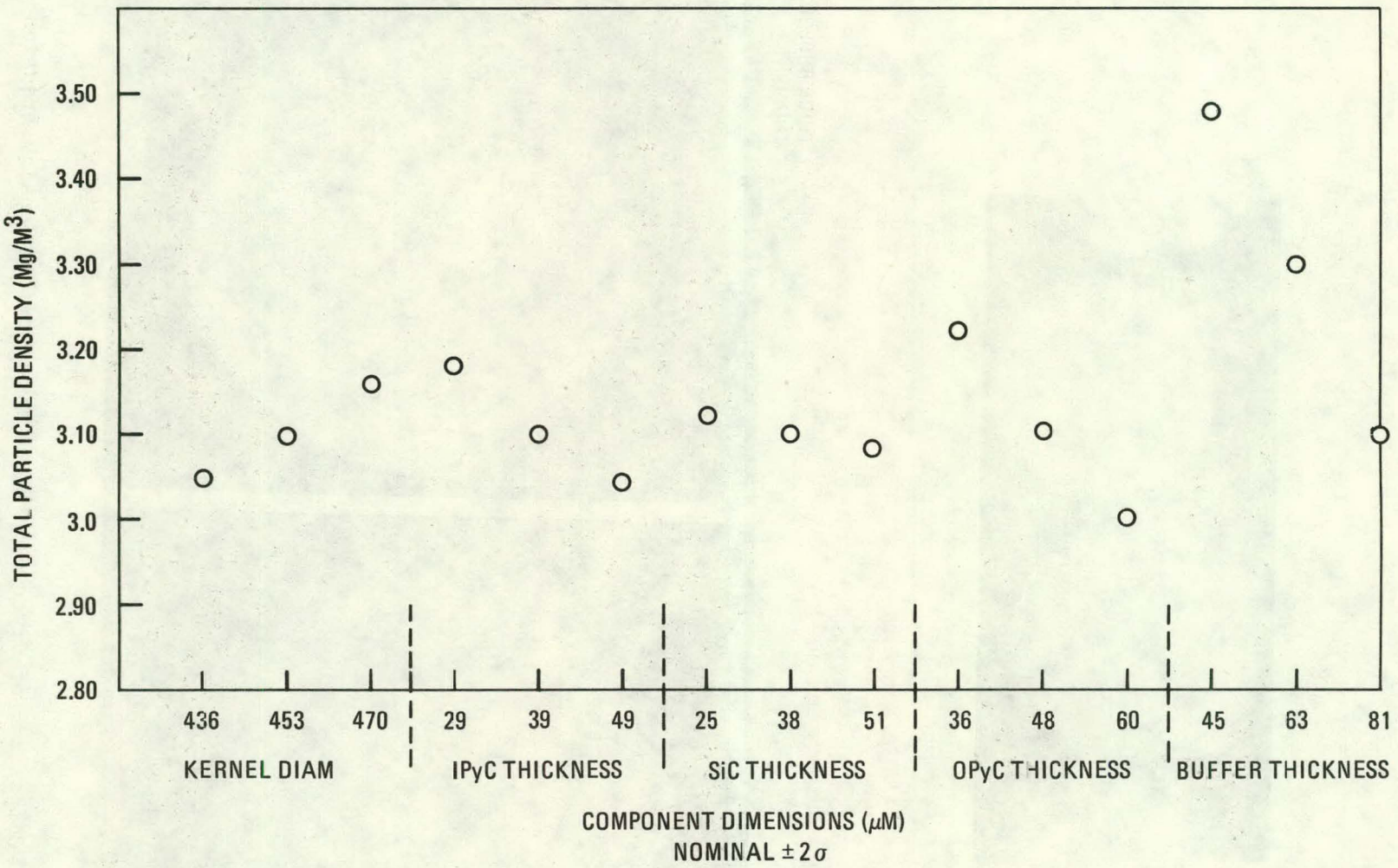

Fig. 3-4. Influence of various particle components on total density (one component varied at a time; other components kept at nominal value)

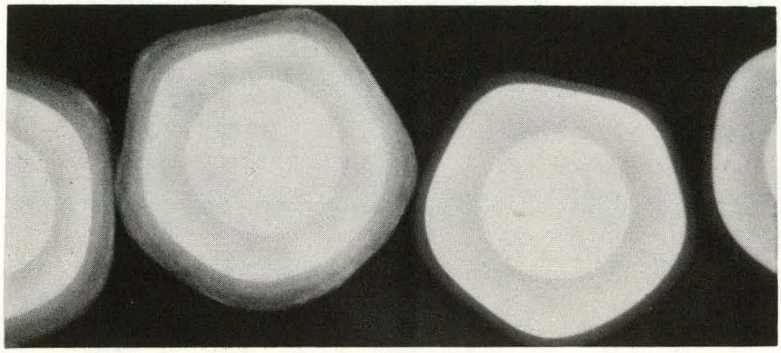

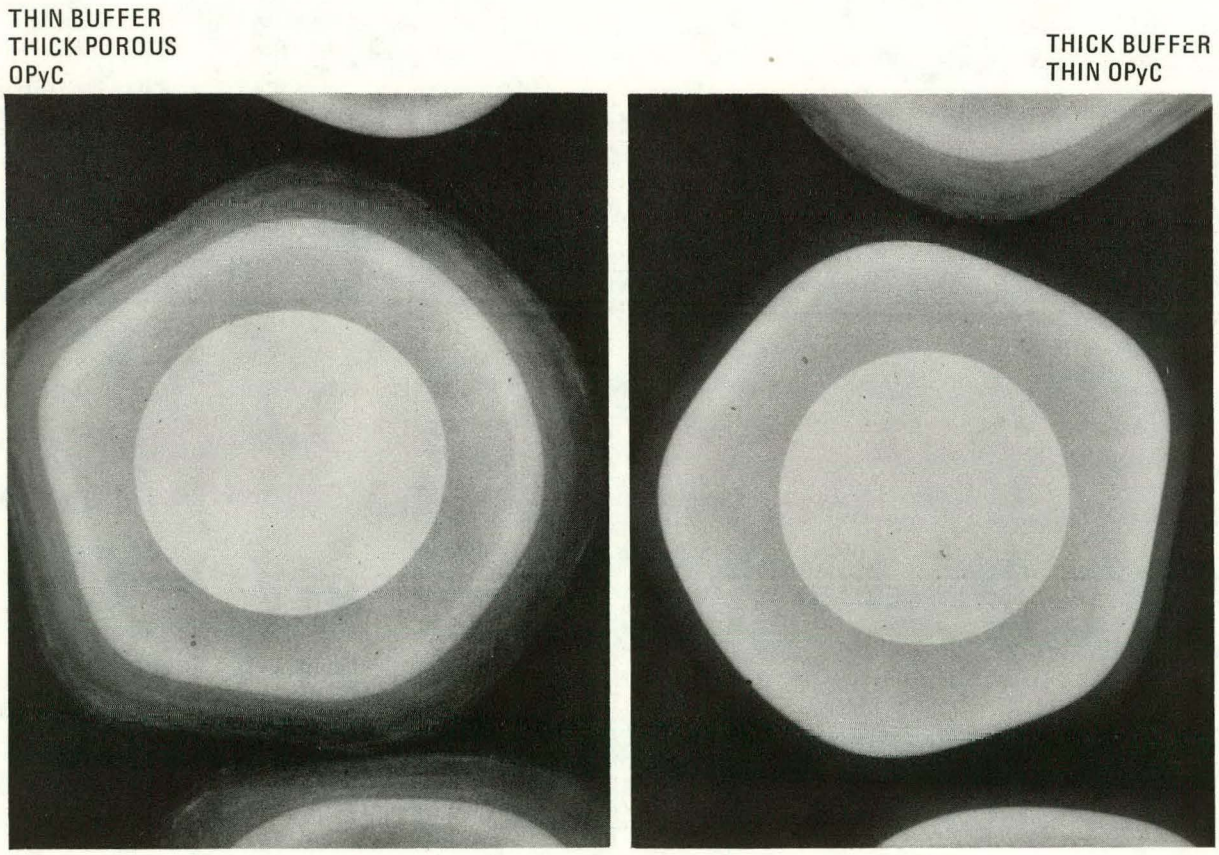

Fig. 3-5. Comparison of diverse particle types in low density fraction from particle batch 6252-14-0200

SP75028 STEREO VIEW

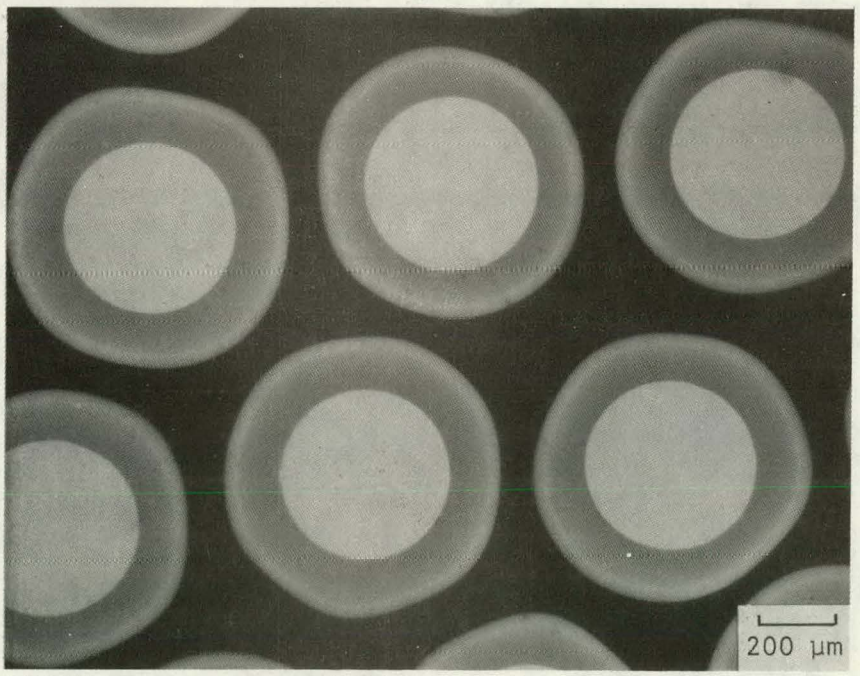

LB 307-2 X-RADIOGRAPH

Fig. 3-6. Representative photomicrographs of TRISO-coated ThO_2 batch 6252-07-020 for capsule HT-34: stereo view and X-radiograph

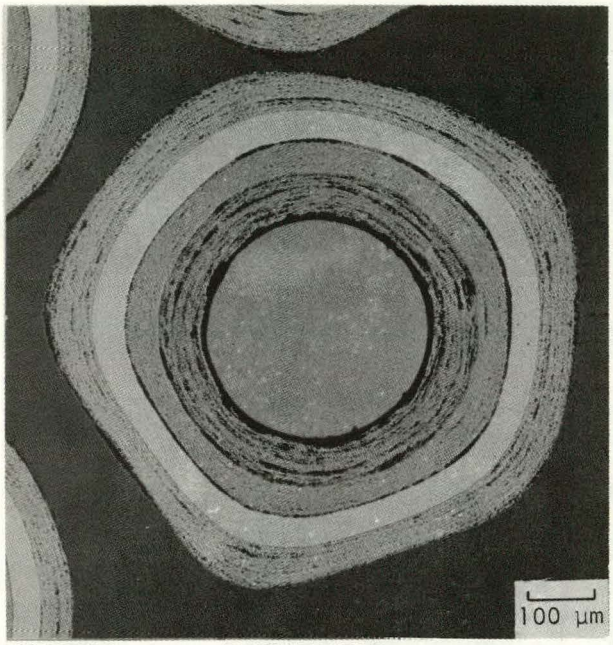

MP75044-1 BRIGHT FIELD

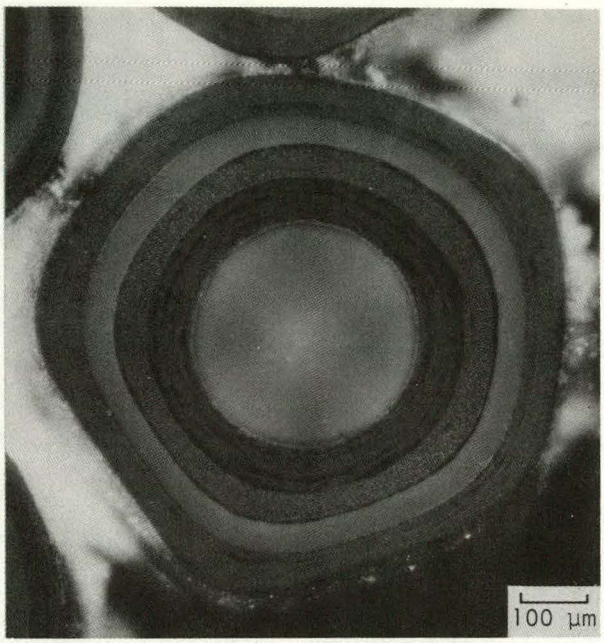

MP75044-2 POLARIZED LIGHT

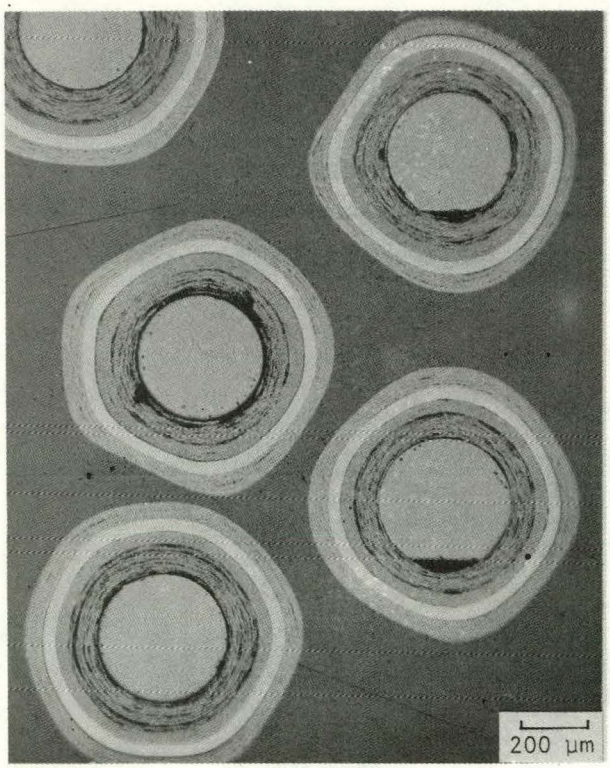

MP75044-6 BRIGHT FIELD

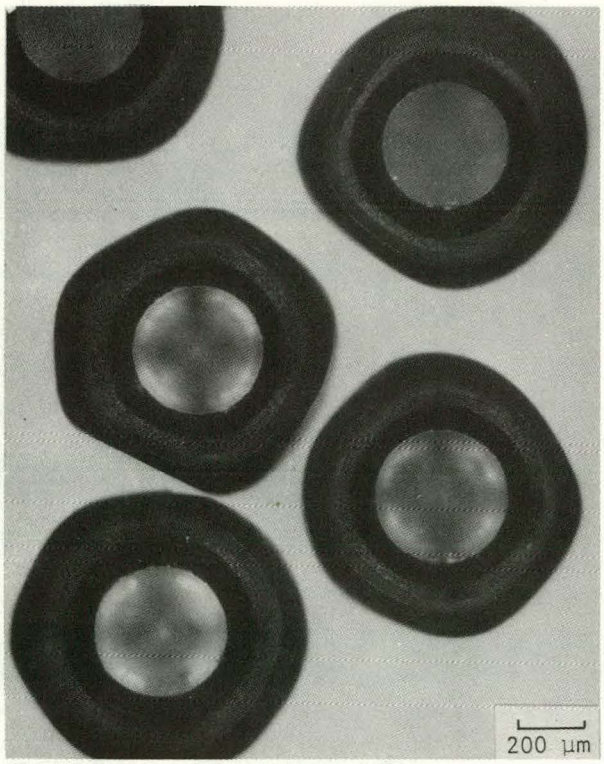

MP75044-7 POLARIZED LIGHT

Fig. 3-7. Representative photomicrographs of TRISO coated ThO_2 batch 6252-07-020 for capsule HT-34: bright field and polarized light

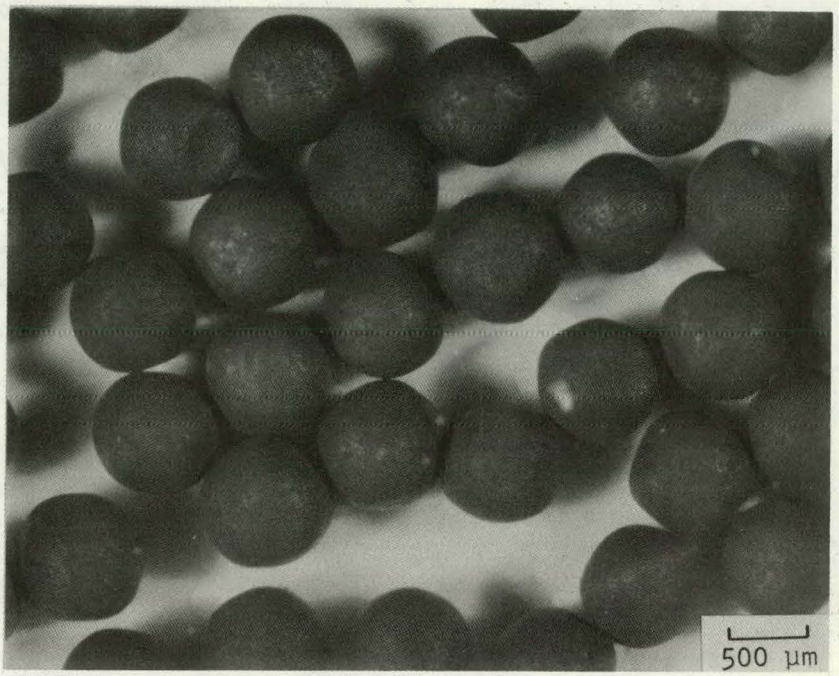

SP77009 STEREO VIEW

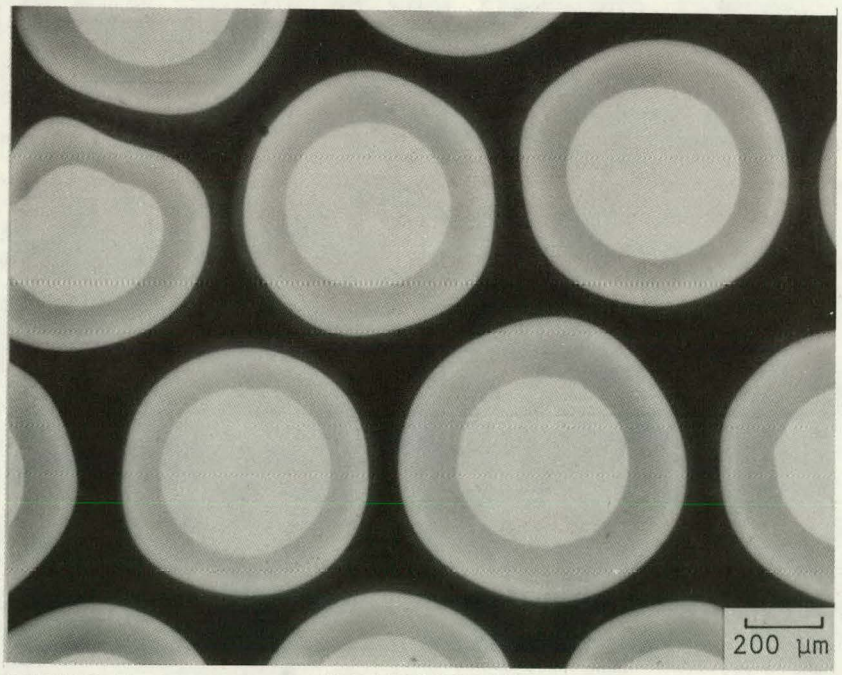

LB692-2 R X-RADIOGRAPH

Fig. 3-8. Representative photomicrographs of TRISO-coated ThO_2 batch 6252-13-010 for capsule HT-34: stereo view and X-radiograph

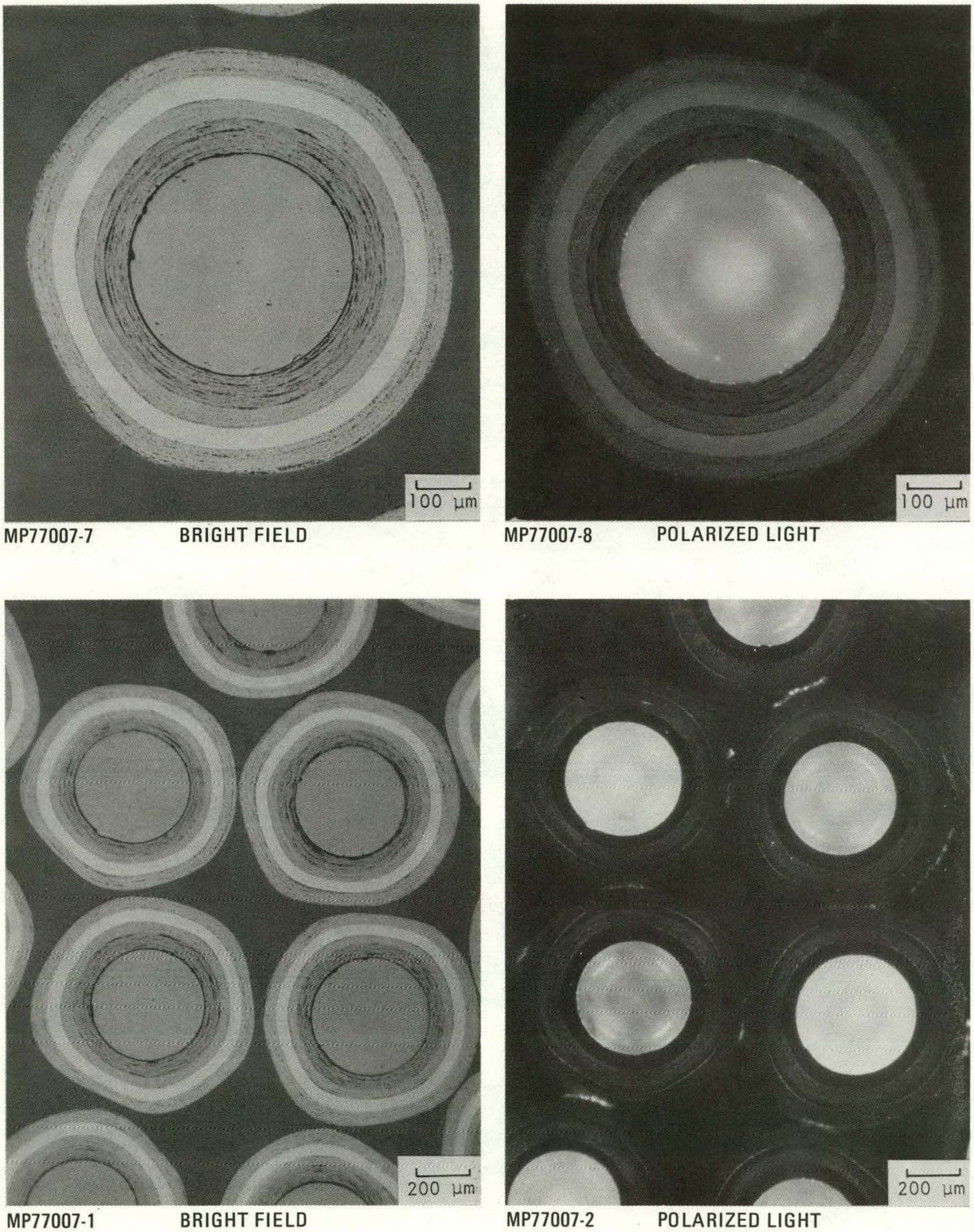

Fig. 3-9. Representative photomicrographs of TRISO-coated ThO_2 batch 6252-13-010 for capsule HT-34: bright field and polarized light

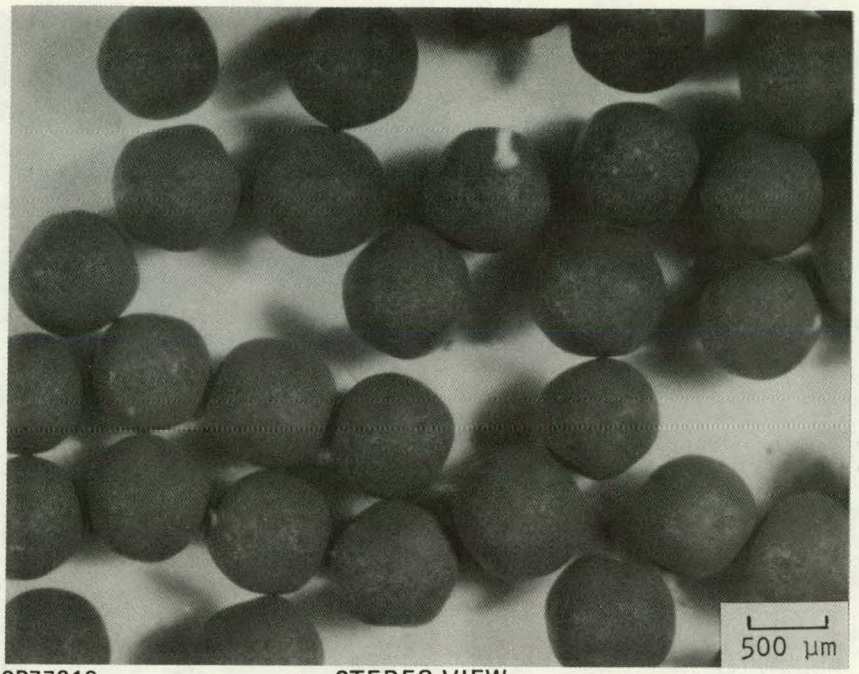

SP77010 STEREO VIEW

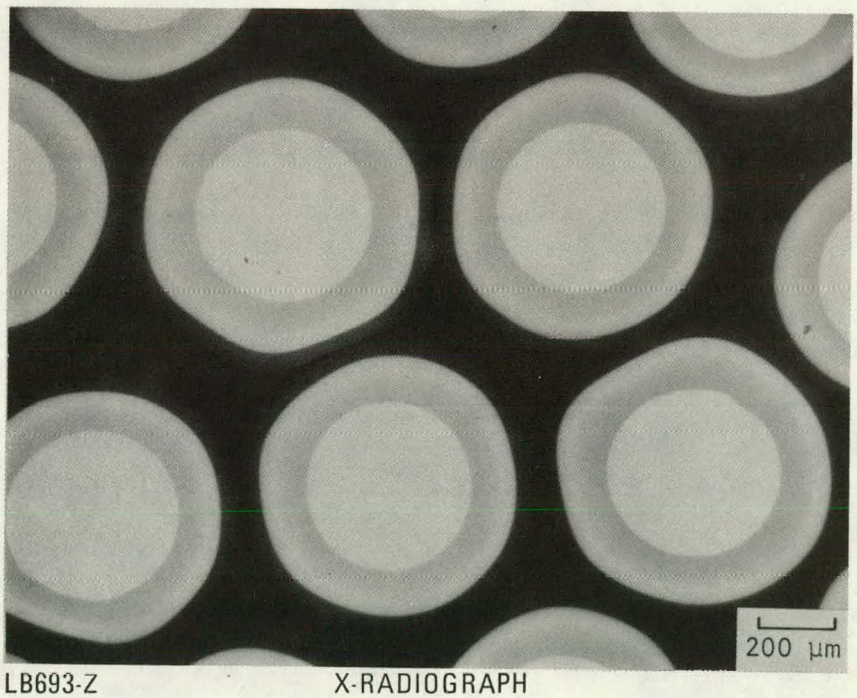

LB693-Z X-RADIOGRAPH

Fig. 3-10. Representative photomicrographs of TRISO-coated ThO_2 batch 6252-14-020 for capsule HT-34: stereo view and X-radiograph

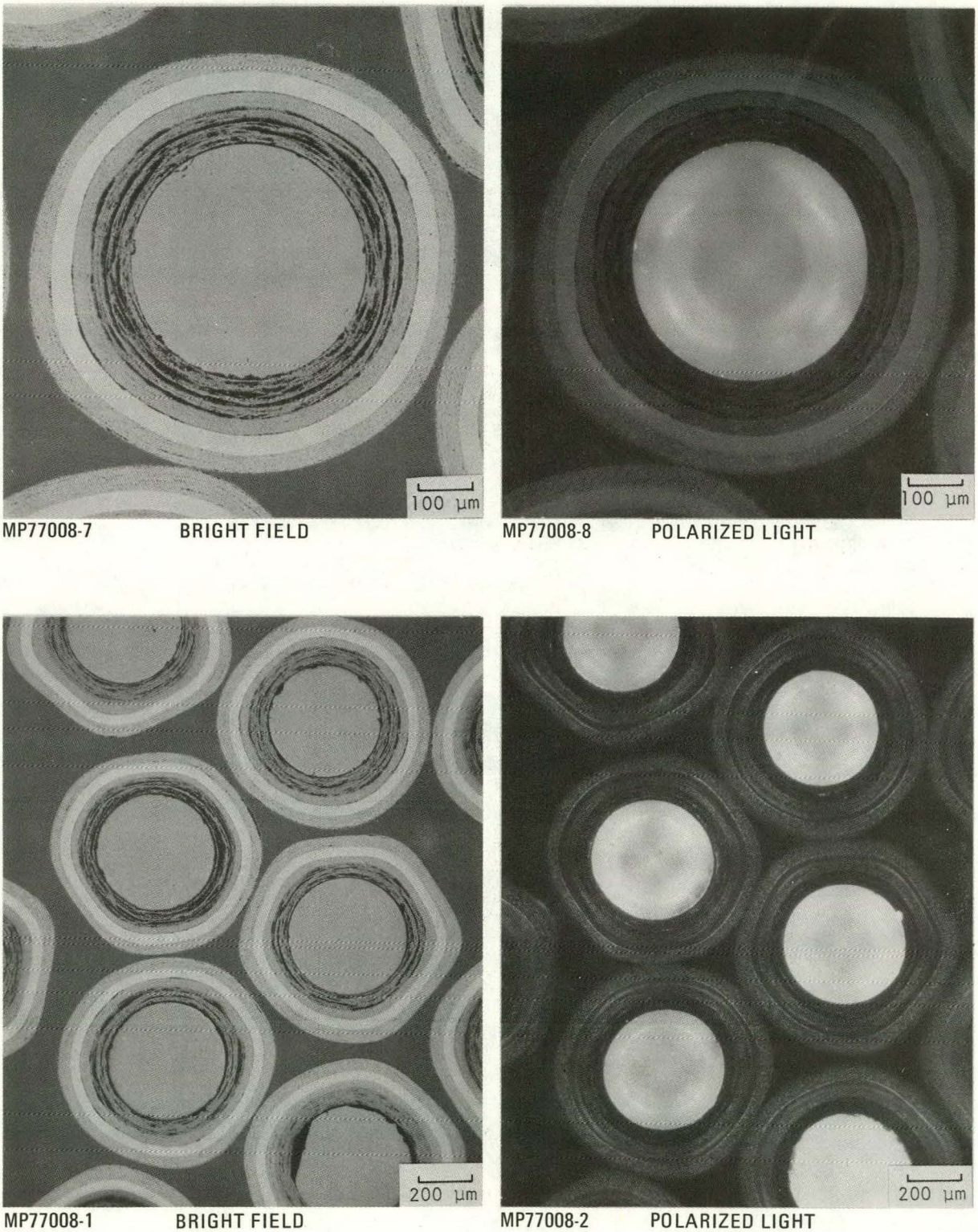

Fig. 3-11. Representative photomicrographs of TRISO-coated ThO_2 batch 6252-14-020 for capsule HT-34: bright field and polarized light

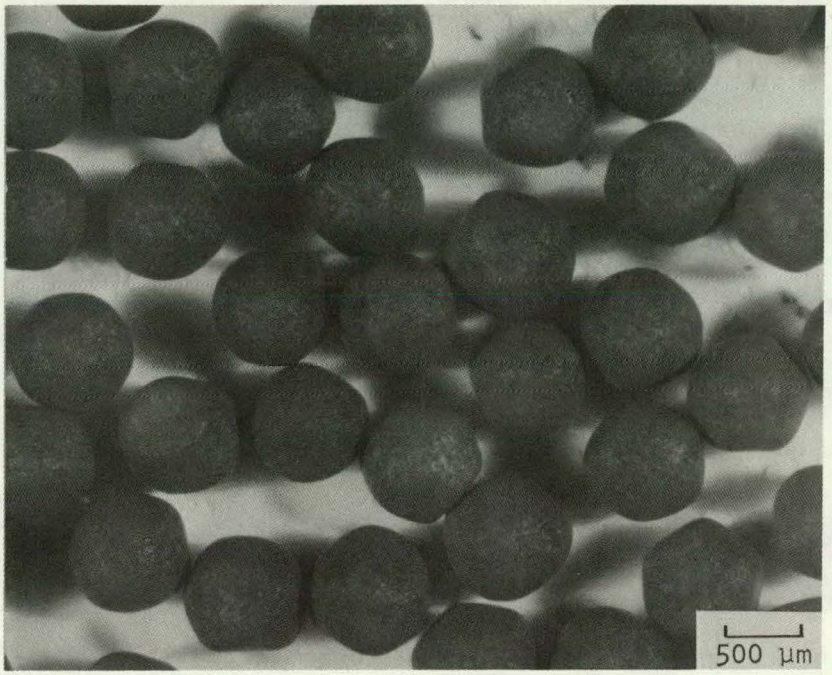

SP77002 STEREO VIEW

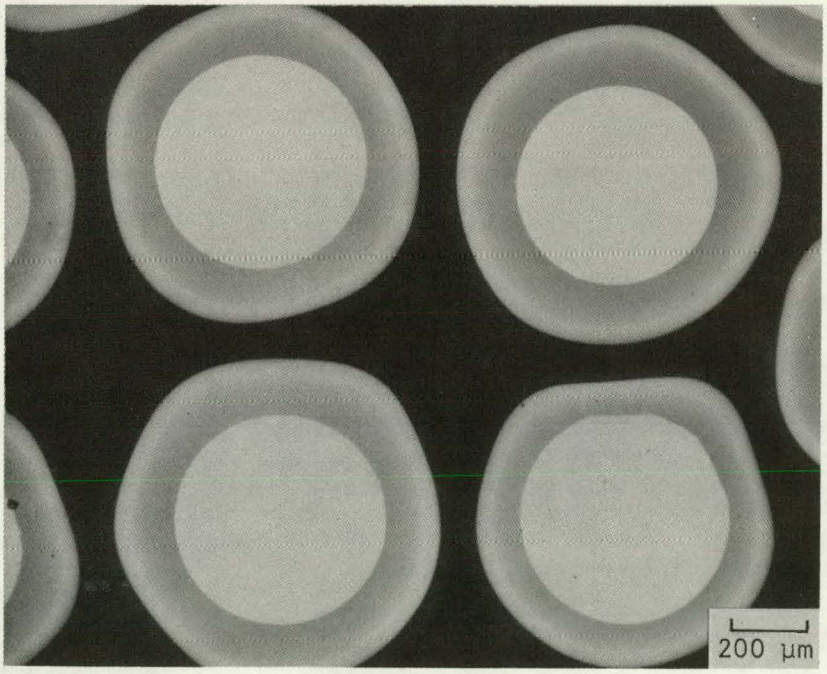

LB 680-2 X-RADIOGRAPH

Fig. 3-12. Representative photomicrographs of TRISO-coated ThO_2 batch 6252-14-020 for capsule HT-34: stereo view and X-radiograph

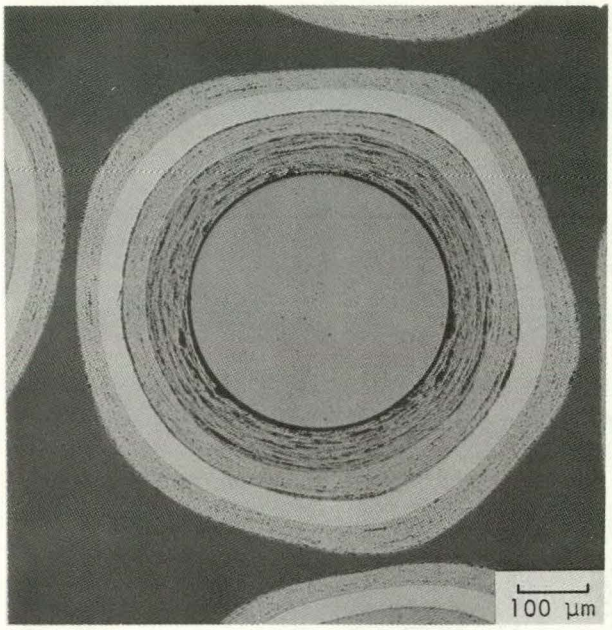

MP77002-7 BRIGHT FIELD

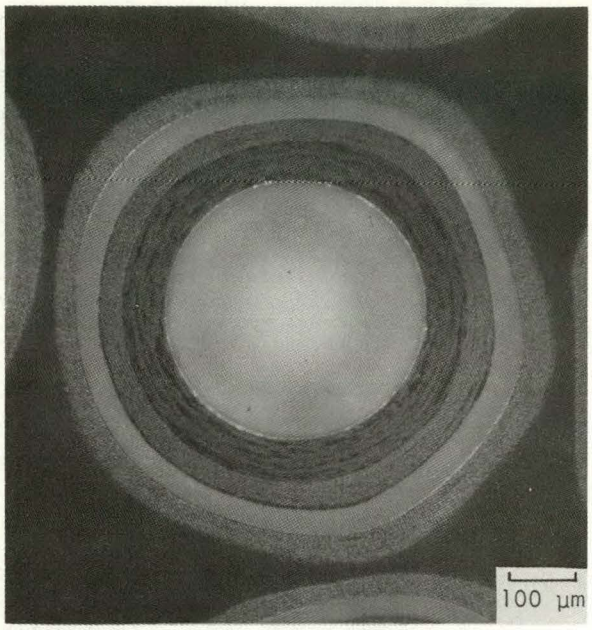

MP77002-8 POLARIZED LIGHT

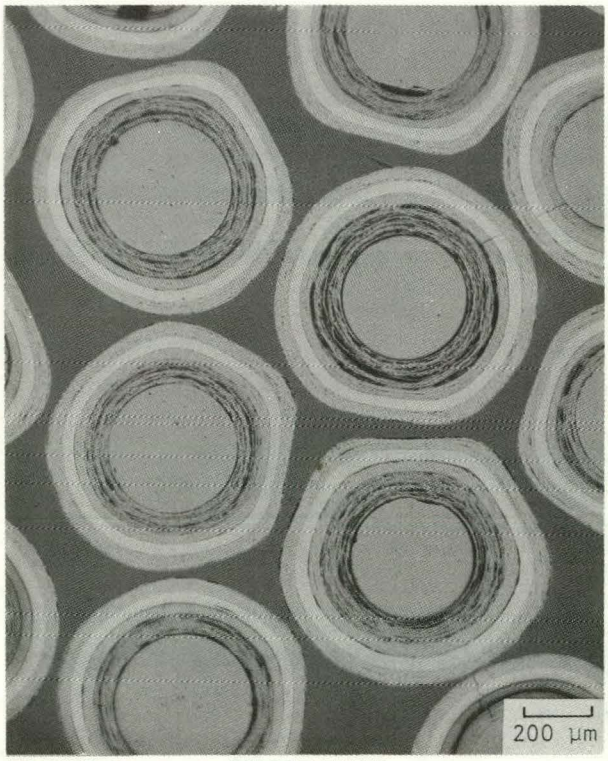

MP77002-1 BRIGHT FIELD

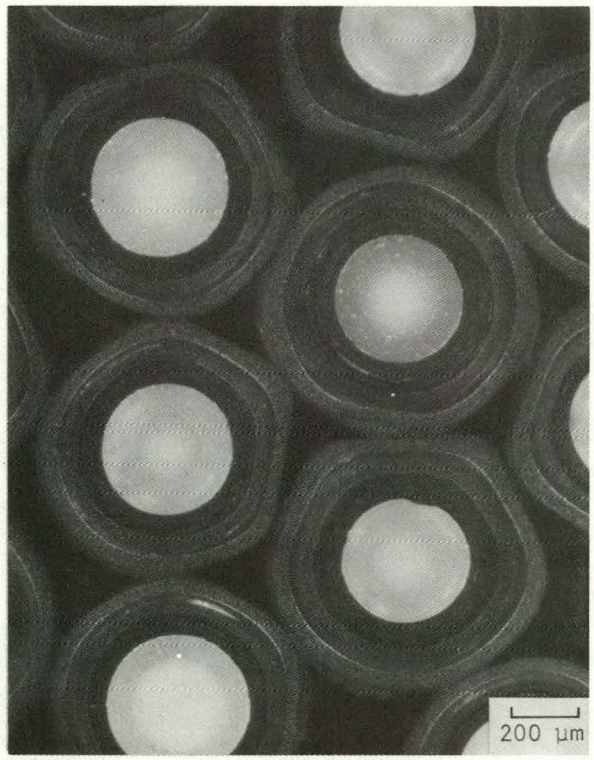

MP77002-2 POLARIZED LIGHT

Fig. 3-13. Representative photomicrographs of TRISO-coated ThO_2 batch 6252-14-020 for capsule HT-34: bright field and polarized light

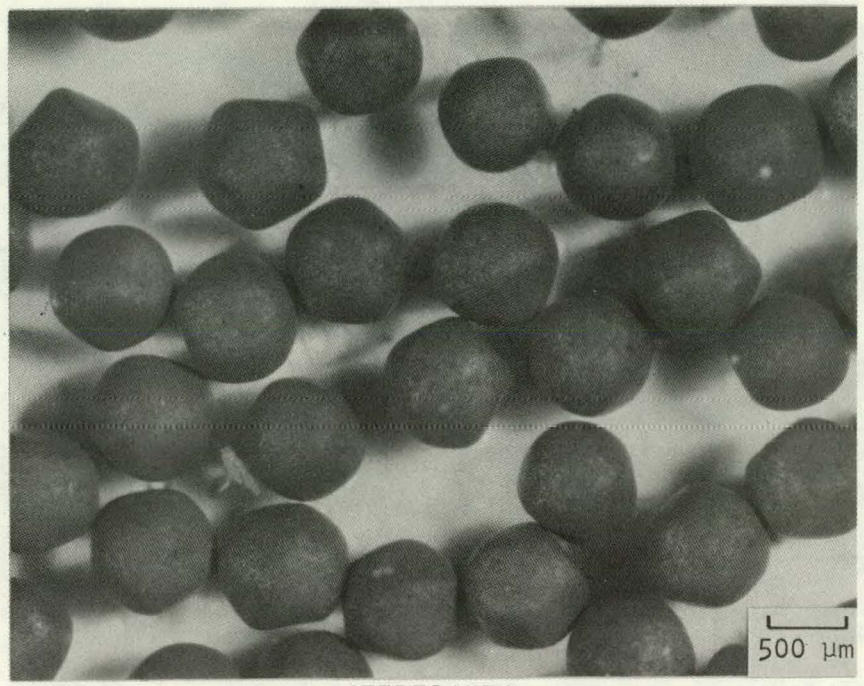

SP77011 STEREO VIEW

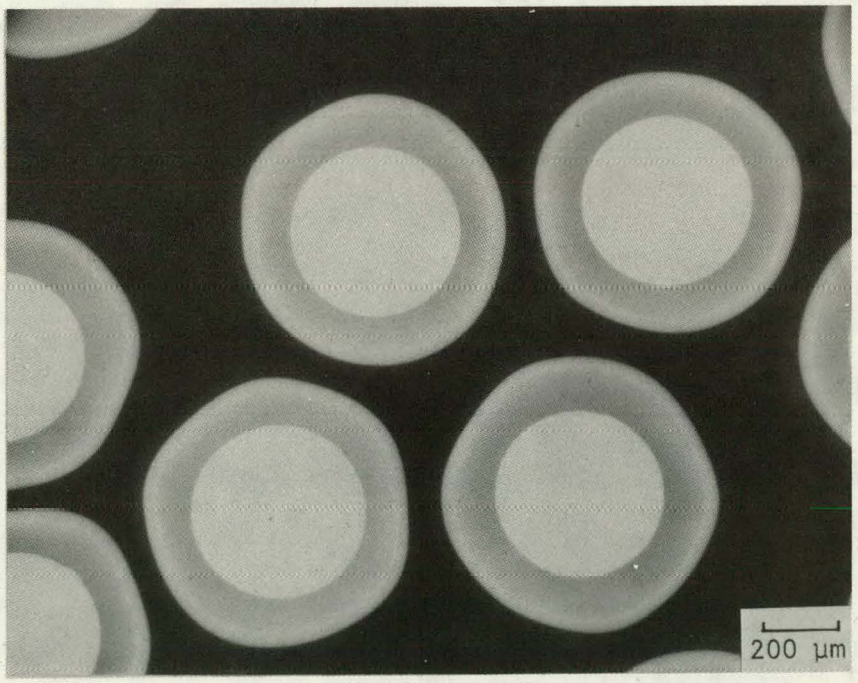

LB694-2 X-RADIOGRAPH

Fig. 3-14. Representative photomicrographs of TRISO-coated ThO_2 batch 6252-15-020 for capsule HT-34: stereo view and X-radiograph

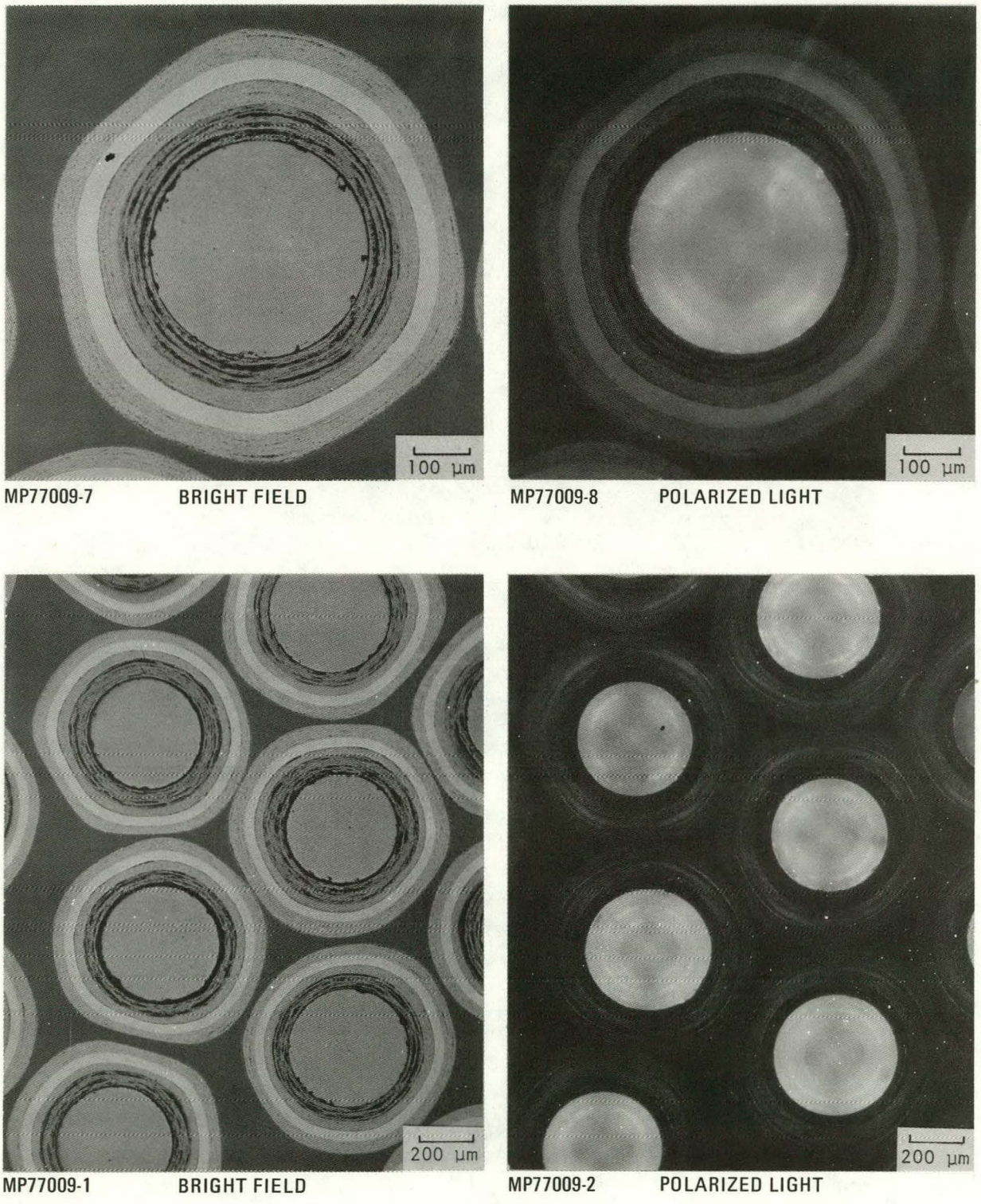

Fig. 3-15. Representative photomicrographs of TRISO-coated ThO_2 batch 6252-15-020 for capsule HT-34: bright field and polarized light

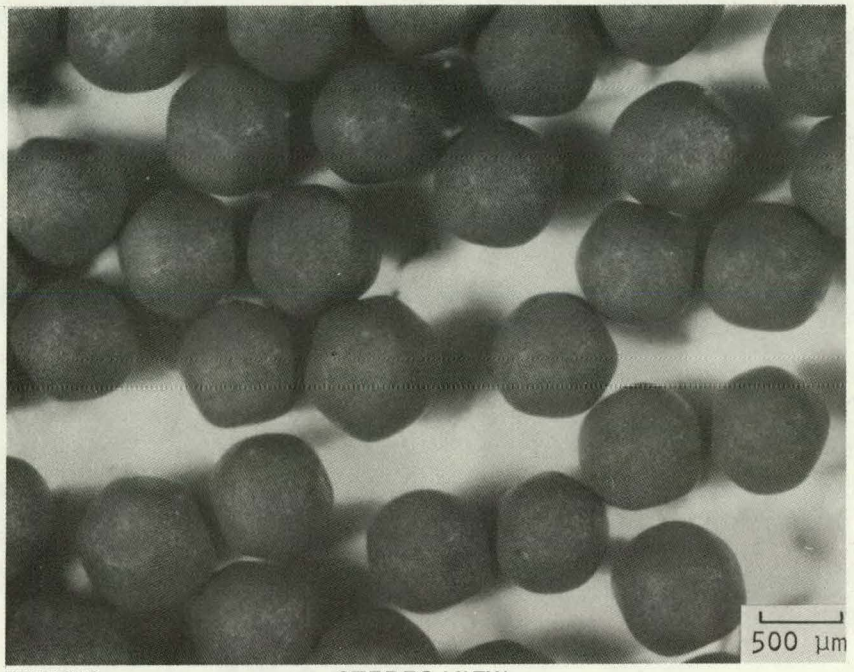

SP77012 STEREO VIEW

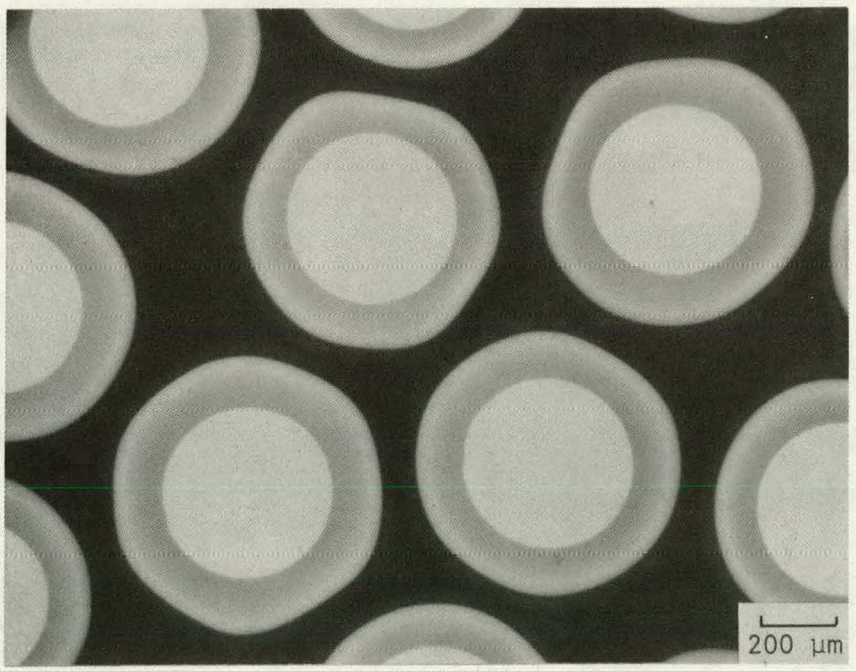

LB695-2 X-RADIOGRAPH

Fig. 3-16. Representative photomicrographs of TRISO-coated ThO_2 batch 6252-16-010 for capsule HT-34: stereo view and X-radiograph

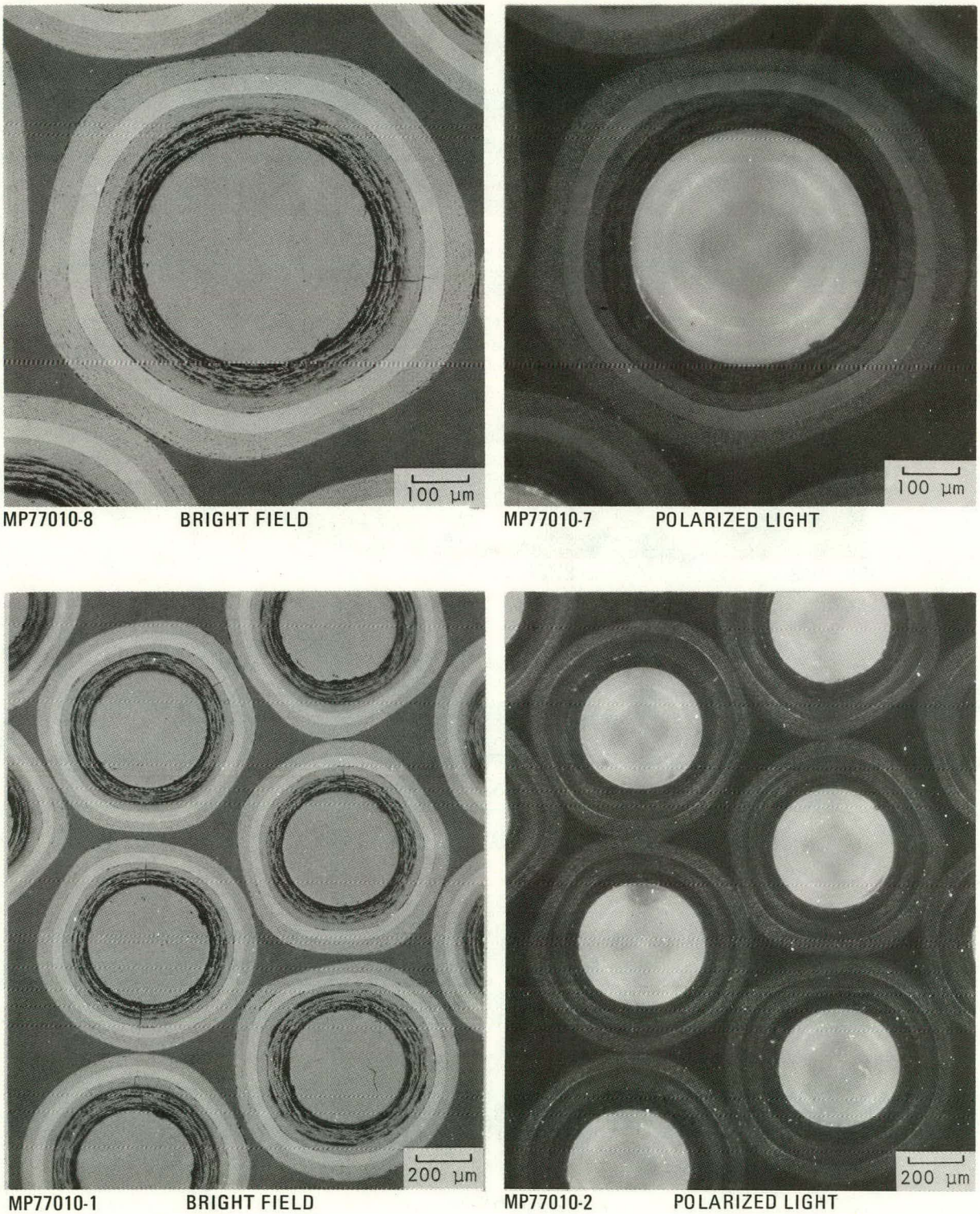

Fig. 3-17. Representative photomicrographs of TRISO-coated ThO_2 batch 6252-16-010 for capsule HT-34: bright field and polarized light

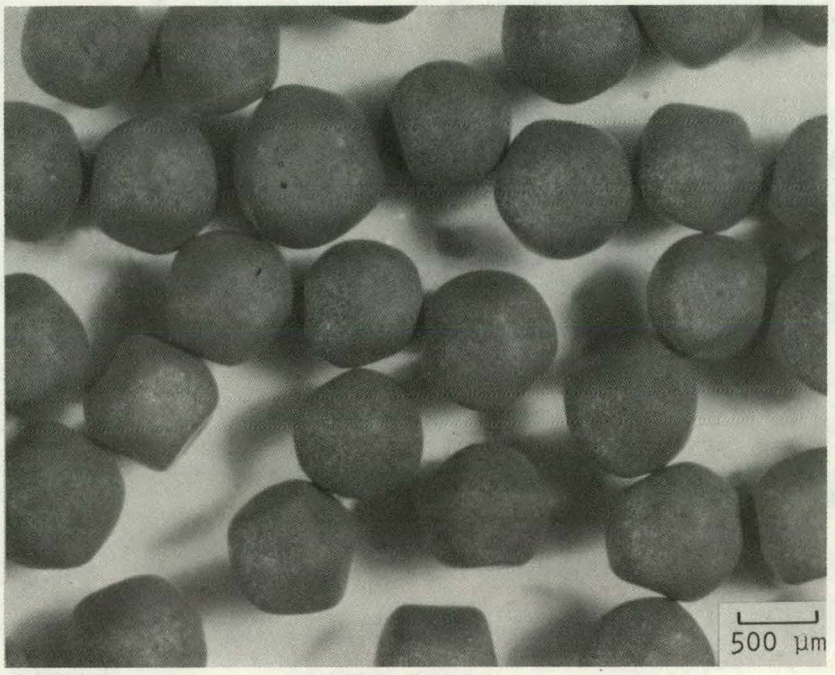

SP77008 STEREO VIEW

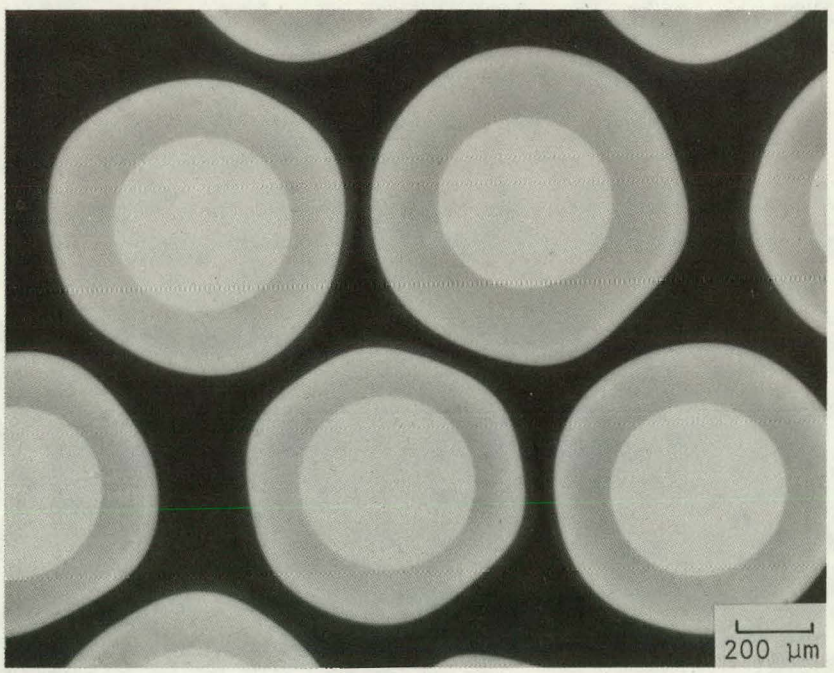

LB686-2 X-RADIOGRAPH

Fig. 3-18. Representative photomicrographs of TRISO-coated ThO_2 batch 6252-17-010 for capsule HT-34: stereo view and X-radiograph

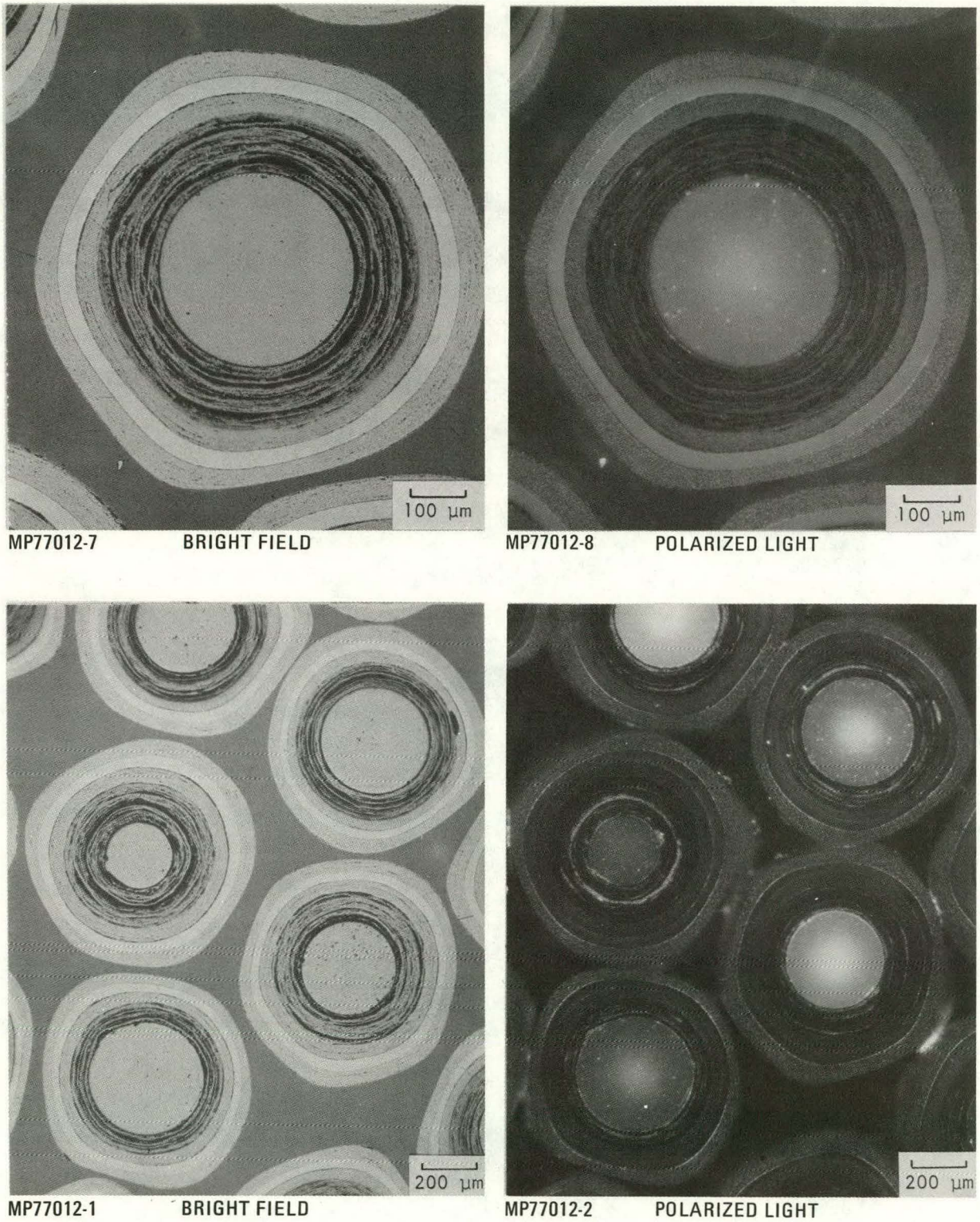

Fig. 3-19. Representative photomicrographs of TRISO-coated ThO_2 batch 6252-17-010 for capsule HT-34: bright field and polarized light

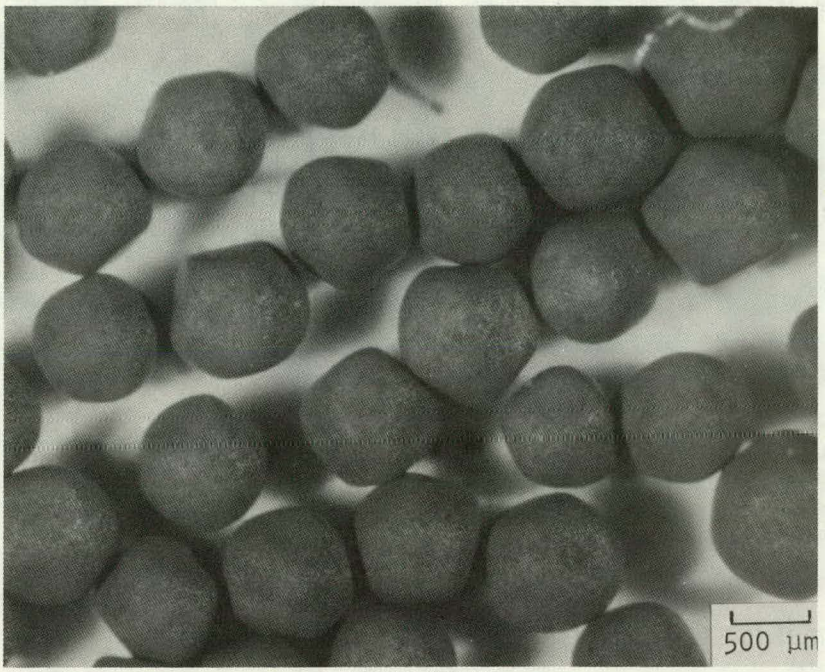

SP77007 STEREO VIEW

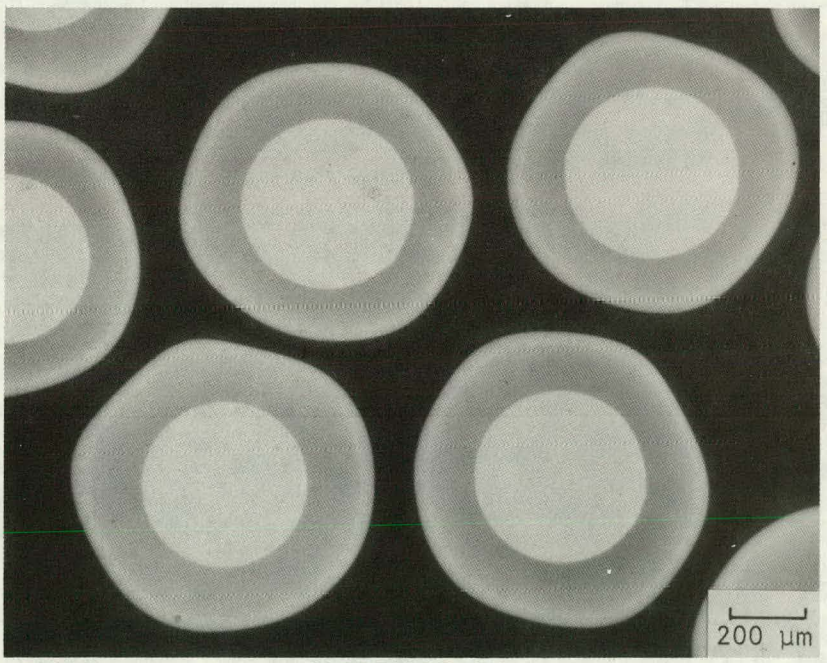

LB685-2 X-RADIOGRAPH

Fig. 3-20. Representative photomicrographs of TRISO-coated ThO_2 batch 6252-20-010 for capsule HT-34: stereo view and X-radiograph

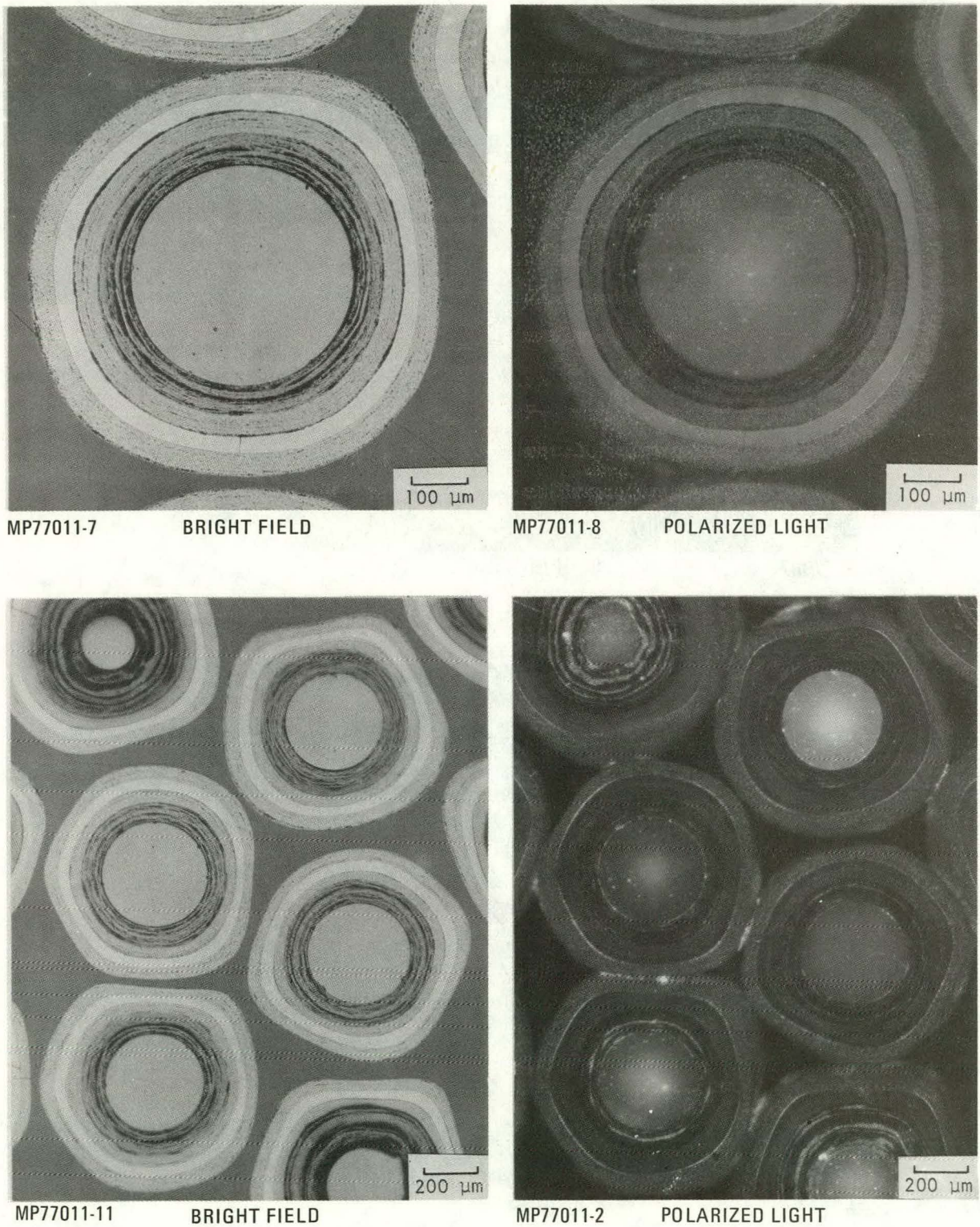

Fig. 3-21. Representative photomicrographs of TRISO-coated ThO_2 batch 6252-20-010 for capsule HT-34: bright field and polarized light

TABLE 3-1
PRIMARY DESIGN VARIABLES OF TRISO ThO_2 PARENT PARTICLE BATCHES FOR CAPSULE HT-34

Parent Batch No.[a]	Buffer Thickness (μm)	SiC Flaws (%)	OPyC				
			Density (Mg/m^3)		Micro-porosity (μℓ/kg)	Coating Rate (μm/min)	Coating Diluent Gas
			Liquid Gradient[b]	Bulk			
6252-13-010	60	10	1.80	1.60	60	8	H_2
6252-14-010	60	10	1.95	1.75	60	8	H_2
6252-14-020	60	30	1.95	1.75	60	8	H_2
6252-15-010	60	10	1.80	1.65	25	5	H_2
6252-16-010	60	10	1.95	1.80	25	5	H_2
6252-20-010	85	6	1.95	1.75	60	8	H_2
6252-17-010	85	6	1.95	1.80	25	5	H_2
6252-07-020[c]	60	38	1.90	1.75	50	6	Ar

[a] The first eight numbers of the parent batch and the corresponding capsule samples are the same, i.e., batch 6252-13-010 is the parent batch of capsule sample 6252-13-0171-001.

[b] Specification density for the OPyC coating.

[c] Batch previously irradiated in capsules HT-31 and HT-33.

TABLE 3-2
VARIABLES TO BE TESTED IN CAPSULE HT-34

Variable	Capsule Samples[a]
1200°C Magazine	
OPyC properties	8,10,11,13
Pressure vessel failure	5,7,10
SiC flaw effect	5,7
Size effect on OPyC	2,10
OPyC-coating diluent gas	All
Standard	4
1500°C Magazine	
Pressure vessel failure	All
Chemical behavior	All
OPyC properties	21,23,24,26
SiC flaw effect	18,20,21
Size effect on OPyC	17,26
Standard	17

[a] Numbers given are the sample positions.

TABLE 3-3
LOCATION AND DESCRIPTION OF PARTICLES IN END PLUGS OF CAPSULE HT-34

End Plug No.(a)	Magazine	Design Irradiation Conditions		Thorium Loading (mg)	Plug Hole No.(b)	Particle Batch(c)	No. Particles
		Fluence [10^{25} n/m^2 (E > 29 fJ)$_{HTGR}$]	Burnup (% FIMA)				
14-3	1200°C	5.2	5.3	22.7	1	BISO-T	19
					2	None	0
					3	BISO-T	19
					4	None	0
					5	BISO-T	18
					6	None	0
14-1	1200°C	3.7	9.1	22.7	1	None	0
					2	TRISO-I	25
					3	BISO-T	14
					4	BISO-T	14
					5	BISO-T	14
					6	BISO-T	14
15-3	1500°C	9.7	10.8	32.5	1	BISO-T	13
					2	BISO-T	14
					3	BISO-T	13
					4	BISO-T	13
					5	BISO-T	14
					6	BISO-T	13
15-1	1500°C	10.9	12.8	32.5	1	None	0
					2	TRISO-I	25
					3	BISO-T	20
					4	BISO-T	20
					5	BISO-T	20
					6	BISO-T	20

(a) See Fig. 2-1 for location of end plugs.

(b) Hole No. 1 has an index mark; other holes are numbered consecutively, clockwise from the top view.

(c) EISO-T = BISO ThO_2 batch 7032-149
TRISO-I = TRISO inert batch 6351-040-0100, burned back.

TABLE 3-4
FABRICATION CONDITIONS OF TRISO ThO_2 PARENT BATCHES FOR CAPSULE HT-34[a]

Parent Batch No.[b]	Buffer			IPyC					SiC					OPyC						
	Coater Charge (kG)	Coating Rate (μm/min)	Deposition Gas/Diluent and Levitating Gas	Coating Rate (μm/min)	Deposition Gas	Diluent Gas/ Levitating Gas	Deposition Temperature		Coater Charge (kG)	Coating Rate (μm/min)	Deposition Gas/Diluent and Levitating Gas	Deposition Temperature		Deposition Control Temperature of Bed (°C)	Coater Charge (kG)	Coating Rate (μm/min)	Deposition Gas	Diluent Gas/ Levitating Gas	Deposition Temperature	
							Bed (°C)	Control (°C)				Bed (°C)	Control (°C)						Bed (°C)	Control (°C)
6252-07-025	15	11.0	C_2H_2/Ar	4.4	C_2H_2/C_3H_6	Ar/Ar	ND[c]	1300	19.5	0.16	CH_3SiCl_3/H_2[d]	ND	1625	1625	11.0	5.3	C_2H_2/C_3H_6	Ar/Ar	ND	1540
6252-13-010	17	9.0	C_2H_2/Ar	4.1	C_2H_2/C_3H_6	H_2/Ar	1185	1350	10.5	0.32	CH_3SiCl_3/H_2	ND	1650	1650	13.5	8.6	C_2H_2/C_3H_6	H_2/Ar	1400	1420
6252-14-010	17	10.0	C_2H_2/Ar	4.0	C_2H_2/C_3H_6	H_2/Ar	ND	1360	11.0	0.31	CH_3SiCl_3/H_2	ND	1650	1650	13.5	8.3	C_2H_2/C_3H_6	H_2/Ar	1295	1315
6252-14-020	17	9.0	C_2H_2/Ar	4.7	C_2H_2/C_3H_6	H_2/Ar	ND	1350	20.5	0.28	CH_3SiCl_3/H_2	ND	1650	1650	13.0	8.0	C_2H_2/C_3H_6	H_2/Ar	1275	1315
6252-15-010	17	10.2	C_2H_2/Ar	4.2	C_2H_2/C_3H_6	H_2/Ar	ND	1360	10.5	0.32	CH_3SiCl_3/H_2	ND	1650	1650	13.5	5.3	C_2H_2/C_3H_6	H_2/Ar	1385	1405
6252-16-010	17	10.2	C_2H_2/Ar	4.2	C_2H_2/C_3H_6	H_2/Ar	ND	1360	10.5	0.33	CH_3SiCl_3/H_2	ND	1650	1650	13.5	6.0	C_2H_2/C_3H_6	H_2/Ar	1280	1310
6252-17-010	17	13.0	C_2H_2/Ar	4.2	C_2H_2/C_3H_6	H_2/Ar	1195	1330	22.5	0.23	CH_3SiCl_3/H_2	ND	1650	1650	14.0	5.4	C_2H_2/C_3H_6	H_2/Ar	1280	1310
6252-20-010	17	13.0	C_2H_2/Ar	4.2	C_2H_2/C_3H_6	H_2/Ar	1195	1330	22.5	0.24	Ch_3SiCl_3/H_2	ND	1650	1650	14.0	9.0	C_2H_2/C_3H_6	H_2/Ar	1275	1315

[a] Coated in 240-mm-i.d. dry coater with a cone gas distributor containing an extension nozzle through center of core. Deposition and diluent gases premixed and enter near top of extension nozzle; levitating gas enters at bottom of cone.

[b] The first eight numbers of the parent batches and the corresponding capsule samples are the same, i.e., batch 6252-13-010 is the parent batch of capsule sample 6252-13-0171-001.

[c] ND = not determined.

[d] Levitating gas was H_2 and argon mixture.

PAGES 3-37 to 3-38

WERE INTENTIONALLY

LEFT BLANK

TABLE 3-5
NUMERICAL CROSS REFERENCE OF HT-34 CAPSULE SPECIMENS

Parent Batch Data Retrieval No.	After Density Separation		After Heat Treatment		Capsule Specimen Data Retrieval No.
	GA Notebook No.	Data Retrieval No.	GA Notebook No.	Data Retrieval No.	
6252-07-0200	2995-114	6252-07-0262	6627-86-13	6252-07-0262	6252-07-0262-001 6252-07-0262-002
6252-13-0100	6627-69-3	6252-13-0110	6627-86-7	6252-13-0111	6252-13-0161-001
6252-13-0100	6627-72-1	6252-13-0120	6627-86-1	6252-13-0171	6252-13-0171-001
6252-14-0100	6627-68-1	6252-14-0130	6627-86-2	6252-14-0131	6252-14-0181-001
6252-14-0100	6627-68-2	6252-14-0110	6627-86-8	6252-14-0111	6252-14-0161-001 6252-14-0161-002
6252-14-0100	6627-68-3	6252-14-0120	6627-86-3	6252-14-0121	6252-14-0171-001
6252-14-0200	6627-59-3	6252-14-0210	6627-86-6	6252-14-0211	6252-14-0261-001
6252-14-0200	6627-73-1	6252-14-0220	6627-86-5	6252-14-0221	6252-14-0271-001
6252-15-0100	6627-70-1	6252-15-0120	6627-86-4	6252-15-0121	6252-15-0171-001
6252-15-0100	6627-70-3	6252-15-0110	6627-86-9	6252-15-0111	6252-15-0161-001
6252-16-0100	6627-71-2	6252-16-0110	6627-86-10	6252-16-0111	6252-16-0161-001
6252-17-0100	6627-56-2	6252-17-0110	6627-86-12	6252-17-0111	6252017-0161-001
6252-20-0100	6627-52-2	6252-20-0110	6627-86-11	6252-20-0111	6252-20-0161-001 6252-20-0161-002

TABLE 3-6
CALCULATION OF PARTICLE LOADINGS FOR CAPSULE HT-34

Sample Batch No.	Particle Density Fraction	Magazine(a)	Density ThO_2 (Mg/m^3)	Kernel Diam ($m \times 10^{-6}$)	Kernel Vol ($m^3 \times 10^{-11}$)	ThO_2/ Particle ($g \times 10^{-10}$)	No. Particles
6252-13-0171-001	Low	High	9.78	442.1	4.52	4.42	85
6252-14-0181-001	Low	High	9.90	445.6	4.63	4.59	82
6252-14-0171-001	High	Low	9.90	451.9	4.83	4.78	56
6252-15-0171-001	Low	High	9.90	447.1	4.68	4.63	81
6252-14-0271-001	Low	High	9.841	445.1	4.62	4.54	83
6252-14-0261-001	High	Low	9.841	451.9	4.83	4.76	56
6252-13-0161-001	Nominal	Low	9.78	449.7	4.76	4.66	57
6252-14-0161-001	Nominal	Low	9.90	447.8	4.70	4.65	57
6252-14-0161-002	Nominal	High	9.90	447.8	4.70	4.65	81
6252-15-0161-001	Nominal	Low	9.90	451.0	4.80	4.75	56
6252-16-0161-001	Nominal	Low	9.90	451.9	4.83	4.78	56
6252-20-0161-001	Nominal	Low	9.78	451.5	4.82	4.71	56
6252-20-0161-002	Nominal	High	9.78	451.5	4.82	4.71	80
6252-17-0161-001	Nominal	High	9.78	450.0	4.77	4.66	81
6252-07-0262-001	Nominal	Low	9.91	447.9	4.70	4.66	57
6252-07-0262-002	Nominal	High	9.91	447.9	4.70	4.66	81

(a) High temp magazine - 1500°C; 0.0331 g Th-232/position.
Low temp magazine - 1200°C; 0.0234 g Th-232/position.

TABLE 3-7
INPUT PARAMETERS USED IN TRISO MONTE-NOCO CODE

Sample Position in Capsule Design Study Numbers[a]	2 DS90	4 DS91	5 DS91	7 DS93	8 DS94	10 DS95	11 DS96	13 DS97	15 DS98	17 DS99	18 DS100	20 DS101	21 DS102	23 DS103	24 DS104	26 DS105
Irradiation parameters																
Fluence (10^{25} n/m^2)$_{HTGR}$	5.3	5.9	6.2	6.8	7.1	7.6	7.9	8.3	9.4	9.8	9.9	10.1	10.2	10.4	10.4	10.4
Burnup (% FIMA)	5.6	6.2	6.5	7.1	7.5	8.1	8.5	9.1	11.0	11.5	11.7	12.1	12.1	12.5	12.6	12.8
Temperature (°C)	1200	1200	1200	1200	1200	1200	1200	1200	1500	1500	1500	1500	1500	1500	1500	1500
Particle parameters																
Kernel																
Density (kg/m^3)	9.78	9.91	9.84	9.90	9.88	9.90	9.90	9.90	9.78	9.91	9.90	9.84	9.90	9.78	9.90	9.88
Diameter (μm)	452	449	455	451	447	448	450	451	452	449	447	443	445	451	448	443
Standard deviation (μm)	7.0	4.8	7.1	10.0	7.4	7.6	7.2	6.8	7.0	4.8	6.8	8.7	7.1	7.0	7.9	7.7
Buffer																
Density (kg/m^3)	0.93	1.12	1.08	1.10	1.13	1.10	1.07	1.07	0.93	1.12	1.10	1.08	1.10	0.93	1.07	1.13
Thickness (μm)	83	60	27	35	57	63	56	57	82	57	62	86	91	80	84	79
Standard deviation (μm)	8.5	7.1	6.0	5.9	6.4	7.0	6.9	6.5	8.1	8.0	7.3	9.0	9.0	9.2	7.7	9.1
IPyC																
Density (kg/m^3)	1.79	1.93	1.83	1.84	1.86	1.84	1.85	1.85	1.79	1.93	1.84	1.83	1.84	1.79	1.85	1.86
Thickness (μm)	40	39	35	32	32	32	36	36	40	39	32	35	32	40	36	32
Standard deviation (μm)	5.1	4.8	4.9	4.4	4.1	4.4	4.4	4.4	5.1	4.8	4.4	4.9	4.4	5.1	4.4	4.1
SiC																
Deposition temp (°C)	1650	1625	1550	1650	1650	1650	1650	1650	1650	1650	1650	1650	1650	1650	1650	1650
Thickness (μm)	36	38	35	35	43	37	38	39	35	37	37	38	37	37	39	43
Standard deviation (μm)	3.7	2.5	3.0	2.5	2.3	2.6	2.1	2.0	3.7	3.1	2.3	3.2	2.6	4.8	2.6	2.5
OPyC																
Deposition temp (°C)	1315	1540	1315	1315	1420	1315	1405	1310	1315	1540	1315	1315	1315	1310	1405	1420
Density (kg/m^3)	1.98	1.80	1.97	1.97	1.79	1.97	1.81	1.96	1.98	1.80	1.97	1.97	1.97	1.95	1.81	1.79
Thickness (μm)	47	45	40	41	48	44	45	48	45	41	44	45	47	45	50	49
Standard deviation (μm)	5.6	5.7	4.9	4.2	6.0	4.8	5.1	5.8	5.4	6.1	4.6	5.7	5.6	5.2	5.5	5.2

[a] General Atomic Company Notebook #7440, unpublished data.

TABLE 3-8

PREDICTED PARTICLE PERFORMANCE FOR CAPSULE HT-34

Particle Batch Data Retrieval Number	Sample Position	Design[a] Study Number	Design Irradiation Conditions			Predicted Failure Fractions			
			Fluence (10^{25} n/m^2)$_{HFIR}$	Burnup (% FIMA)	Temperature (°C)	OPyC Intact		OPyC Failed	
6252-20-0161-001	2	DS90	5.3	5.6	1200	0[b]	(0 - 0)[c]	0[b]	(1.0-0)[c]
-07-0262-001	4	DS91	5.9	6.2	1200	0	(.18-0)	0.87	(1.0-0)
-14-0261-001	5	DS92	6.2	6.5	1200	0.59	(.98-.13)	1.0	(1.0-.86)
-14-0171-001	7	DS93	6.8	7.1	1200	0.51	(.99-.01)	1.0	(1.0-.85)
-13-0161-001	8	DS94	7.1	7.5	1200	0	(.77-0)	1.0	(1.0-0)
-14-0161-001	10	DS95	7.6	8.1	1200	0	(.78-0)	1.0	(1.0-.02)
-15-0161-001	11	DS96	7.9	8.5	1200	0	(.84-0)	1.0	(1.0-.05)
-16-0161-001	13	DS97	8.3	9.1	1200	0	(.91-0)	1.0	(1.0-.13)
-20-0161-002	15	DS98	9.4	11.0	1500	0	(.80-0)	1.0	(1.0-.07)
-07-0262-002	17	DS99	9.8	11.5	1500	0.94	(1.0-.31)	1.0	(1.0-1.0)
-14-0161-002	18	DS100	9.9	11.7	1500	0.90	(1.0-.11)	1.0	(1.0-.99)
-14-0271-001	20	DS101	10.1	12.1	1500	0.11	(1.0-0)	1.0	(1.0-.57)
-14-0181-001	21	DS102	10.2	12.2	1500	0.12	(1.0-0)	1.0	(1.0-.70)
-17-0161-001	23	DS103	10.4	12.5	1500	0.09	(.97-0)	1.0	(1.0-.43)
-15-0171-001	24	DS104	10.4	12.6	1500	0.04	(.99-0)	1.0	(1.0-.70)
-13-0171-001	26	DS105	10.4	12.8	1500	0.36	(1.0-.01)	1.0	(1.0-.93)

[a] Referenced from GA internal document.

[b] Predicted failure fraction based on a mean Apparent Failure Stress of -0.34×10^4 psi.

[c] Range of predicted failure fractions based on an Apparent Failure Stress range (two tailed test at 90% confidence level) of -2.03×10^4 to 1.35×10^4 psi.

TABLE 3-9
KERNEL PROPERTIES OF TRISO ThO_2 PARENT BATCHES FOR CAPSULE HT-34

Particle Batch No.	Kernel Batch No.		Diameter[a] (μm)		Density[b] (Mg/m^3)	Impurities (ppm-wt)		
	Data Retrieval No.	Manufacturer	Mean	SD		Fe	Cr	Ni
6252-07-025	4222-08-0130	FKB-1075-1-3	453	8.3	9.91	28	52	17
6252-13-010	4222-09-0300	88-1-118-2-2/3	454	8.3	9.88	64	16	42
6252-14-010	4222-09-0400	90-1-120	451	9.1	9.90	55	16	40
6252-14-020	4222-09-0100	88-1-118-2	451	8.1	9.84	61	35	76
6252-15-010	4222-09-0400	90-1-120	456	8.4	9.90	55	16	40
6252-16-010	4222-09-0400	90-1-120	455	8.4	9.90	55	16	40
6252-17-010	4222-09-0200	88-1-118-3	455	8.9	9.78	53	13	40
6252-20-010	4222-09-0200	88-1-118-3	456	8.6	9.78	53	13	40

[a] Measured by X-radiography.

[b] Measured by mercury porosimetry.

THIS PAGE

WAS INTENTIONALLY

LEFT BLANK

TABLE 3-10
COATING PROPERTIES OF TRISO ThO_2 PARENT BATCHES FOR CAPSULE HT-34

Parent Batch No.	Buffer			IPyC						SiC					OPyC								
	Thickness[a,b] (μm)		Density (Mg/m^3)	Thickness[b,c] (μm)		Liquid Gradient Density (Mg/m^3)		BAF_o[d]		Thickness[b] (μm)		Liquid Gradient Density (Mg/m^3)		Flaw[e] Frequency (%)	Thickness[b] (μm)		Density (mg/m^3) Liquid Gradient		Bulk	Accessible Porosity[f] (ml/kg)	Oriented Porosity (%)	Faceting[g]	BAF_o[d]	
	Mean	SD		Mean	SD	Mean	SD	Mean	SD	Mean	SD	Mean	SD		Mean	SD	Mean	SD					Mean	SD
6252-07-025	63	11.4	1.12	39	4.8	1.93	0.011	1.10	0.011	38	3.3	3.21	0.004	38	48	6.2	1.80	0.025	1.65	48	0	ND[h]	1.027	0.0030
6252-13-010	55	9.7	1.13	32	4.1	1.86	0.032	1.06	0.007	42	2.3	3.22	0.002	16	50	4.9	1.79	0.006	1.61	57	0	6.09	1.031	0.0027
6252-14-010	62	12.0	1.10	32	4.4	1.84	0.028	1.06	0.006	37	2.5	3.22	<0.001	9	48	5.2	1.97	0.005	1.76	57	0	7.09	1.041	0.0042
6252-14-020	55	10.7	1.08	35	4.9	1.83	0.014	1.06	0.006	36	2.7	3.21	<0.001	30	45	6.3	1.97	0.004	1.79	54	0	7.91	1.040	0.0048
6252-15-010	54	11.4	1.07	36	4.4	1.85	0.020	1.06	0.006	38	2.4	3.22	0.003	12	48	6.3	1.81	0.011	1.68	21	0	8.76	1.033	0.0032
6252-16-010	58	12.3	1.07	36	4.4	1.85	0.020	1.06	0.007	39	2.0	3.21	0.005	12	50	5.7	1.96	0.003	1.82	25	0	8.31	1.048	0.0048
6252-17-010	90	22.3	0.93	40	5.1	1.79	0.014	1.05	0.008	36	3.4	3.22	0.005	6	49	7.1	1.95	0.004	1.80	28	0	9.69	1.049	0.0043
6252-20-010	86	19.2	0.93	40	5.1	1.79	0.014	1.05	0.006	37	3.4	3.21	0.003	6	48	5.8	1.98	0.005	1.74	59	0.02	8.58	1.041	0.0046

(a) Calculated (after SiC coating deposited) by subtracting IPyC thickness from measured buffer and IPyC thickness.

(b) Measured by contact X-radiography on ≥200 particles.

(c) Measured at BISO stage.

(d) Measured with the Seibersdorf unit at GA using a 24-μm spot on 50 particles.

(e) Counted by a visual examination of gold spots in the SiC coatings, % of particles with flaws.

(f) The amount of mercury which penetrates the coatings from 250 to 10,000 psi.

(g) Measured using line-intercept technique on 100 particles on X-radiograph plates.
Equation used:

$$100X \frac{\sqrt{2}}{n} \sum_{i=1}^{n} \left(\frac{X_{1i} - X_{2i}}{X_{1i} + X_{2i}} \right)$$

where n = number of particles
X_1 = OPyC thickness on one side of particle
X_2 = OPyC thickness on other side of particle

(h) ND = not determined.

THIS PAGE

WAS INTENTIONALLY

LEFT BLANK

TABLE 3-11
PROPERTIES OF TOTAL COATED PARTICLES OF TRISO ThO_2 PARENT BATCHES FOR CAPSULE HT-34

Kernel Batch No.		Total Diam[a] (μm)		Particle Density (Mg/m^3)			Chemical Composition					Particle Defects						
					Liquid Gradient		Th Content (wt %)	C (wt %)	Si (wt %)	Impurities (ppm-wt)		Fraction Defective SiC Coating		Excessive Fuel Dispersion[a,e]	Fraction of Missing or Incomplete Coating[a,e]		Th Contamination[c] (kgTh/kgTh)	Fission Gas Release[f] (R/B)
Data Retrieval	Manufacturer	Mean	SD	Hg Porosimeter	Mean	SD				Fe	Be Equivalent[b]	Burn-Leach Test[c]	Burn-Visual Test[d]		Buffer and/or IPyC	OPyC		
6252-07-025	6780-13-0	822	28.0	3.32	3.34	0.139	43.41	35.89	13.39	72	1.8	2.9×10^{-4}	1.0×10^{-4}	0	0	0	1.1×10^{-5}	1.6×10^{-5}
6252-13-010	6252-12Q-02A	811	26.8	3.39	3.43	0.139	45.00	33.94	14.85	74	2.0	4.3×10^{-4}	9.7×10^{-4}	0	0	3.1×10^{-4}	4.9×10^{-5}	1.2×10^{-5}
6252-14-010	6252-12Q-07A	808	28.9	3.37	3.42	0.163	46.20	35.25	13.20	60	2.0	2.4×10^{-3}	4.1×10^{-3}	0	3.0×10^{-4}	0	8.3×10^{-5}	4.2×10^{-5}
6252-14-020	6780-141-02B	791	25.6	3.49	3.54	0.147	47.60	33.50	12.75	71	1.7	1.1×10^{-3}	1.5×10^{-3}	0	1.3×10^{-3}	0	6.1×10^{-4}	3.9×10^{-5}
6252-15-010	6252-12Q-08A	807	30.5	3.36	3.39	0.113	45.85	34.73	13.58	54	2.1	1.9×10^{-4}	2.7×10^{-4}	0	0	0	4.9×10^{-6}	4.0×10^{-6}
6252-16-010	6252-12Q-08B	816	29.2	3.37	3.39	0.160	44.78	36.37	13.42	60	2.0	8.9×10^{-5}	3.7×10^{-4}	0	0	0	9.8×10^{-6}	2.5×10^{-6}
6252-17-010	6780-147-03B	882	51.6	2.98	3.03	0.193	41.65	39.00	14.16	140	2.3	1.3×10^{-3}	1.2×10^{-3}	0	3.3×10^{-4}	0	2.1×10^{-5}	2.1×10^{-5}
6252-20-010	6780-147-03A	874	44.1	2.98	3.09	0.157	41.79	39.65	13.55	87	2.3	2.9×10^{-3}	2.3×10^{-3}	0	1.3×10^{-3}	0	2.5×10^{-4}	7.3×10^{-5}

[a] Measured by contact X-radiography.

[b] The following elements were measured by spectrographic analysis: Al, Be, Cd, Fe, Mo, P, Sn, V, B, Bi, Cr, Mg, Na, Pb, Sr, Zn, Ba, Ca, Mn, Ni, Si, Tl.

[c] 25 g samples leached for 24 hr in ultraleach.

[d] ≥10 g sample examined.

[e] Measured on ≥3000 particles.

[f] Release rate/birth rate for Kr-85 m at 1100°C for ∿20 g samples.

THIS PAGE

WAS INTENTIONALLY

LEFT BLANK

TABLE 3-12
MEASURED PROPERTIES OF PARTICLE SAMPLES FOR CAPSULE HT-34

Sample Batch No.	Kernel Diam[a] (μm)		Buffer Coating Calculated Thickness[a,b] (μm)		Buffer Coating Rate (μm/min)	IPyC Coating Calculated Thickness[a,c] (μm)		IPyC Coating Rate (μm/min)	SiC Coating Thickness[a] (μm)		SiC Coating Rate (μm/min)	OPyC Coating Thickness[a] (μm)		OPyC Coating Rate (μm/min)	OPyC BAF_o[d]		Total Particle Diam[a] (μm)		Total Particle Density[e] (Mg/m^3)		Radiograph Plate No.
	Mean	SD	Mean	SD		Mean	SD		Mean	SD		Mean	SD		Mean	SD	Mean	SD	Mean	SD	
6252-07-0262-001	449	4.8	60	7.1	9.68	39	4.8	4.4	38	2.5	0.17	45	5.7	5.0	ND[f]	ND	816	15.3	3.35	0.002	LB720
6252-07-0262-002	449	4.8	57	8.0	9.19	39	4.8	4.4	37	3.1	0.16	41	6.1	4.6	ND	ND	808	19.2	3.35	0.002	LB719
6252-13-0161-001	447	7.4	57	6.4	9.50	32	4.1	4.1	43	2.3	0.33	48	6.0	8.3	1.031	0.0025	808	18.8	3.39	0.017	LB734
6252-13-0171-001	443	7.7	79	9.1	13.17	32	4.1	4.1	43	2.5	0.33	49	5.2	8.5	1.031	0.0025	848	20.3	3.13	0.021	LB728
6252-14-0161-001	448	7.6	63	7.0	9.69	32	4.4	4.0	37	2.6	0.31	44	4.8	7.6	1.047	0.0046	798	17.2	3.42	0.039	LB727
6252-14-0161-002	447	6.8	62	7.3	9.54	32	4.4	4.0	37	2.3	0.31	44	4.6	7.6	1.047	0.0046	796	19.0	3.42	0.039	LB726
6252-14-0171-001	451	10.0	35	5.9	5.38	32	4.4	4.0	35	2.5	0.29	41	4.2	7.1	1.047	0.0046	736	19.0	3.93	0.041	LB730
6252-14-0181-001	445	7.1	91	9.0	14.00	32	4.4	4.0	37	2.6	0.31	47	5.6	8.1	1.047	0.0046	854	20.8	3.06	0.026	LB729
6252-14-0261-001	455	7.1	27	6.0	4.35	35	4.9	4.7	35	3.0	0.27	40	4.9	7.1	ND	ND	729	17.5	3.96	0.011	LB736
6252-14-0271-001	443	8.7	86	9.0	13.87	35	4.9	4.7	38	3.2	0.29	45	5.7	8.0	ND	ND	849	24.4	3.11	0.062	LB732
6252-15-0161-001	450	7.2	56	6.9	9.33	36	4.4	4.2	38	2.1	0.32	45	5.1	5.0	1.035	0.0036	798	13.9	3.38	0.022	LB725
6252-15-0171-001	448	7.9	84	7.7	14.00	36	4.4	4.2	39	2.6	0.33	50	5.5	5.6	1.035	0.0036	865	21.0	3.07	0.020	LB731
6252-16-0161-001	451	6.8	57	6.5	9.50	36	4.4	4.2	39	2.0	0.33	48	5.8	5.3	1.052	0.0056	813	17.2	3.41	0.011	LB724
6252-17-0161-001	451	7.0	80	9.2	11.43	40	5.1	4.2	37	4.8	0.24	45	6.2	5.0	ND	ND	858	23.1	3.11	0.017	LB721
6252-20-0161-001	450	7.3	83	8.5	11.86	40	5.1	4.2	36	3.7	0.23	47	5.6	8.4	ND	ND	862	22.1	3.06	0.030	LB723
6252-20-0161-002	452	7.0	82	8.1	11.71	40	5.1	4.2	35	3.7	0.23	45	5.4	8.0	ND	ND	854	23.3	3.06	0.030	LB722

(a) Measured by contact X-radiography of ≥200 particles.

(b) Calculated (after SiC coating deposited) by subtracting the IPyC thickness from measured buffer and IPyC thickness.

(c) Measured at BISO stage on parent batch.

(d) Measured with Seibersdorf unit at GA using 24-μm-spot on 50 companion particles.

(e) Measured by a liquid gradient technique on companion sample.

(f) ND = Not determined.

THIS PAGE

WAS INTENTIONALLY

LEFT BLANK

TABLE 3-13
SUMMARY OF TRISO ThO_2 PARTICLE SAMPLES FOR CAPSULE HT-34

		Coatings														Total Coated Particle			
		Buffer		IPyC		SiC			OPyC										
Sample Batch No.	Kernel Diam[a] (μm)	Thickness[a,b] (μm)	Density[c] (Mg/m^3)	Thickness[c,d] (μm)	Liquid Gradient Density[c] (Mg/m^3)	Thickness[a] (μm)	Density[c] (Mg/m^3)	Flaw Content[c] (%)	Thickness[a] (μm)	Density[c] (Mg/m^3) Liquid Gradient	Density[c] (Mg/m^3) Bulk	BAF_o[c]	Accessible Porosity[c] (ml/kg)	Coating Rate[a] (μm/min)	Coating Diluent Gas[c]	Diam[a] (μm)	Defective SiC Coating[c,e]	Thorium Contamination[c,f] (kgTh/kgTh)	Fission Gas Release[c,g] (R/B)
6252-07-0262-001	449	60	1.12	39	1.93	38	3.21	38	45	1.80	1.65	1.027	48	5.0	Ar	816	1.0×10^{-4}	1.1×10^{-5}	1.6×10^{-5}
6252-07-0262-002	449	57	1.12	39	1.93	37	3.21	38	41	1.80	1.65	1.027	48	4.6	Ar	808	1.0×10^{-4}	1.1×10^{-5}	1.6×10^{-5}
6252-13-0161-001	447	57	1.13	32	1.86	43	3.22	16	48	1.79	1.61	1.031	57	8.3	H_2	808	9.7×10^{-4}	4.9×10^{-5}	1.2×10^{-5}
6252-13-0171-001	443	79	1.13	32	1.86	43	3.22	16	49	1.79	1.61	1.031	57	8.5	H_2	848	9.7×10^{-4}	4.9×10^{-5}	1.2×10^{-5}
6252-14-0161-001	448	63	1.10	32	1.84	37	3.22	9	44	1.97	1.76	1.041	57	7.6	H_2	798	4.1×10^{-3}	8.3×10^{-5}	4.2×10^{-5}
6252-14-0161-002	447	62	1.10	32	1.84	37	3.22	9	44	1.97	1.76	1.041	57	7.6	H_2	796	4.1×10^{-3}	8.3×10^{-5}	4.2×10^{-5}
6252-14-0171-001	451	35	1.10	32	1.84	35	3.22	9	41	1.97	1.76	1.041	57	7.1	H_2	736	4.1×10^{-3}	8.3×10^{-5}	4.2×10^{-5}
6252-14-0181-001	445	91	1.10	32	1.84	37	3.22	9	47	1.97	1.76	1.041	57	8.1	H_2	854	4.1×10^{-3}	8.3×10^{-5}	4.2×10^{-5}
6252-14-0261-001	455	27	1.08	35	1.83	35	3.21	29	40	1.97	1.79	1.040	54	7.1	H_2	729	1.5×10^{-3}	6.1×10^{-4}	3.9×10^{-5}
6252-14-0271-001	443	86	1.08	35	1.83	38	3.21	29	45	1.97	1.79	1.040	54	8.0	H_2	849	1.5×10^{-3}	6.1×10^{-4}	3.9×10^{-5}
6252-15-0161-001	450	56	1.07	36	1.85	38	3.22	12	45	1.81	1.68	1.033	21	5.0	H_2	798	2.7×10^{-4}	4.9×10^{-6}	4.0×10^{-6}
6252-15-0171-001	448	84	1.07	36	1.85	39	3.22	12	50	1.81	1.68	1.033	21	5.6	H_2	865	2.7×10^{-4}	4.9×10^{-6}	4.0×10^{-6}
6252-16-0161-001	451	57	1.07	36	1.85	39	3.21	12	48	1.96	1.82	1.048	25	5.3	H_2	813	3.7×10^{-4}	9.8×10^{-6}	2.5×10^{-6}
6252-17-0161-001	451	80	0.93	40	1.79	37	3.22	6	45	1.95	1.80	1.049	28	5.0	H_2	858	1.2×10^{-3}	2.1×10^{-5}	2.1×10^{-5}
6252-20-0161-001	450	83	0.93	40	1.79	36	3.21	6	47	1.98	1.74	1.041	59	8.4	H_2	862	2.3×10^{-3}	2.5×10^{-4}	7.3×10^{-5}
6252-20-0161-002	452	82	0.93	40	1.79	35	3.21	6	45	1.98	1.74	1.041	59	8.0	H_2	854	2.3×10^{-3}	2.5×10^{-4}	7.3×10^{-5}

[a] Measured or calculated on capsule sample.
[b] Calculated (after SiC coating deposited) by subtracting the IPyC thickness from measured buffer and IPyC thickness.
[c] Measured or calculated on parent batch.
[d] Measured at BISO stage.
[e] Measured by burn-visual examination technique.
[f] Leached for 24 hr in ultraleach.
[g] Release rate/birth rate for Kr-85m at 1100°C.

THIS PAGE

WAS INTENTIONALLY

LEFT BLANK

TABLE 3-14
COMPARISON OF HT-34 PARENT BATCHES WITH CAPSULE SPECIMENS

Sample Batch No.	Density Fraction	Kernel Diam (μm) Mean	Kernel Diam (μm) σ	Buffer Thickness (μm) Mean	Buffer Thickness (μm) σ	IPyC Thickness (μm) Mean	SiC Thickness (μm) Mean	SiC Thickness (μm) σ	OPyC Thickness (μm) Mean	OPyC Thickness (μm) σ	Total Particle Diam (μm) Mean	Total Particle Diam (μm) σ	Radiograph Plate No.	No. Particles	Liquid Gradient Density (Mg/m^3)	BAF_o (μm) Mean	BAF_o (μm) σ
6252-07-0200(a)	--	452.60	8.32	62.93	11.35	39	37.69	3.27	47.50	6.19	821.80	28.02	--	--	3.340	1.027	0.0030
6252-07-0262-001	Nominal	448.55	4.80	59.93	7.13	39	38.36	2.54	45.28	5.73	815.62	15.31	LB720	57	3.340	ND	ND
6252-07-0262-002	Nominal	448.53	4.83	56.50	8.02	39	37.21	3.06	41.42	6.11	807.97	19.23	LB719	81	3.340	ND	ND
6252-13-0100(a)	--	453.53	8.33	55.03	9.67	32	42.46	2.33	49.92	4.87	810.86	26.76	--	--	3.430	1.031	0.0027
6252-13-0161-001	Nominal	447.20	7.43	56.87	6.41	32	43.45	2.26	48.25	6.04	808.45	18.85	LB734	57	3.391	1.031	0.0025
6252-13-0171-001	Low	442.71	7.72	79.01	9.06	32	42.78	2.50	49.12	5.18	848.37	20.29	LB728	85	3.126	1.031	0.0025
6252-14-0100(a)	--	451.23	9.12	62.75	12.04	32	37.35	2.48	47.60	5.17	808.01	28.93	--	--	3.420	1.041	0.0042
6252-14-0161-002	Nominal	447.73	7.59	62.66	7.04	32	37.00	2.61	44.39	4.84	797.66	17.23	LB727	57	3.421	1.047	0.0046
6252-14-0161-002	Nominal	447.68	6.82	62.22	7.27	32	36.64	2.34	44.49	4.60	796.18	18.99	LB726	81	3.421	1.047	0.0046
6252-14-0171-001	High	451.30	9.98	34.95	5.87	32	35.21	2.51	40.57	4.21	735.63	18.79	LB730	56	3.929	1.047	0.0046
6252-14-0181-001	Low	444.63	7.08	91.02	8.97	32	36.78	2.59	46.62	5.60	854.44	20.77	LB729	82	3.057	1.047	0.0046
6252-14-0200(a)	--	450.60	8.07	54.63	10.66	35	35.70	2.73	43.25	5.71	791.30	25.63	--	--	3.540	1.040	0.0048
6252-14-0261-001	High	454.59	7.106	27.32	6.02	35	34.77	2.95	39.63	4.86	728.86	17.48	LB736	56	3.958	ND	ND
6252-14-0271-001	Low	442.38	8.71	86.32	8.99	35	38.42	3.24	45.13	5.69	848.58	24.44	LB732	83	3.107	ND	ND
6252-15-0100(a)	--	455.33	8.43	54.04	11.37	36	38.08	2.35	48.00	6.29	807.28	30.47	--	--	3.394	1.033	0.0032
6252-15-0161-001	Nominal	449.74	7.23	55.83	6.87	36	37.77	2.06	45.21	5.13	797.93	13.91	LB725	56	3.380	1.035	0.0036
6252-15-0171-001	Low	448.90	7.94	84.49	7.72	36	39.09	2.58	49.95	5.45	864.82	21.04	LB731	81	3.070	1.035	0.0036
6252-16-0100(a)	--	454.52	8.43	57.84	12.29	36	38.69	2.04	49.97	5.65	815.70	29.18	--	--	3.392	1.048	0.0048
6252-16-0161-001	Nominal	450.84	6.77	57.49	6.48	36	38.51	2.02	47.84	5.81	813.26	17.19	LB724	56	3.413	1.052	0.0056
6252-17-0100(a)	--	454.50	8.93	89.71	22.32	40	36.27	3.35	43.60	7.06	882.10	51.61	--	--	3.030	1.049	0.0043
6252-17-0161-001	Nominal	451.24	7.02	79.61	9.22	40	36.92	4.77	44.53	6.19	858.43	23.11	LB721	81	3.109	ND	ND
6252-20-0100(a)	--	455.85	8.63	85.77	15.17	40	36.60	3.37	48.36	5.76	873.60	44.05	--	--	3.090	1.041	0.0046
6252-20-0161-001	Nominal	449.77	7.27	82.97	8.49	40	36.02	3.68	47.34	5.59	862.12	22.13	LB723	56	3.057	ND	ND
6252-20-0161-002	Nominal	451.55	6.98	82.32	8.13	40	35.24	3.69	45.04	5.36	854.23	23.26	LB722	80	3.057	ND	ND

(a) Parent batch.

Note: σ = standard deviation
ND = not determined

Blank

4. CAPSULE PARAMETERS

4.1. OPERATING HISTORY

Capsule HT-34 was inserted into the C-6 target position of the HFIR reactor on July 25 and removed on November 23, 1977. The capsule was irradiated for five cycles for a total of 2686 hs at 100-MW power. The operating history (Ref. 14) of the capsule is given in Table 4-1.

4.2. FLUENCE AND BURNUP ANALYSIS

The fast-fluence data for capsule HT-34 are reported in Table 4-2; they were calculated by ORNL (Ref. 14). The fluence ranged from 5.1 to 8.2 x 10^{29} n/m^2 $(E > 29\ fJ)_{HTGR}$ for the low-temperature magazine and 9.2 to 10.2 x 10^{25} n/m^2 $(E > 29\ fJ)_{HTGR}$ for the high-temperature magazine.

The burnups of the irradiated ThO_2 samples were calculated by ORNL (Ref. 14) and GA (Ref. 15), and the values are reported in Table 4-2. The GA calculations were based on reaction rates determined from the analytical burnup measurements of capsule samples HT-31 and HT-33. The details of this analysis are given in Ref. 16. The GA values were 8% to 12% lower than the ORNL values for the 1200°C samples and 2% lower to 4% higher for the 1450°C samples. This is good agreement, considering the numerous uncertainties associated with burnup calculations. The GA values will be reported in the following sections of this document.

4.3. THERMAL ANALYSIS

Actual temperatures were not monitored during the irradiation. ORNL performed a detailed thermal analysis (Ref. 17) using the thermal modeling code HTCAP 1, which is a modified version of HTCAP (Ref. 18). This code

calculates total heat generation within the capsule, performs a modified, one-dimensional heat transfer analysis, then predicts the maximum particle surface operating temperature at one-day intervals during each irradiation cycle.

The results of the thermal analysis (Ref. 19) are plotted in Fig. 4-1, which shows the graphite annulus temperature, particle surface temperature, and power per particle. Tables 4-3 and 4-4 present the time-averaged particle surface temperature and power/particle/cycle for each sample, respectively. The results showed that the temperatures increased with time and that the highest maximum surface temperature for the last cycle was 1340°C for the low-temperature magazine and 1530°C for the other magazine. The time-averaged maximum surface temperatures were 1180° to 1250°C and 1430°C to 1450°C for the two magazines. The power/particle for the last cycle averaged 0.29 to 0.42 watts for the low-temperature magazine and 0.48 to 0.51 watts for the high-temperature magazine.

Based on the thermal analysis data supplied by ORNL, the time-volume averaged temperature of the kernel was calculated (Ref. 20) for each cycle and is summarized in Table 4-5. Particle dimensions and conductivities, surface temperature, and power generation for each sample were input into the calculations. The analysis was modeled after a general study made on the temperature distribution inside a TRISO particle (Ref. 21). For the HT-34 calculations, no gaps were assumed between coatings, which could mean the actual kernel temperatures were higher. The kernel temperatures were 30° to 50°C higher than the surface temperatures for the low-temperature samples and 50° to 70°C higher for the high-temperature samples. The average kernel temperature for the two magazines reached 1410° and 1620°C during the last cycle.

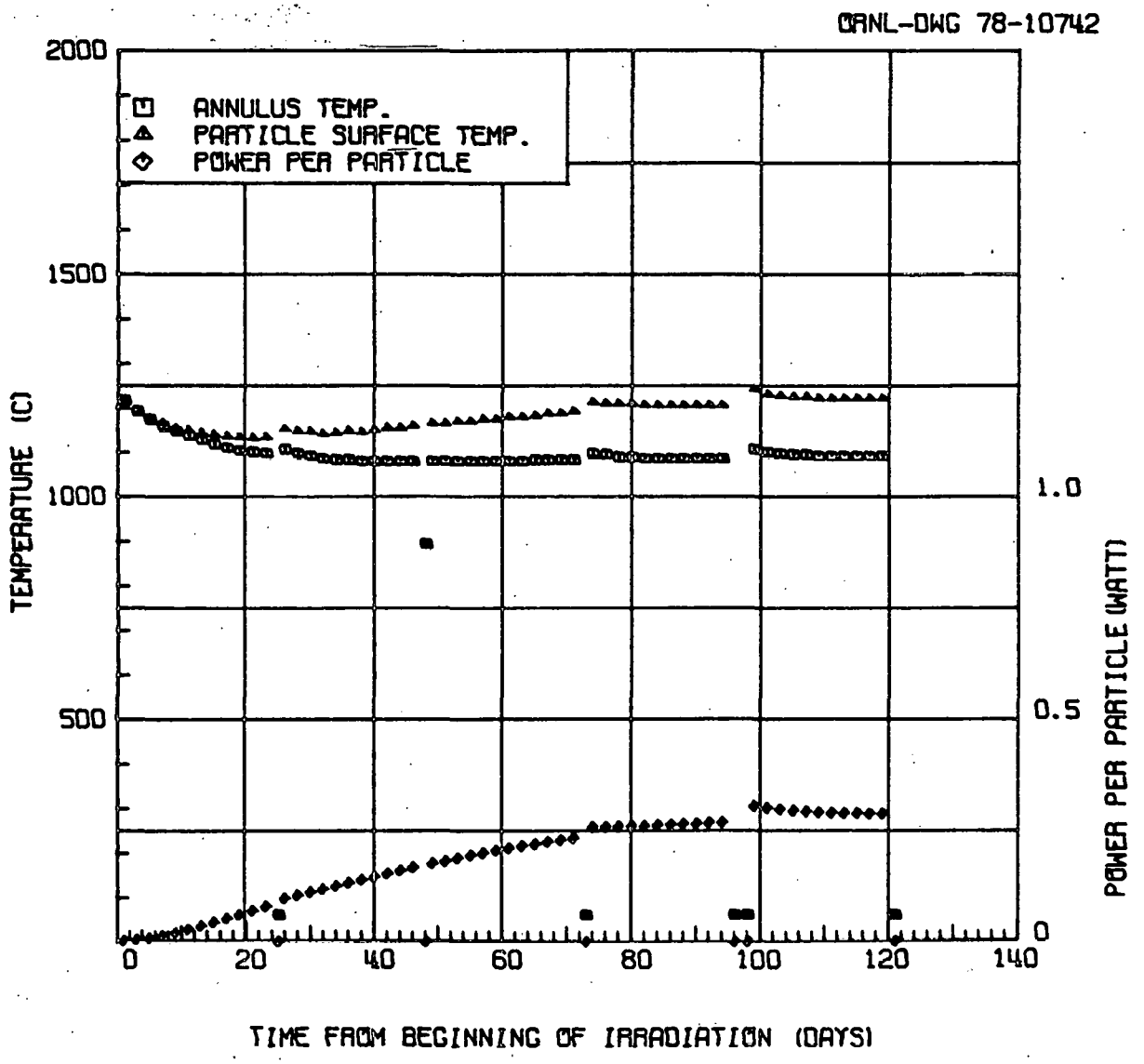

Fig. 4-1. Results of ORNL thermal analysis (sheet 1 of 16)

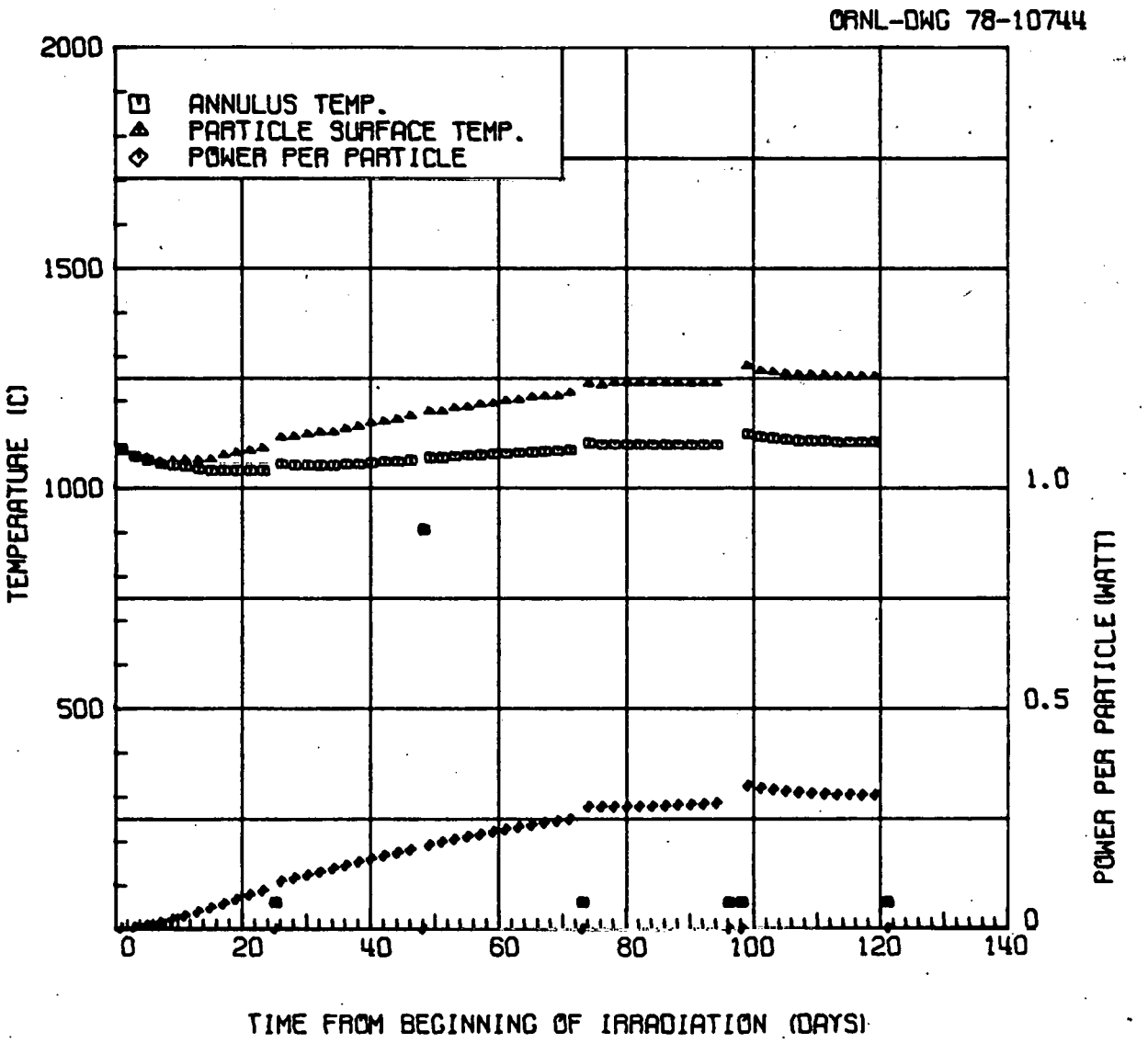

Fig. 4-1. Results of ORNL thermal analysis (sheet 2 of 16)

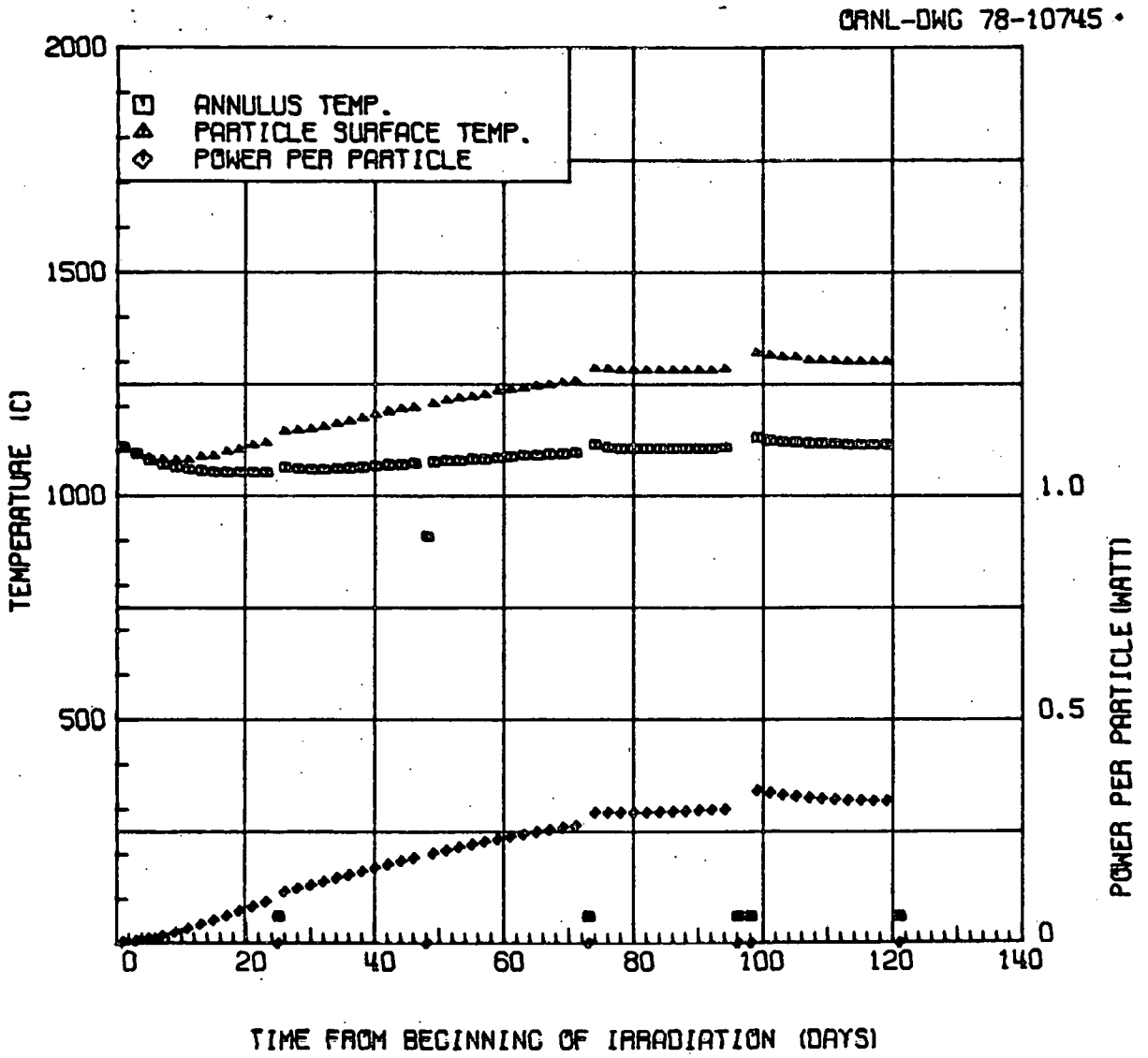

Fig. 4-1. Results of ORNL thermal analysis (sheet 3 of 16)

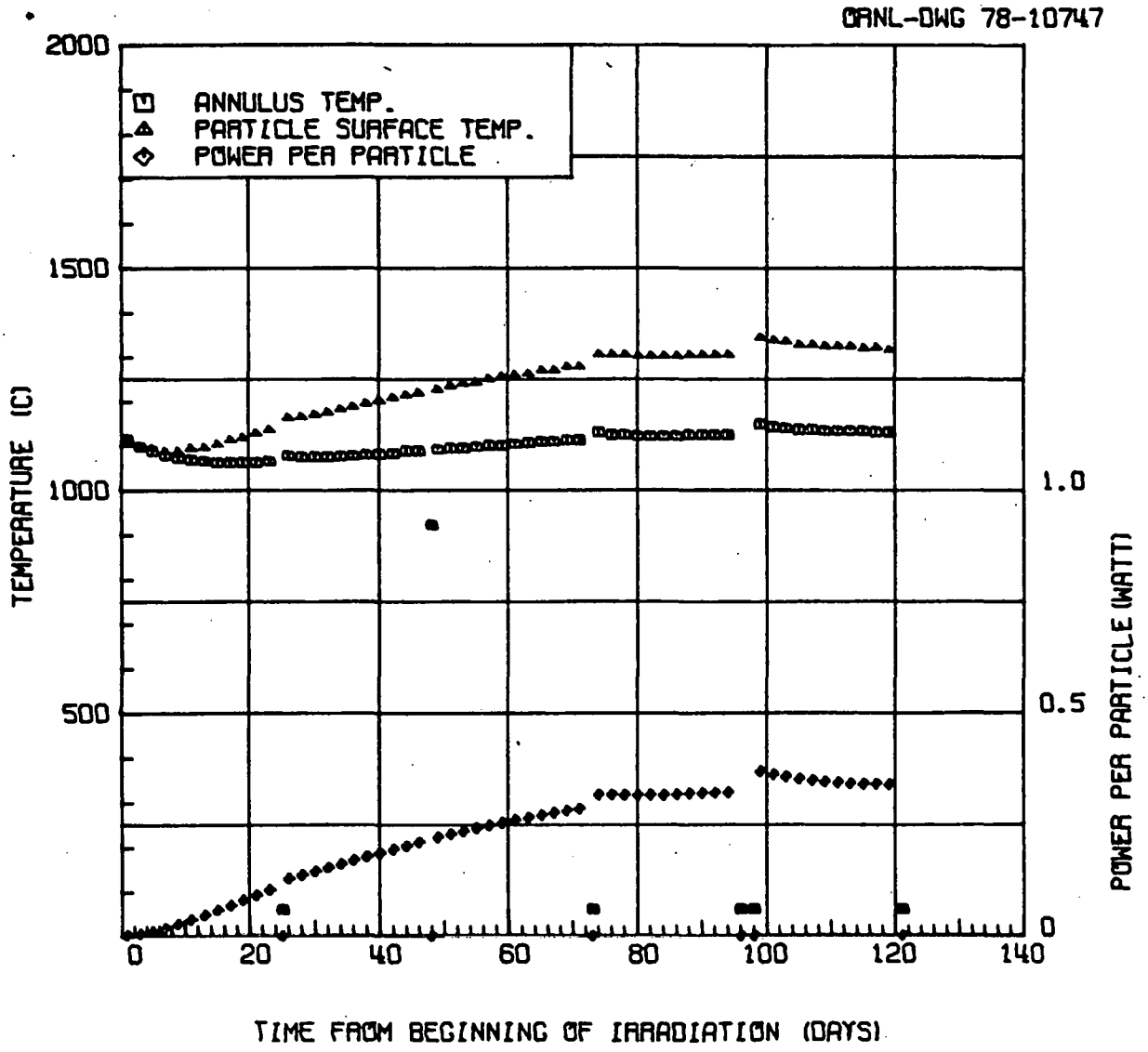

Fig. 4-1. Results of ORNL thermal analysis (sheet 4 of 16)

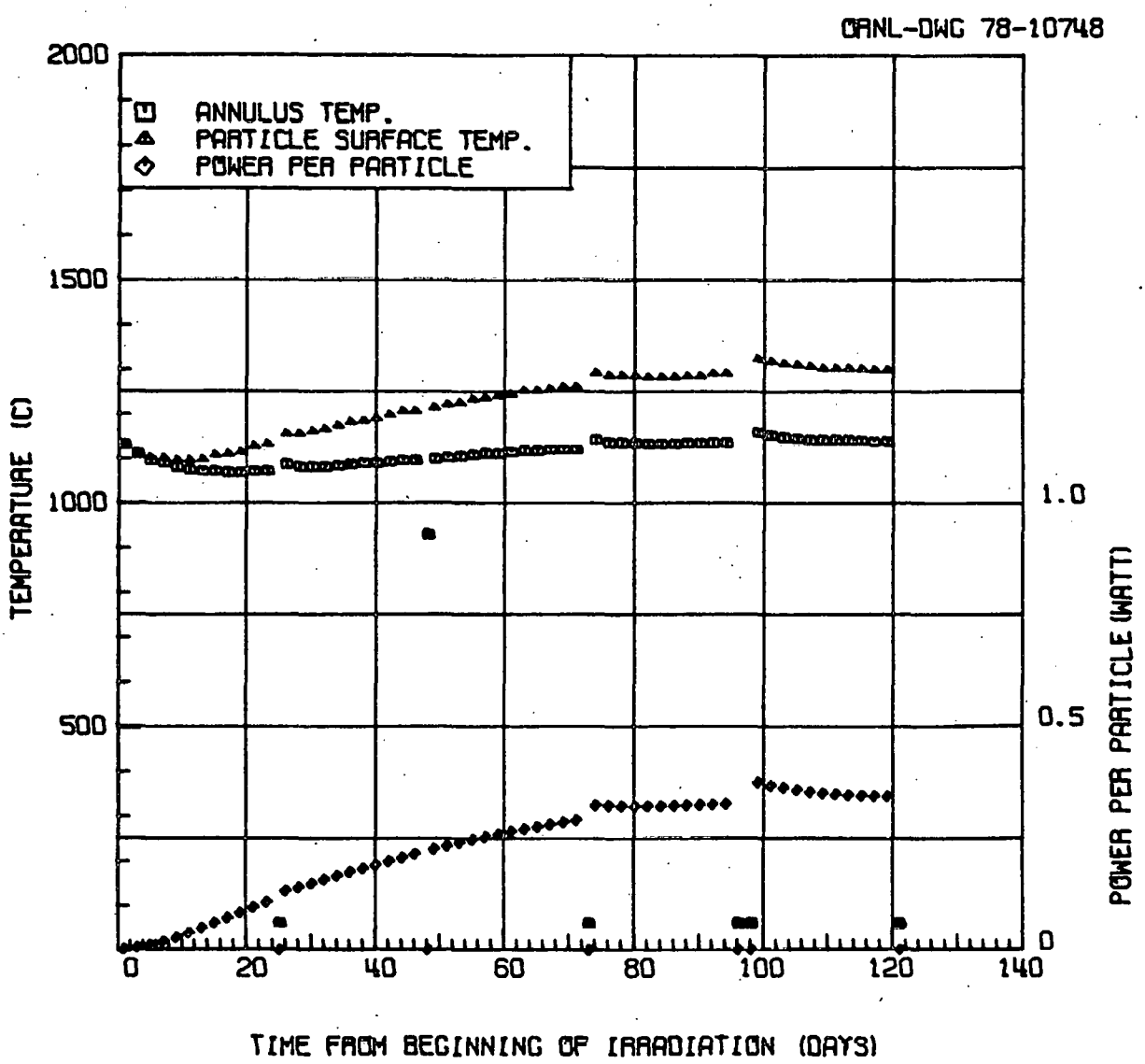

Fig. 4-1. Results of ORNL thermal analysis (sheet 5 of 16)

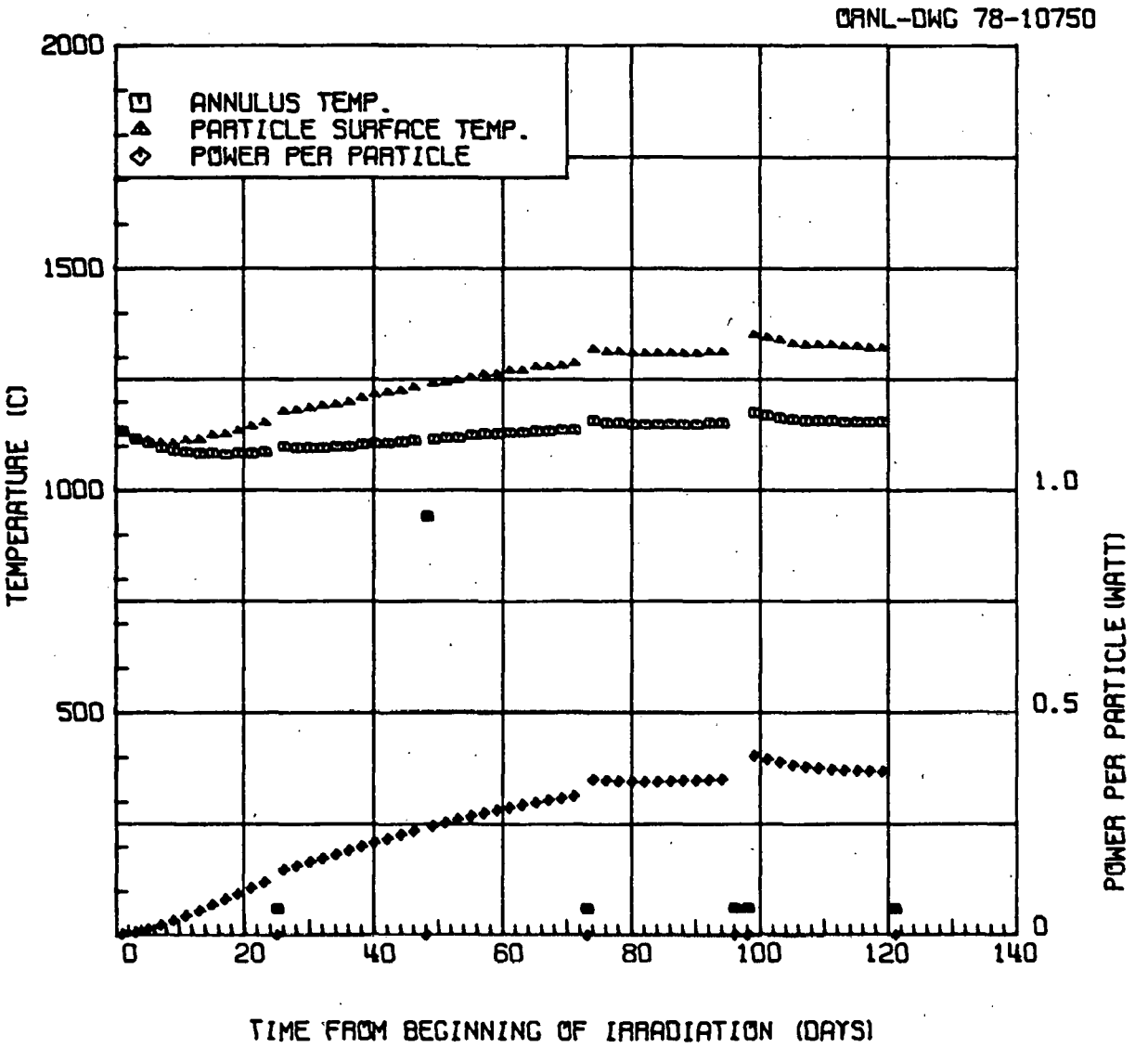

HT-34 PARTICLE HOLDER 10 BATCH 14-0161-001
800.0 MICRON PARTICLE DIAMETER

Fig. 4-1. Results of ORNL thermal analysis (sheet 6 of 16)

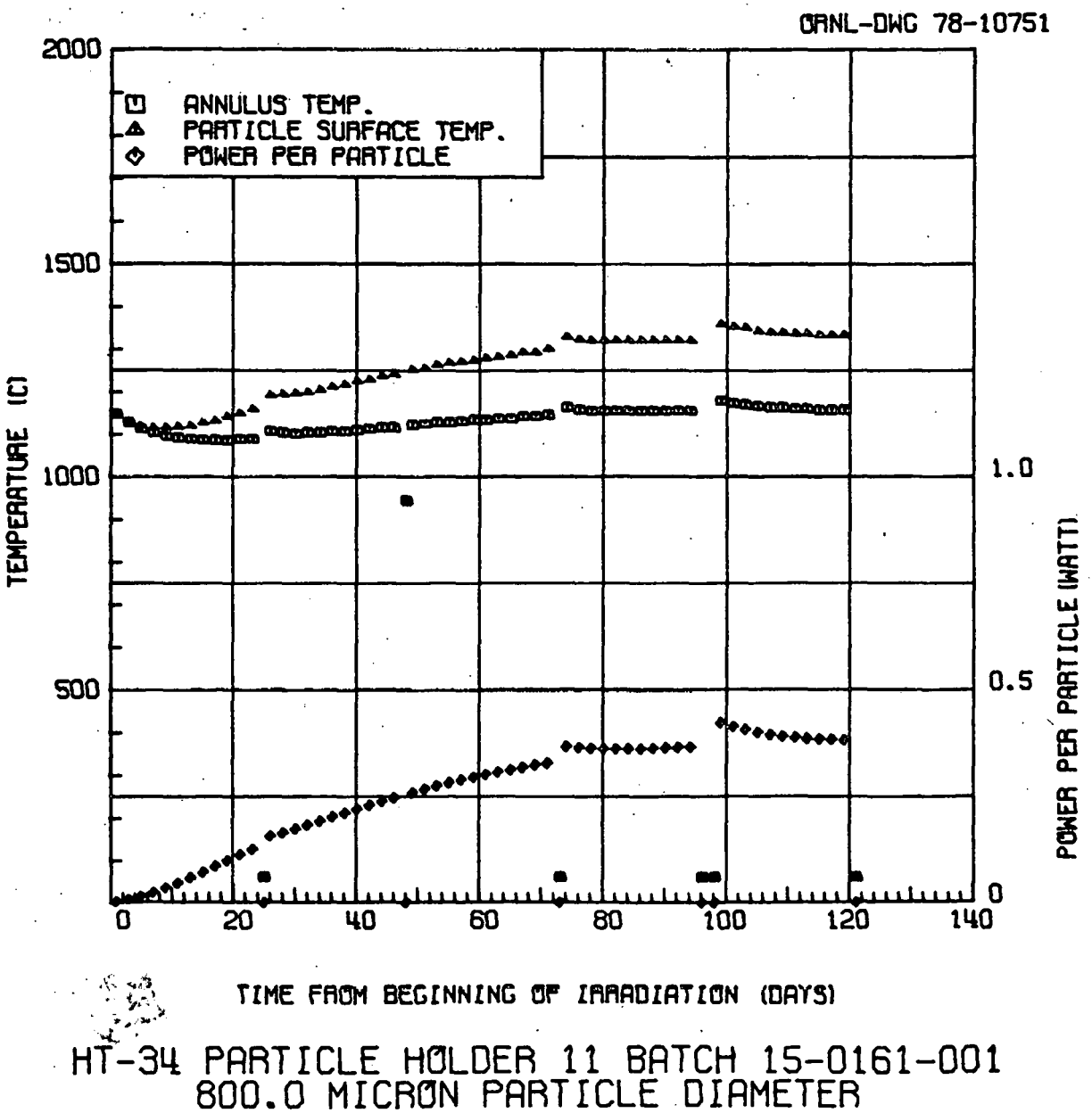

Fig. 4-1. Results of ORNL thermal analysis (sheet 7 of 16)

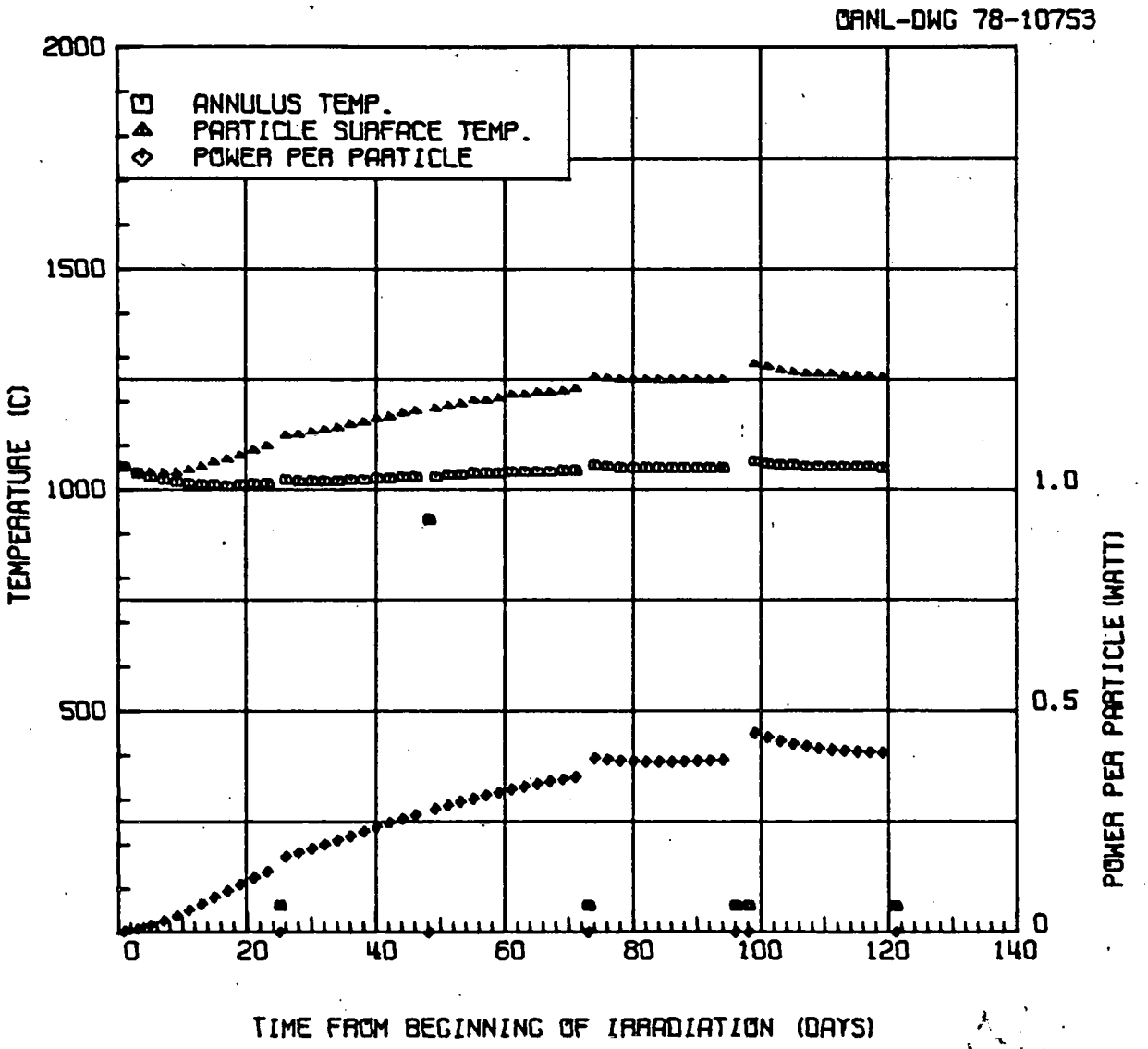

Fig. 4-1. Results of ORNL thermal analysis (sheet 8 of 16)

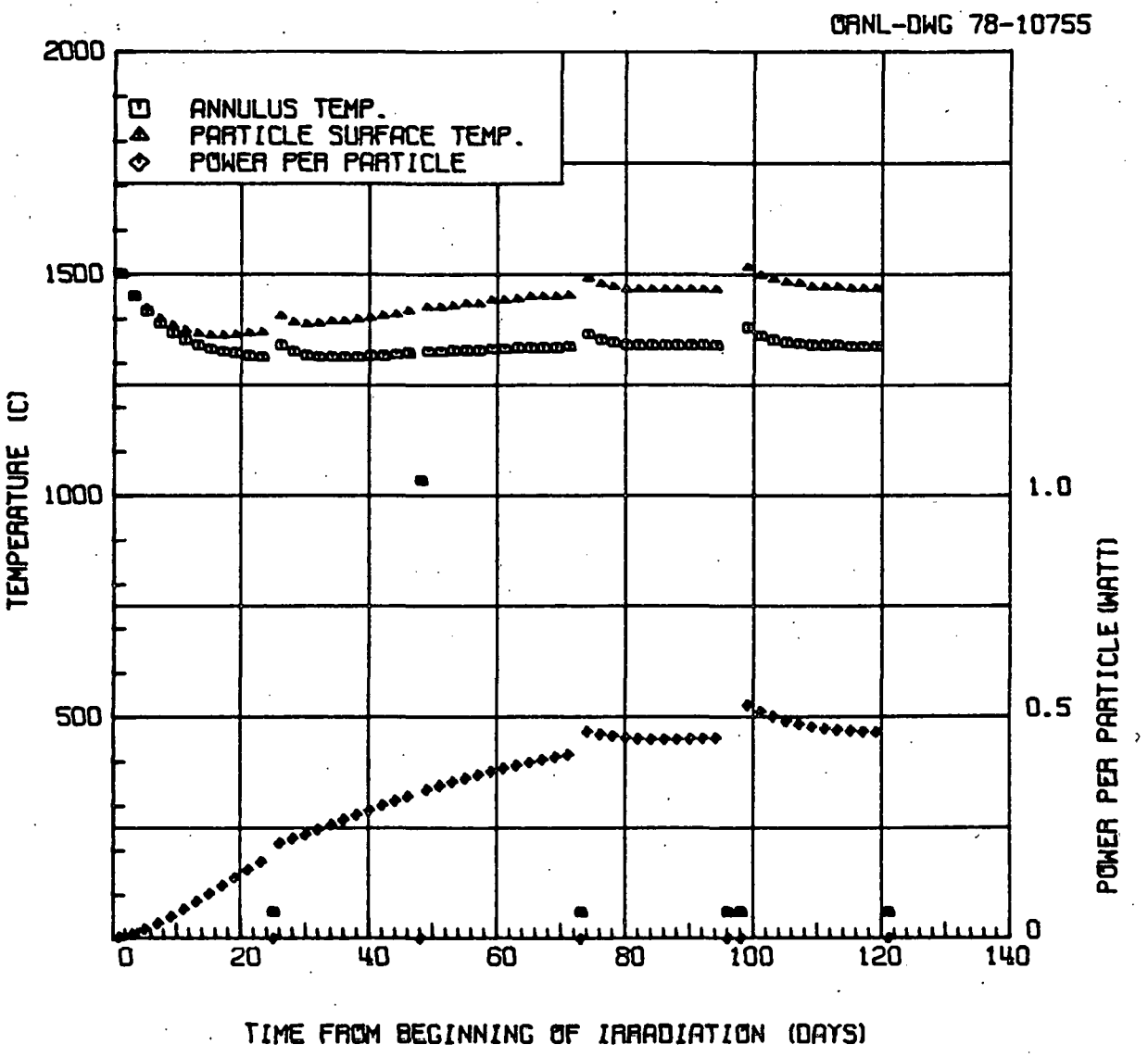

Fig. 4-1. Results of ORNL thermal analysis (sheet 9 of 16)

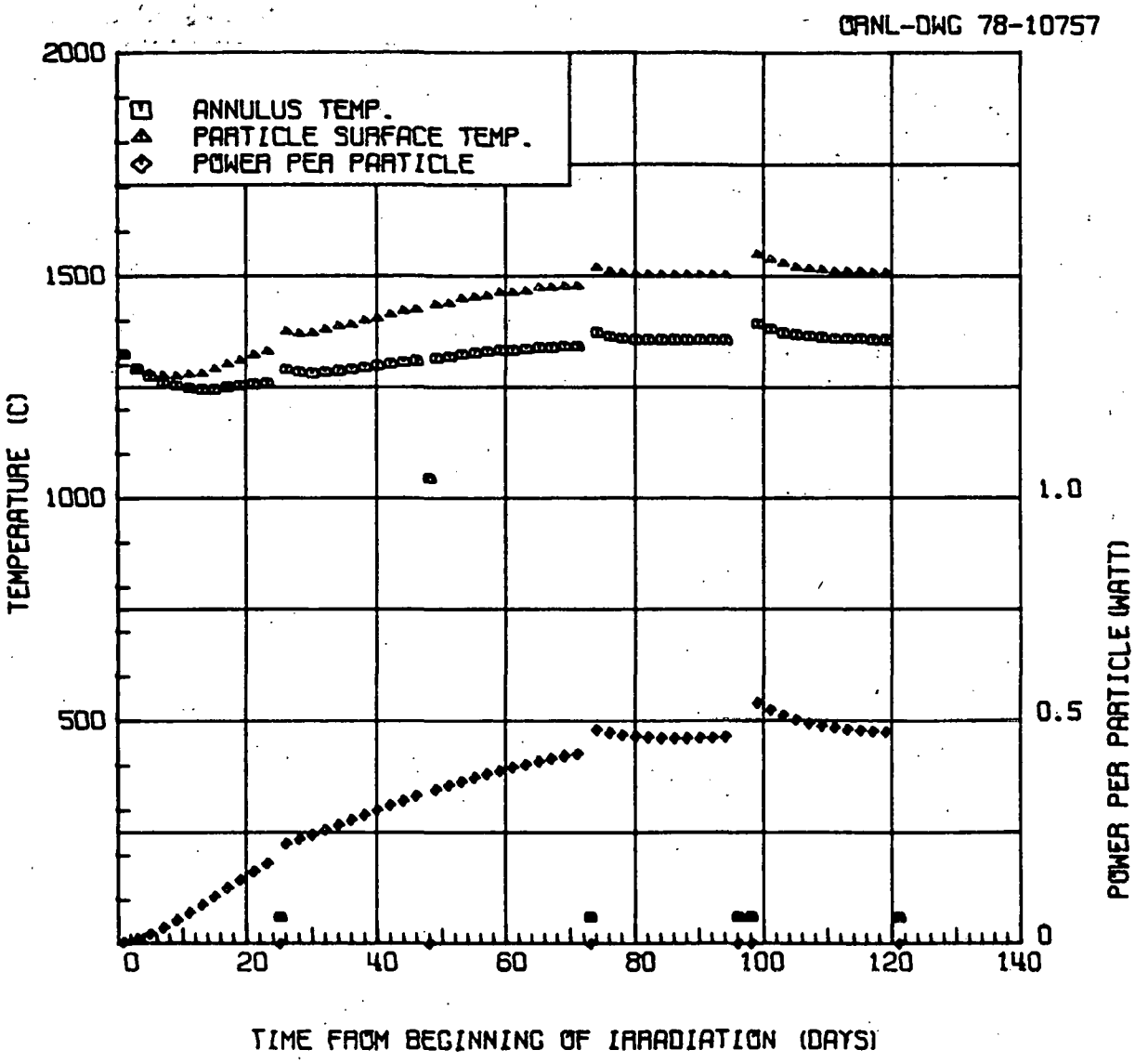

Fig. 4-1. Results of ORNL thermal analysis (sheet 10 of 16)

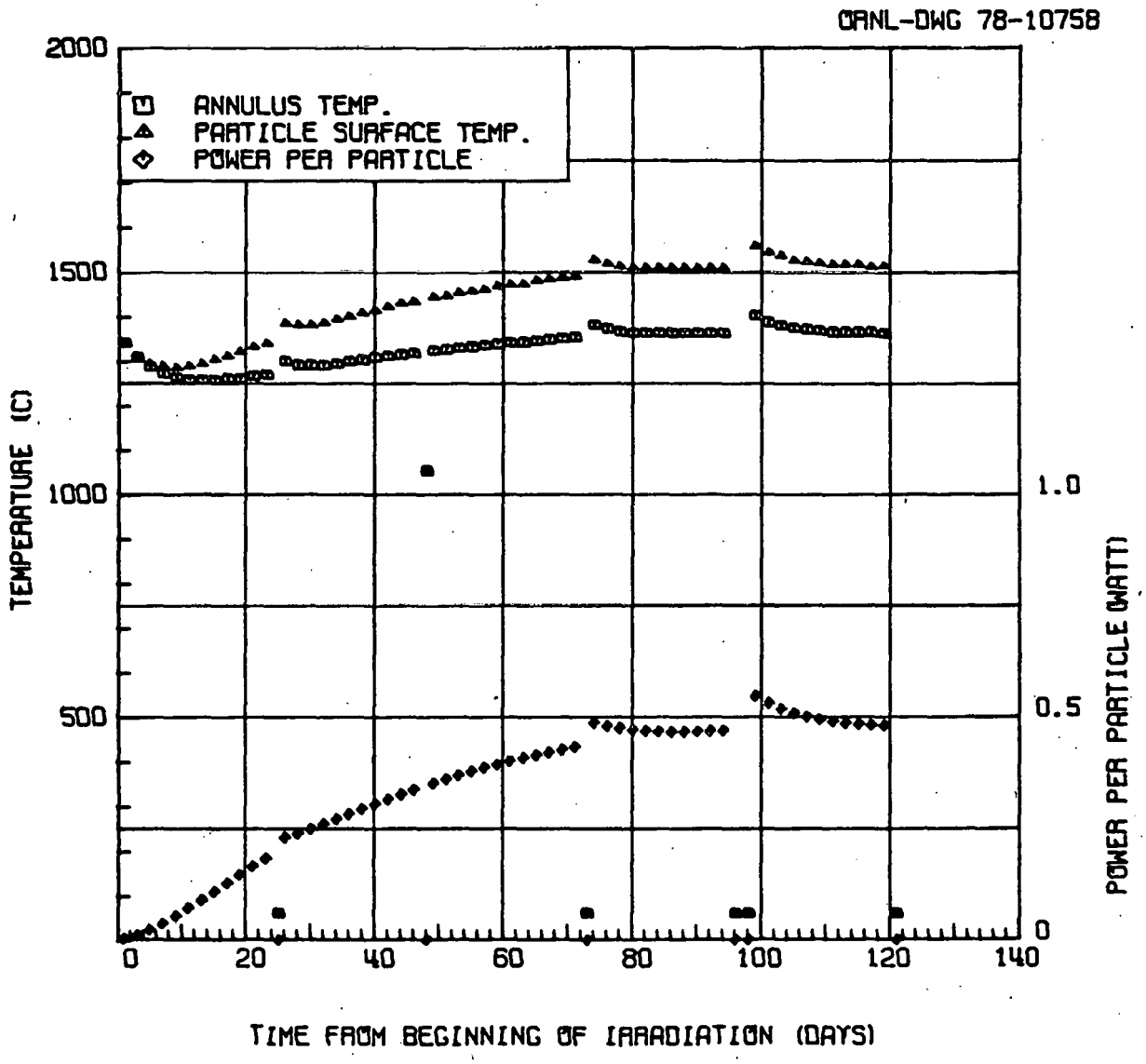

HT-34 PARTICLE HOLDER 18 BATCH 14-0161-002
798.0 MICRON PARTICLE DIAMETER

Fig. 4-1. Results of ORNL thermal analysis (sheet 11 of 16)

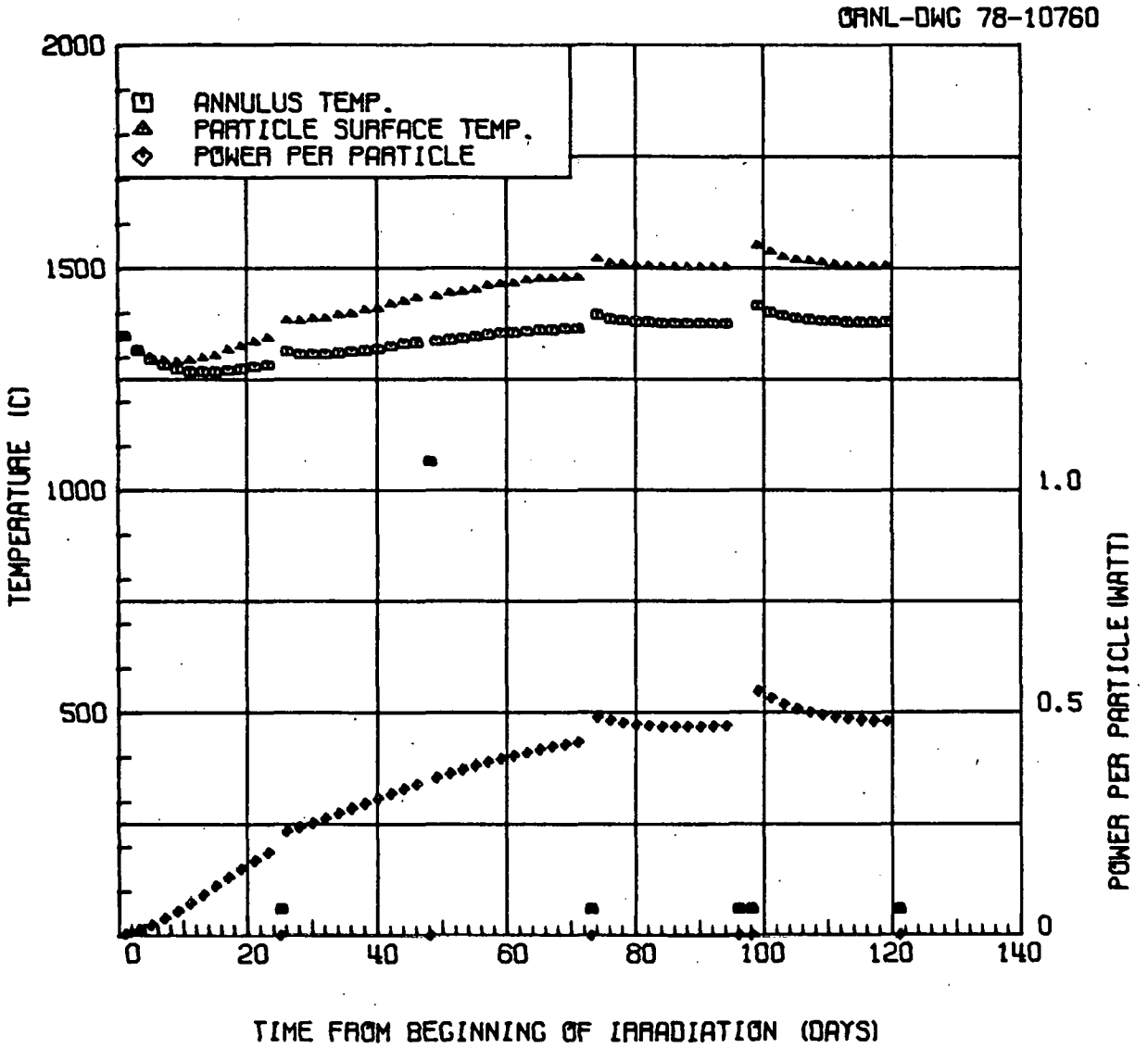

Fig. 4-1. Results of ORNL thermal analysis (sheet 12 of 16)

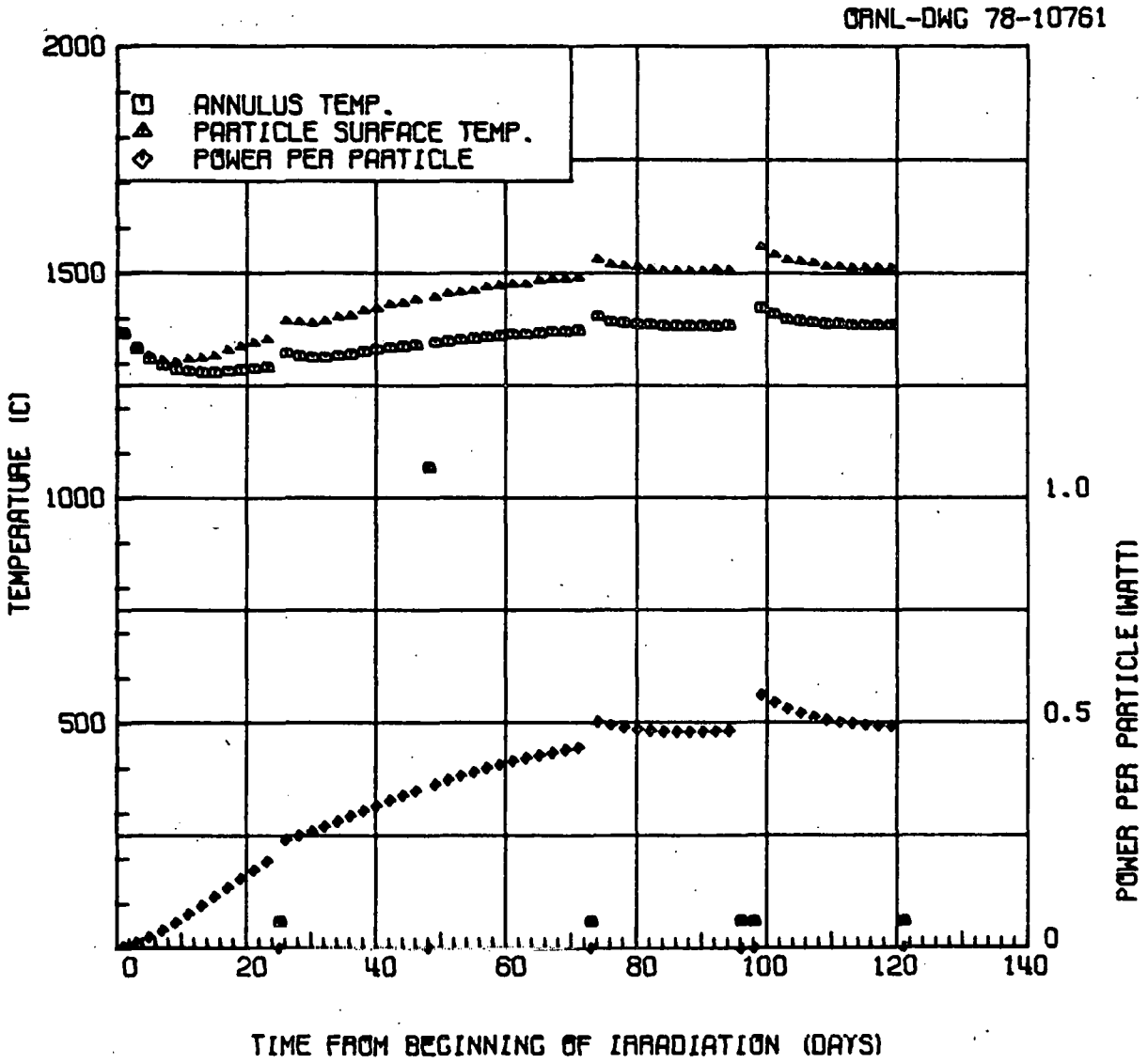

Fig. 4-1. Results of ORNL thermal analysis (sheet 13 of 16)

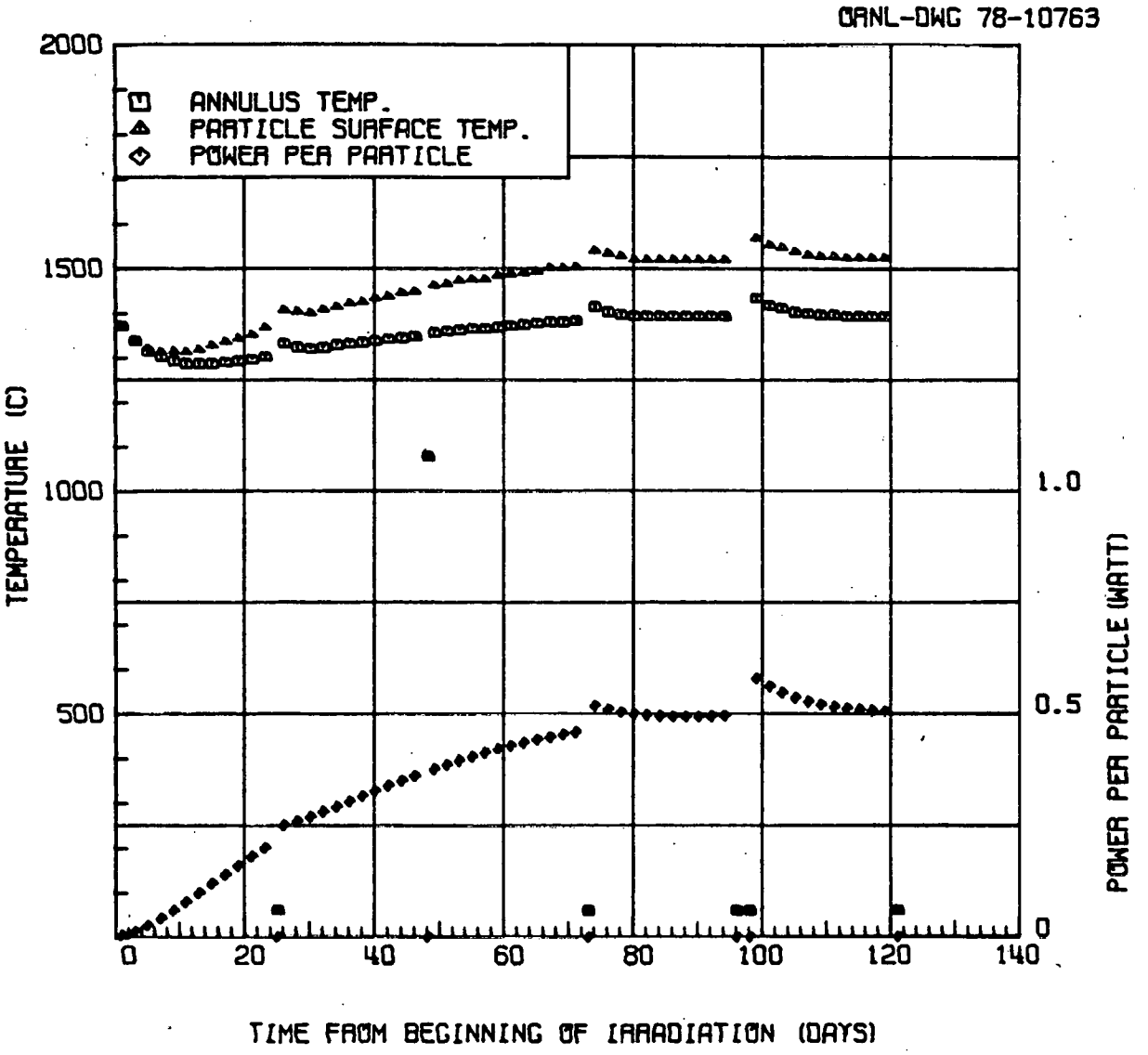

Fig. 4-1. Results of ORNL thermal analysis (sheet 14 of 16)

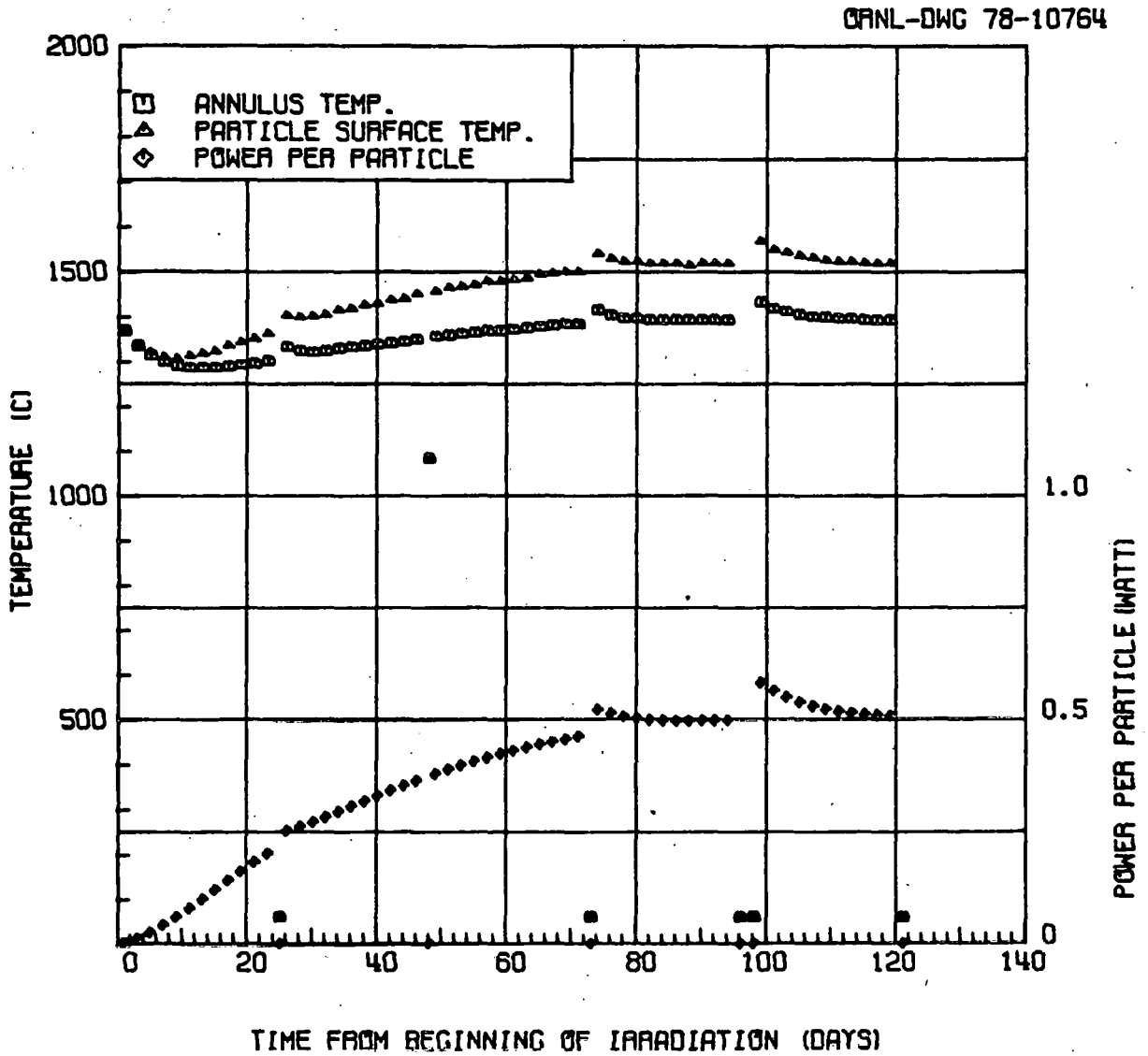

Fig. 4-1. Results of ORNL thermal analysis (sheet 15 of 16)

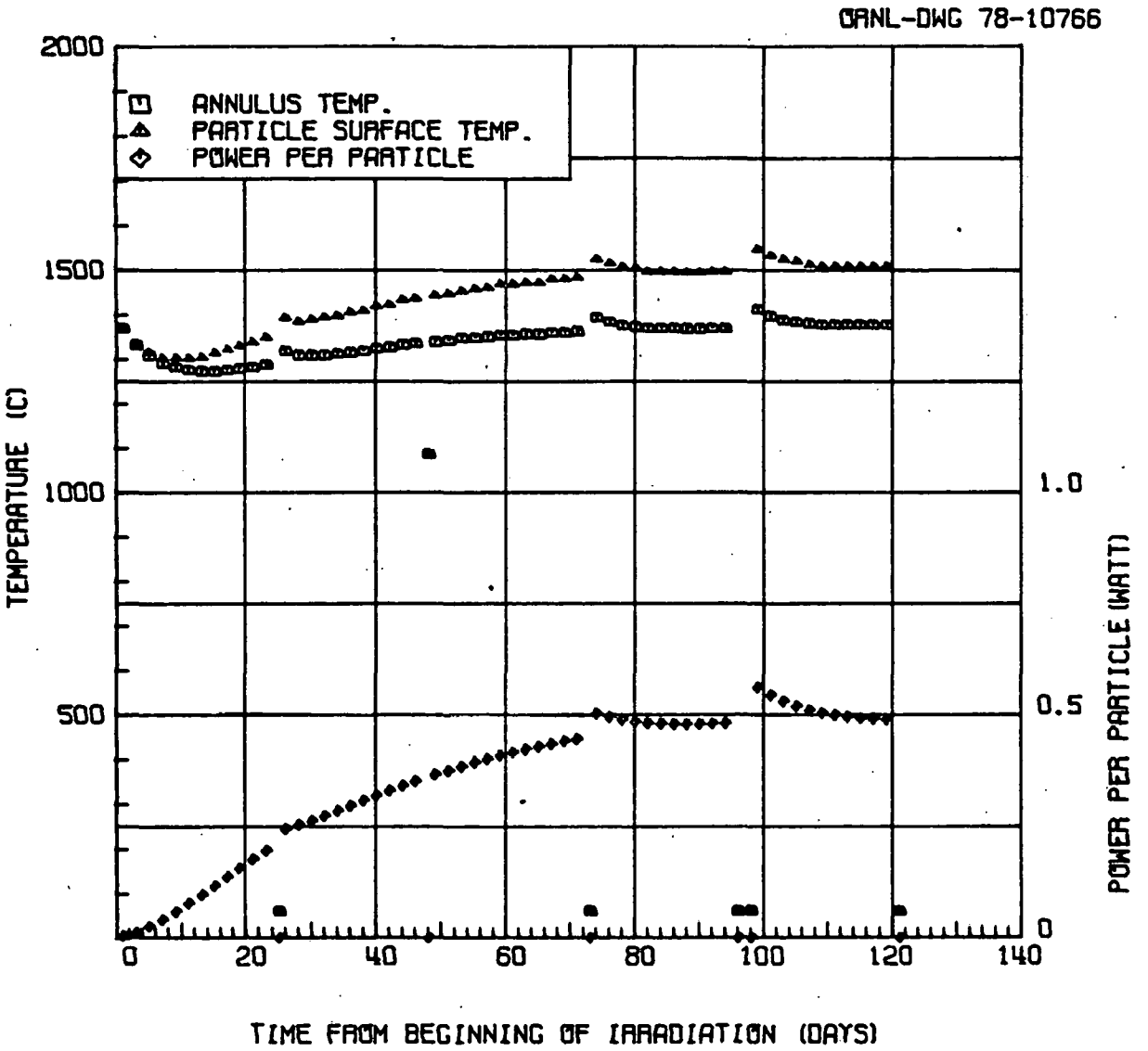

Fig. 4-1. Results of ORNL thermal analysis (sheet 16 of 16)

TABLE 4-1

REACTOR OPERATING HISTORY[a]

HFIR Cycle	Cycle Dates				Irradiation Time[b] (hr)	
	Begin		End			
	Day	Time	Day	Time	During Cycle	Accumulated
150	07/27/77	19:00	08/17/77	16:00	549	549
151	08/19/77	04:51	09/11/77	02:27	547	1096
152	09/11/77	18:39	10/04/77	11:35	545	1641
153	10/06/77	19:09	10/29/77	04:00	538	2179
154[c]	10/31/77	17:30	11/23/77	04:00	507	2686

[a] Ref. 14

[b] Time at 100 MW

[c] The reactor was shutdown for 55.3 hrs (from 05:00 11/07/77 to 12:00 11/09/77)

TABLE 4-2

NEUTRON FLUENCES AND BURNUPS OF SAMPLES

Capsule Position	Fast Fluence[a] ($\times 10^{25}$ n/m^2) (E > 29 fJ)$_{HTGR}$	Burnup		
		% FIMA		Difference[c] (%)
		ORNL[a]	GA[b]	
Low Temperature Magazine				
2	5.1	5.6	5.1	9.8
4	5.8	6.4	5.7	12.2
5	6.1	6.7	6.0	11.7
7	6.7	7.3	6.7	10.4
8	7.0	7.6	7.0	8.6
10	7.5	8.3	7.6	9.2
11	7.7	8.6	7.9	8.9
13	8.2	9.2	8.5	8.2
High Temperature Magazine				
15	9.2	10.7	10.5	1.9
17	9.4	11.0	10.9	.9
18	9.5	11.2	11.2	0
20	9.7	11.5	11.6	-0.8
21	9.8	11.6	11.9	-2.5
23	10.0	11.9	12.2	-2.5
24	10.1	12.0	12.4	-3.2
26	10.2	12.2	12.7	-3.9

[a] Ref. 14

[b] Ref. 15

[c] [(ORNL-GA) ÷ GA] x 100

TABLE 4-3

TIME-AVERAGED MAXIMUM SURFACE TEMPERATURES[(a)] OF SAMPLES

Capsule Position	Time-Averaged Maximum Surface Temperature (°C)					
	Cycle 1	Cycle 2	Cycle 3	Cycle 4	Cycle 5	Average of Cycles
Low Temperature Magazine						
2	1150	1150	1180	1210	1220	1180
4	1070	1140	1200	1240	1260	1180
5	1090	1170	1240	1280	1300	1210
7	1100	1190	1260	1300	1320	1230
8	1110	1180	1240	1280	1300	1220
10	1120	1200	1270	1310	1330	1240
11	1130	1210	1280	1320	1340	1250
13	1060	1150	1210	1250	1260	1180
High Temperature Magazine						
15	1390	1400	1440	1470	1480	1430
17	1290	1400	1460	1500	1520	1430
18	1310	1400	1470	1510	1520	1440
20	1310	1400	1470	1500	1500	1440
21	1320	1410	1470	1510	1520	1440
23	1330	1420	1490	1520	1530	1460
24	1330	1420	1480	1520	1530	1450
26	1320	1410	1470	1500	1510	1400

[(a)] Ref. 17.

TABLE 4-4

POWER PER PARTICLE OF SAMPLES

Capsule Position	Time-Averaged Power/Particle (Watts)					
	Cycle 1	Cycle 2	Cycle 3	Cycle 4	Cycle 5	Average for Capsule
2	.03	.14	.21	.26	.29	.18
4	.04	.15	.23	.28	.31	.20
5	.04	.16	.24	.29	.32	.21
7	.05	.17	.26	.32	.35	.23
8	.05	.18	.26	.32	.35	.23
10	.05	.19	.29	.34	.38	.25
11	.06	.20	.30	.36	.39	.26
13	.06	.22	.32	.38	.42	.28
15	.08	.27	.38	.45	.48	.33
17	.08	.28	.39	.42	.49	.33
18	.08	.29	.40	.47	.50	.34
20	.09	.29	.40	.47	.50	.35
21	.09	.30	.41	.48	.51	.35
23	.09	.31	.43	.50	.53	.37
24	.09	.31	.43	.50	.53	.37
26	.09	.30	.42	.48	.51	.36

TABLE 4-5

TIME-AVERAGED KERNEL TEMPERATURES OF SAMPLES

Capsule Position	Time-Volume-Averaged Kernel Temperatures (°C)					
	Cycle 1	Cycle 2	Cycle 3	Cycle 4	Cycle 5	Average for Capsule
2	1160	1170	1220	1260	1270	1210
4	1080	1160	1240	1290	1310	1210
5	1100	1190	1270	1320	1350	1240
7	1110	1220	1300	1350	1370	1270
8	1120	1210	1280	1330	1360	1260
10	1130	1230	1320	1370	1390	1290
11	1140	1240	1330	1380	1410	1300
13	1070	1190	1260	1310	1330	1230
15	1400	1450	1510	1550	1560	1490
17	1300	1450	1530	1570	1600	1490
18	1320	1450	1540	1590	1600	1500
20	1330	1450	1540	1580	1590	1500
21	1340	1460	1540	1590	1610	1510
23	1350	1470	1560	1610	1620	1520
24	1350	1470	1560	1610	1620	1520
26	1340	1460	1540	1580	1600	1500

Blank

5. RESULTS OF POSTIRRADIATION EXAMINATIONS

The irradiation capsule was disassembled at ORNL. The ends of the capsule containment were cut off and the four graphite magazines were removed. All GA sample holders were pushed out of the top two magazines. The particles from each graphite holder were removed, visually examined, and photographed in-cell. Selected fuel particles were gamma-counted at ORNL. The samples were then shipped to GA for completion of the postirradiation characterization, which included visual examinations, fission gas release measurements, and metallographic examinations.

5.1. VISUAL EXAMINATION

The visual examination was performed at ORNL using an in-cell stereomicroscope with a magnification range of 6x to 27x. Each sample was examined for particle failure immediately after the particles were unloaded from the graphite holder. The results are reported in Table 5-1 along with the irradiation conditions, 95% confidence limits, and the predicted particle failure.

The visual examination of the 1200°C magazine indicated that no pressure vessel failure (both OPyC and SiC coatings cracked) occurred in any of the samples. The OPyC coating failure was zero for five samples, 1.8% for two, and 8.9% for one, and was apparently caused by fast neutron damage, as shown in Fig. 5-1. A typical sample exhibiting zero pressure vessel and OPyC coating failure is shown in Fig. 5-2.

The visual examination of the 1450°C magazine samples showed that the OPyC plus SiC coating failure ranged from 6.2 to >80%. The ThO_2 kernels of the failed particles fragmented and converted to carbide by the end of the irradiation. The OPyC coating failure was the same as the pressure vessel failure. An example of the failure is shown in Fig. 5-3.

The two end plugs containing the burned-back TRISO inert particles (batch 6351-040-0100) were examined at GA. The end plugs were unloaded at ORNL, and the particles were shipped to GA.

End plug 14-1 was irradiated at 1200°C. Totals of 36 Si-doped BISO particles (batch 7032-149) and 14 TRISO particles were examined. No coating failures were observed in either batch. The SiC coating of the burned-back inerts was visibly in good condition. Twenty BISO and 11 TRISO particles were lost during unloading at ORNL.

End plug 15-2 was irradiated at ~1500°C. Forty-five BISO particles and one TRISO particle were counted and all particles were intact. The SiC coating of the one TRISO particle was shiny and appeared to be in good condition. Thirty-five BISO and 24 TRISO particles were missing from the sample.

The burned-back TRISO inert particles were placed in capsule HT-34 to determine if the exposed SiC coating volatilized during irradiation. The visual examination indicated that volatilization did not occur, because the SiC surface still appeared shiny through the microscope at 27x. No other analyses were performed on these particles.

5.2. METALLOGRAPHIC EXAMINATION

Six particle samples were examined metallographically to evaluate the microstructure of the coatings and kernels after irradiation. Approximately 15 particles from each specimen were mounted. The mounts were ground, reimpregnated with mounting resin to prevent kernel pullout, reground, and finally polished. The polished sections were examined under bright field illumination and polarized light with a Lietz metallograph. The results of the examination are presented in Table 5-2 and given in terms of number of observations rather than percentages, because the sample sizes were very small. The data are useful for a qualitative evaluation.

The integrity of the sample particles was indicated by the metallographic examination. Zero SiC and OPyC coating failure was observed in the polished sections of four 1200°C magazine samples. This agrees with the visual results. The two 1450°C samples exhibited high SiC coating failure but low OPyC coating failure. These data are also consistent with the visual results, because SiC failure would not be detected if the OPyC were still intact. The anisotropy of the OPyC and IPyC coatings, which was observed under polarized light, increased slightly during irradiation, as shown in Fig. 5-4. The IPyC coating cracked and/or debonded in the majority of particles examined. Figure 5-4 also indicates that redeposition of the buffer coating was observed. The metallographic examination showed that the particles with the 27-μm buffer (6252-14-0261-001) performed well. An example is given in Fig. 5-5.

The shape and microstructure of the kernels changed with temperature and burnup. At a temperature of 1240°C and a burnup of 6.0% FIMA the kernels were round, and the grain boundaries and a fine porosity were visible, as shown in Fig. 5-5. The kernels irradiated at 1280°C to a burnup of 7.6% FIMA were similar, but no grain boundaries were visible (Fig. 5-4). A white metallic phase approximately 1 to 2 μm in size appeared throughout the kernels. At temperatures of 1490°C and a burnup of 10.5% to 10.9% FIMA, the kernels elongated, the microstructure showed larger pores, and the amount of the white metallic phase increased (Fig. 5-6).

Different types of chemical attack of the SiC coating were observed in both the 1200° and 1450°C samples. The metallographic evaluation showed that two kinds of chemical reactions occurred in three of the four samples irradiated at 1180° to 1240°C. The SiC coating of the majority of these three samples exhibited $\leq$2-μm pores distributed around the entire SiC coating. The pores were observed across the SiC coating thickness, but were concentrated near the inner surface of the SiC. The amount of porosity varied from particle to particle. Figure 5-7 gives examples of this phenomenon. The other type of attack in the three 1200°C specimens was a localized reaction at the inner surface of the SiC coating, as shown in Fig. 5-8.

In five out of 45 particles examined, there was a penetration of 9 to 18 μm of the SiC coating (nominal thickness was 35 μm). A white metallic phase was observed in the front of the reaction zone in one of the five areas (see Fig. 5-8d).

The two 1450°C specimens also showed localized attack of the SiC coating, but the appearance of the reaction was different from that in the 1200°C samples. In some instances, the corrosion was completely through the SiC coating in a localized area. The reaction zone was always on the hot side of the particle, because the attack was opposite the advancing face of the migrated kernel. No metallic phases were observed at the reaction zone. In some cases there was a buildup of white phase, which was bonded to the SiC coating near the reaction zone. It had the appearance of being SiC. Photomicrographs of the 1450°C SiC attack are presented in Fig. 5-6.

An unusual SiC coating fracture also occurred in the three 1200°C samples that had SiC attack. Figure 5-9 gives an example of the cracking. The fractures began at the inner surface of the SiC and propagated tangentially along the SiC at roughly 5 μm from the inner surface. The longest crack measured ~170 μm. The fracture pattern was similar for all the cracks. The cracks did not cause the SiC coating to fail.

The metallographic examination showed that a significant fraction (5 and 13 out of 15) of the particles that were irradiated to a temperature of 1490°C and a burnup of 10.9% exhibited kernel migration. Rejected graphite was observed on the cool side of kernels. An example of the migration is shown in Fig. 5-10. The maximum migration distance was approximately 60 μm.

5.3. GAMMA-RAY SPECTROMETRY ANALYSIS

Gamma-ray spectrometry was used to determine fission product inventories of the TRISO ThO_2 samples. The loss of metallic fission products gave a measure of SiC failure.

Oak Ridge National Laboratory measured the gamma-ray spectra on selected samples, using the Irradiated-Microsphere Gamma Analyzer (IMGA) (Ref. 22). The IMGA system automatically gamma counted each particle from a sample. The GA samples were counted approximately 310 days after the end of irradiation.

Eight 1200°C and four 1450°C magazine samples were gamma counted. All or most particles from each sample were analyzed. The visual examination indicated that all particles measured had intact SiC coatings. The results of the IMGA measurements are given in Table 5-3. The measured activity for the isotopes Zr-95, Ru-106, Cs-134, Cs-137, Ce-144, and Pa-233 are specified for each sample. Also, the predicted quantities were calculated by GA. The GA values were determined by the computer program "Curie" (Ref. 15). Considering all the uncertainties in calculating the fission product inventory, the agreement between the measured and predicted values is fairly good.

In addition, certain fission product ratios were calculated for each particle gamma counted from a sample. The data are summarized in Table 5-4, the distributions of Cs-137/Zr-95 ratios are plotted in Fig. 5-11, and the predicted fission product ratios are given in both. The figure shows that particles from four low-temperature and all four high-temperature samples released Cs; this will be discussed in Section 6.

5.4. FISSION GAS RELEASE

Fission gas release data were obtained by neutron activation in the GA TRIGA reactor facility on six 1200°C samples. The primary objective of the postirradiation FGR measurements was to evaluate the fuel failure.

The samples were examined under stereomicroscope, and washed with nitric acid to remove possible surface contamination picked up during sample unloading.

Fission gas release measurements were made by irradiating the fuel specimens in a graphite tube furnace designed to fit into a fuel element position of the TRIGA reactor core (Ref. 23). The furnace allowed measurements to be made at high temperatures, independent of the power generated in the fuel. The rods were irradiated at appropriate power levels for 0.5 h to produce approximately 10^{14} fissions in each fuel specimen. During irradiation, the released fission gases were swept with helium into a liquid-nitrogen-cooled charcoal trap. The trapped gases were assayed for fission product isotopes by gamma-ray spectroscopy (Ref. 24), using a Ge(Li) detector and a 4096-channel analyzer. The fission product isotope birth fractions were calculated using the neutron flux in the TRIGA core and the end-of-life (EOL) fissionable material loadings given in Table 5-5. The adjusted EOL fissile fuel loading for each specimen was determined by expressing the sum of the weights of all remaining fissionable material (U-233 and U-235) in terms of U-235, producing the equivalent Kr-85m yield. The Kr-85m isotope was selected as the reference isotope because it has a short half-life (4.4 hours) and its gamma-ray energy peak can easily be resolved. A reference temperature of 1100°C was used for analysis of fuel failure levels. The results of the measurements are presented in Table 5-5.

The failure fraction of each sample was calculated from the FGR measurement. The fission gas released during TRIGA activation comes primarily from heavy metal contamination outside the particle coatings and from failed coatings. Since the particles were washed in nitric acid, the amount of surface contamination was minimized. Therefore, to determine the coating failure fractions it was assumed that the fission gas released was all due to failed particles (this gives a maximum particle failure). The fractional release for failed particle (R/b_f) is given by the following equation (Ref. 25) for failed ThO_2 particles:

$$r/b_f = 0.0013 + 0.00186\ (\%\ FIMA)^{0.9} \quad . \qquad (5\text{-}1)$$

The failure fraction (F) was determined by the following equation:

$$F = \frac{R/B_{TRIGA}}{r/b_f} \quad . \qquad (5\text{-}2)$$

The number of failed particles per sample was then calculated by multiplying the failure fraction by the total number of particles activated. If the number of failed particles was less than 0.5 of a particle, it was assumed that a particle was not failed and the fission gas released was a result of contamination. The results of the calculations are given in Table 5-5. Four of the samples showed zero failure, while samples 6252-13-0161-001 and 6252-15-0161-001 exhibited one particle failed (1.8%). This is not a true indication of the number of particles per sample with failed SiC coatings, because the OPyC coating was intact on most particles. An OPyC coating prevents or slows the diffusion of Kr-85m in a particle with a failed SiC coating. The gamma-counting results to be discussed in Section 6 show that the SiC failure is higher, based on metallic fission product release.

5.5. ELECTRON MICROPROBE EXAMINATION

An electron microprobe examination was performed at ORNL on one 1200°C and one 1450°C sample. The microprobe examination was done on two metallographically polished sections prepared at GA.

Sample 10 was selected from the 1200°C samples, because metallic fission products were seen in the localized reaction zone of the SiC coating. Figure 5-12 gives the optical light photograph and the electron microprobe scans of the area examined. Palladium was associated with the reaction zone. Chlorine was detected in between the buffer and IPyC and next to the inner surface of the SiC coating. No U, Th, rare earths, or Ag were detected at the reaction zone. No elements were detectd in the small pores in the SiC coating.

Sample 17, which was irradiated at ~1450°C, was selected because of the corrosion of the SiC coating. Figure 5-13 gives the optical light photograph and electron microprobe scans of the areas examined. The results show that the Si was transported to the area adjacent to the reaction zone. No Cl, fission products, U, or Th were measured at the SiC reaction zone. The large white phase in the middle of the kernel and the white specks scattered around the kernel were rich in Mo and Ru. Iron and Cr were detected in the large void of the particle. However, it is believed that they were from the steel-mesh polishing wheel. Chromium and Fe were measured at <50 ppm each on the as-coated particle batch.

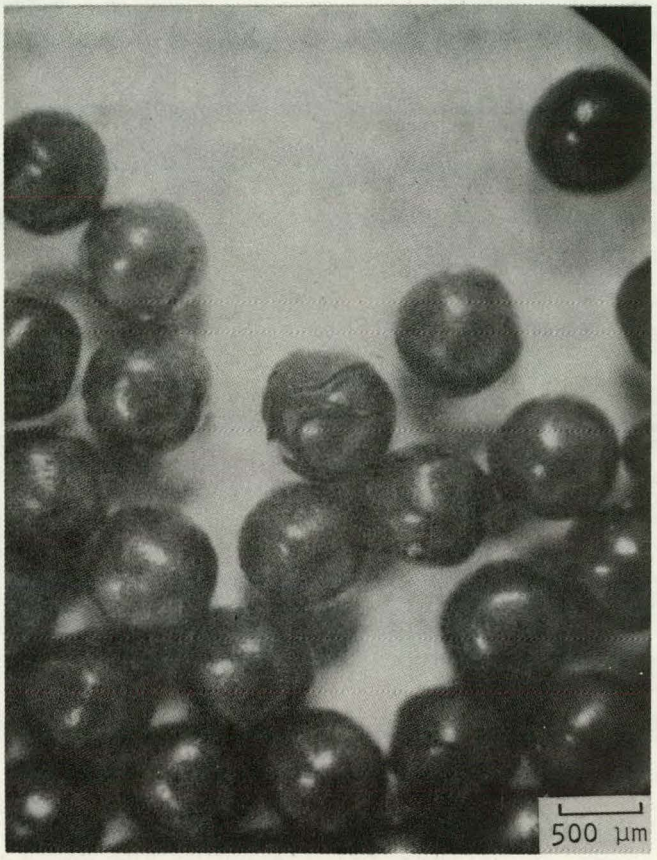

S7909-9

Fig. 5-1. Photomicrograph of a representative example of OPyC coating failure of a particle irradiated in the low temperature magazine; sample 10 had an average temperature of 1240°C and a fluence of 7.5×10^{25} n/m^2 $(E > 29 \text{ fJ})_{HTGR}$.

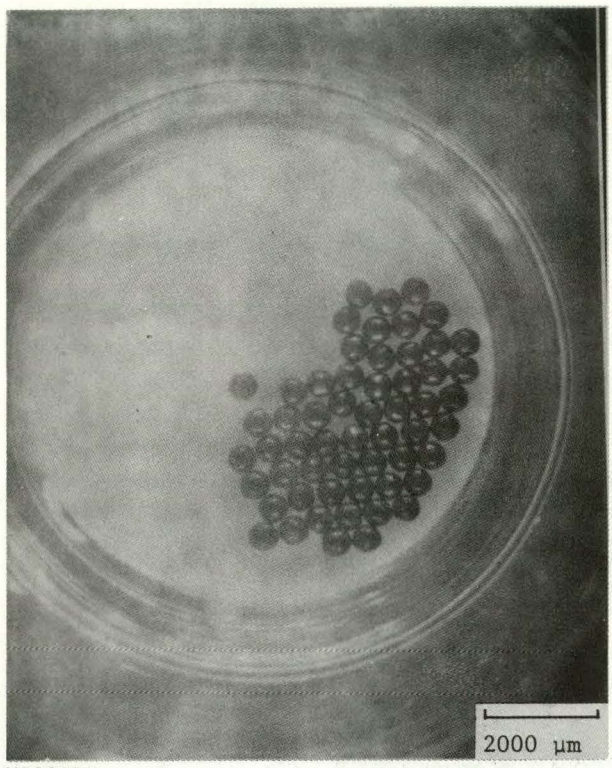

N78015-1

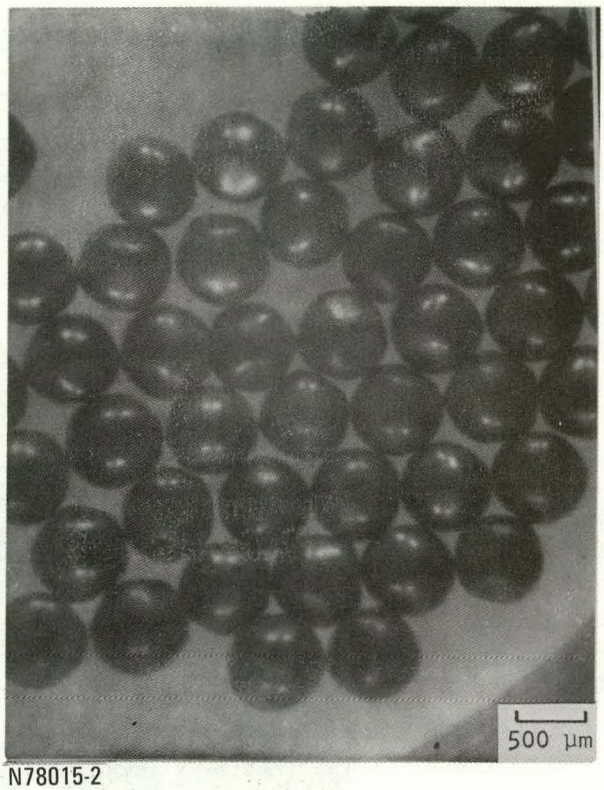

N78015-2

Fig. 5-2. Photomicrographs of a typical sample with zero pressure vessel and OPyC coating failure irradiated in the low temperature magazine; sample 8 had an average temperature of 1220°C and a fluence of 7.0×10^{25} n/m^2 $(E > 29\ fJ)_{HTGR}$.

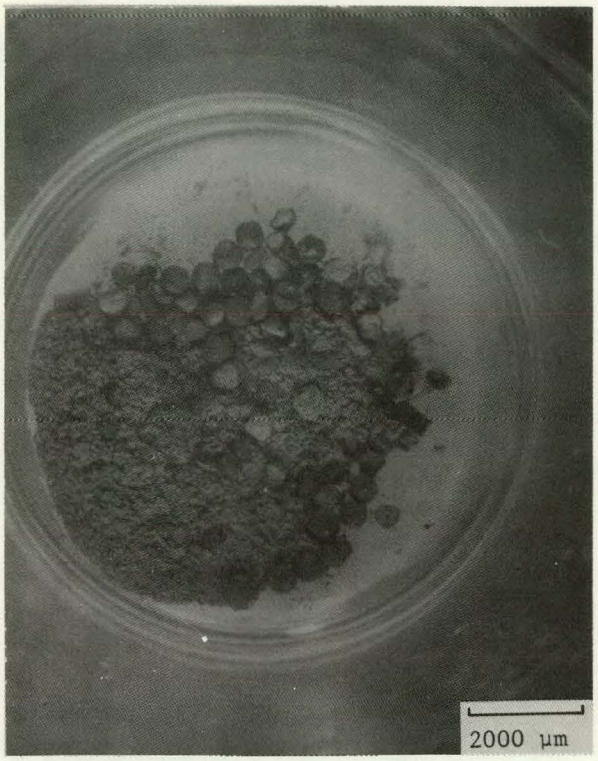

N78013-1

N78013-2

Fig. 5-3. Photomicrographs of total coating failure observed in a sample (6252-17-0161-001) irradiated at 1460°C to a fluence of 10.0×10^{25} n/m^2 (E > 29 fJ)$_{HTGR}$

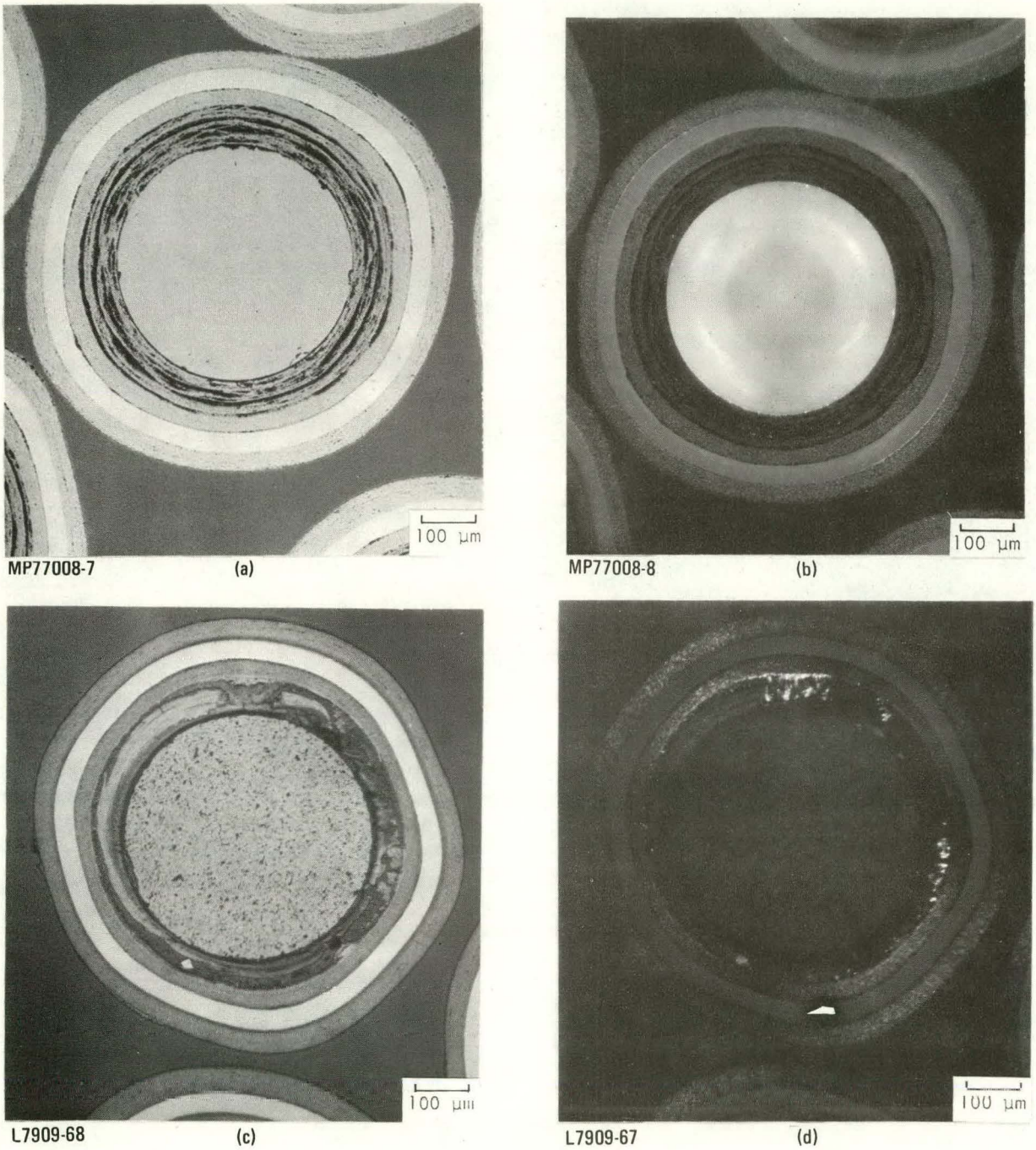

Fig. 5-4. Photomicrographs of sample 6252-14-0161-001: (a) and (b) as coated; (c) and (d) after irradiation at 1240°C to a fluence of 7.6×10^{25} n/m^2 $(E > 29\ fJ)_{HTGR}$; (a) and (c) are bright field; (b) and (d) are polarized light. Note redeposition of the buffer in (c).

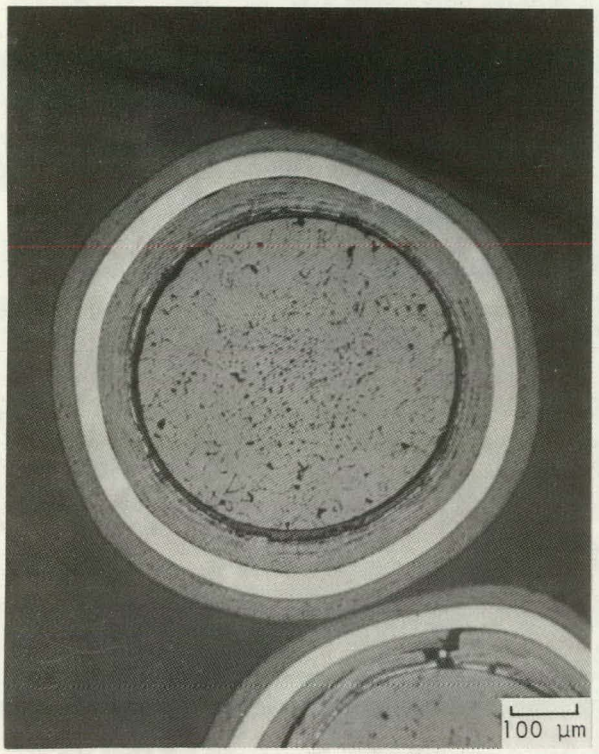

L7907-47

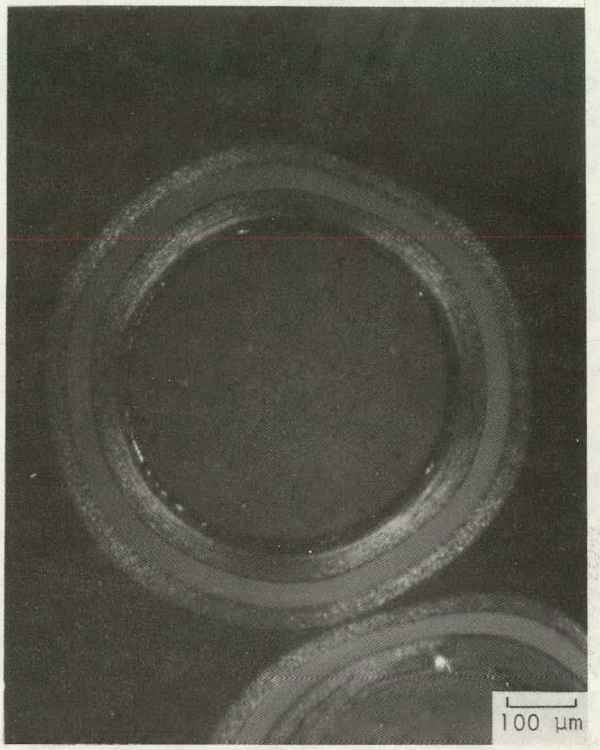

L7909-48

Fig. 5-5. Photomicrographs of typical particle with a 27-µm-thick buffer (6252-14-0261-002) irradiated at 1210°C to a burn-up of 6.0% FIMA

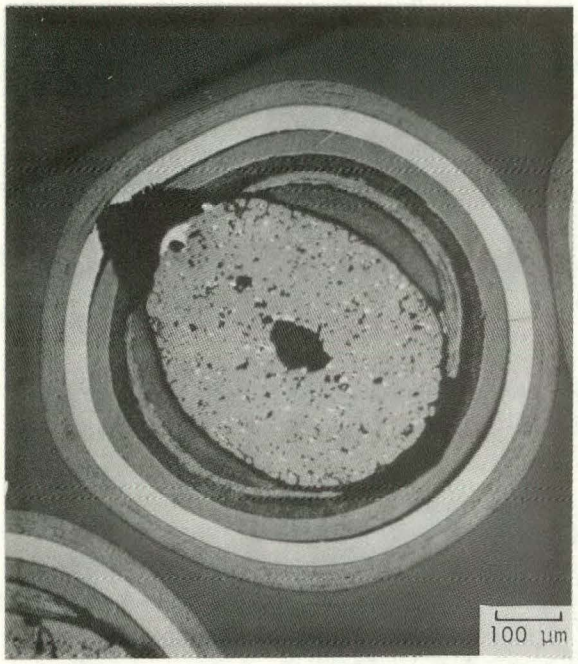

L7909-32

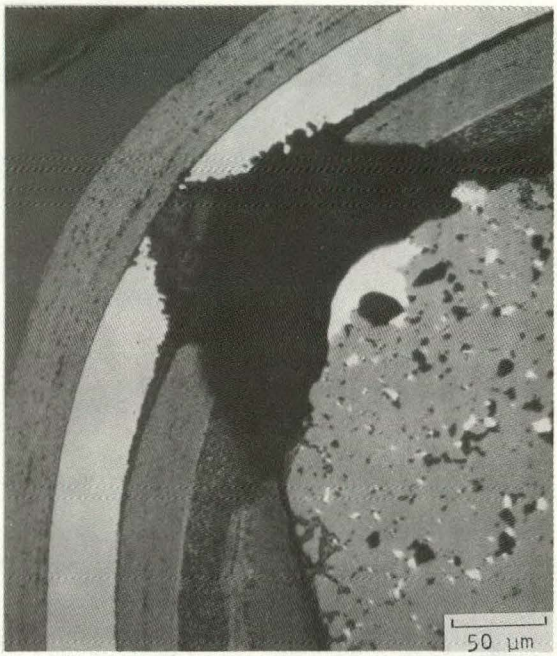

L7909-34

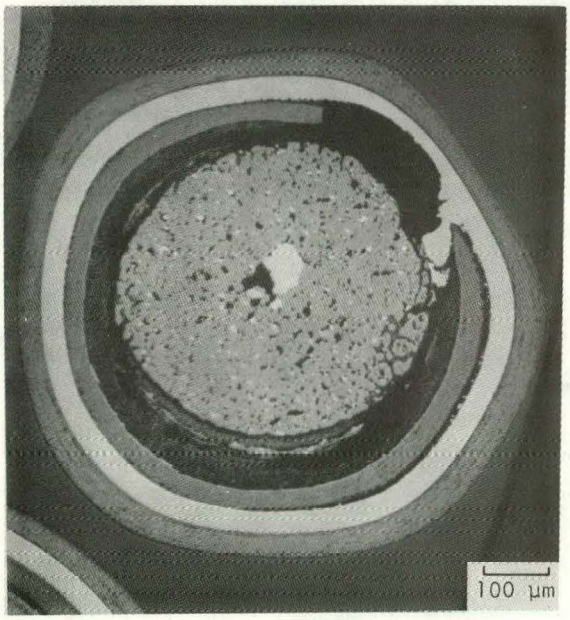

L7909-35

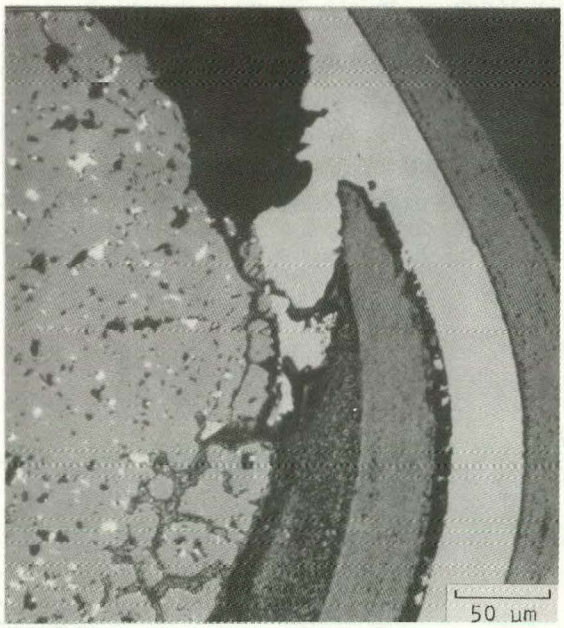

L7909-36

Fig. 5-6. Photomicrographs of two particles (6252-07-0262-002) irradiated at 1430°C to a burnup of 10.9% FIMA and a fluence of 9.4 x 10^{25} n/m^2 $(E > 29\ fJ)_{HTGR}$

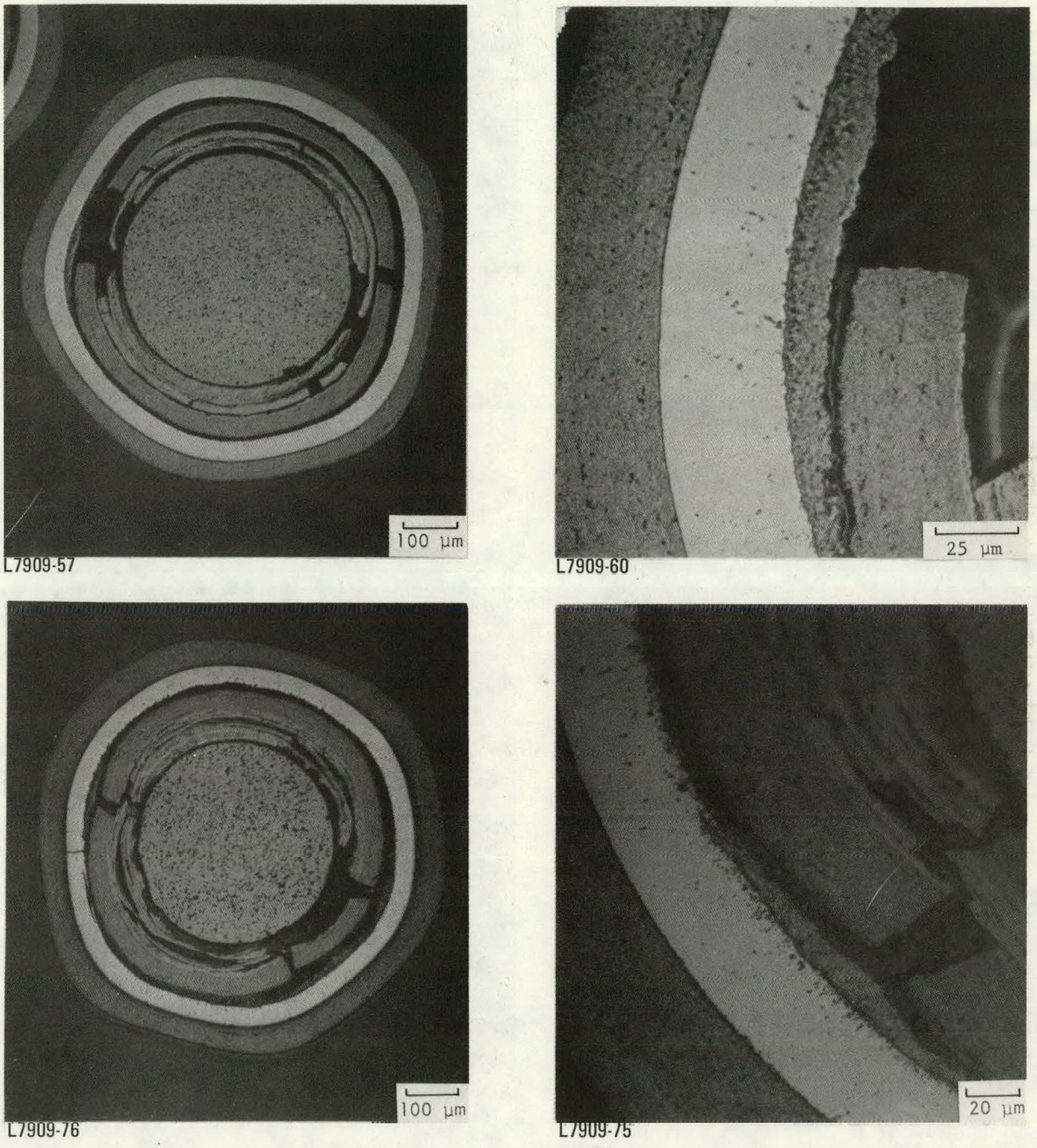

Fig. 5-7. Photomicrographs of representative particles irradiated at 1240°C to a burn-up of 7.9% FIMA which showed SiC coatings attacked around the circumference of the coating

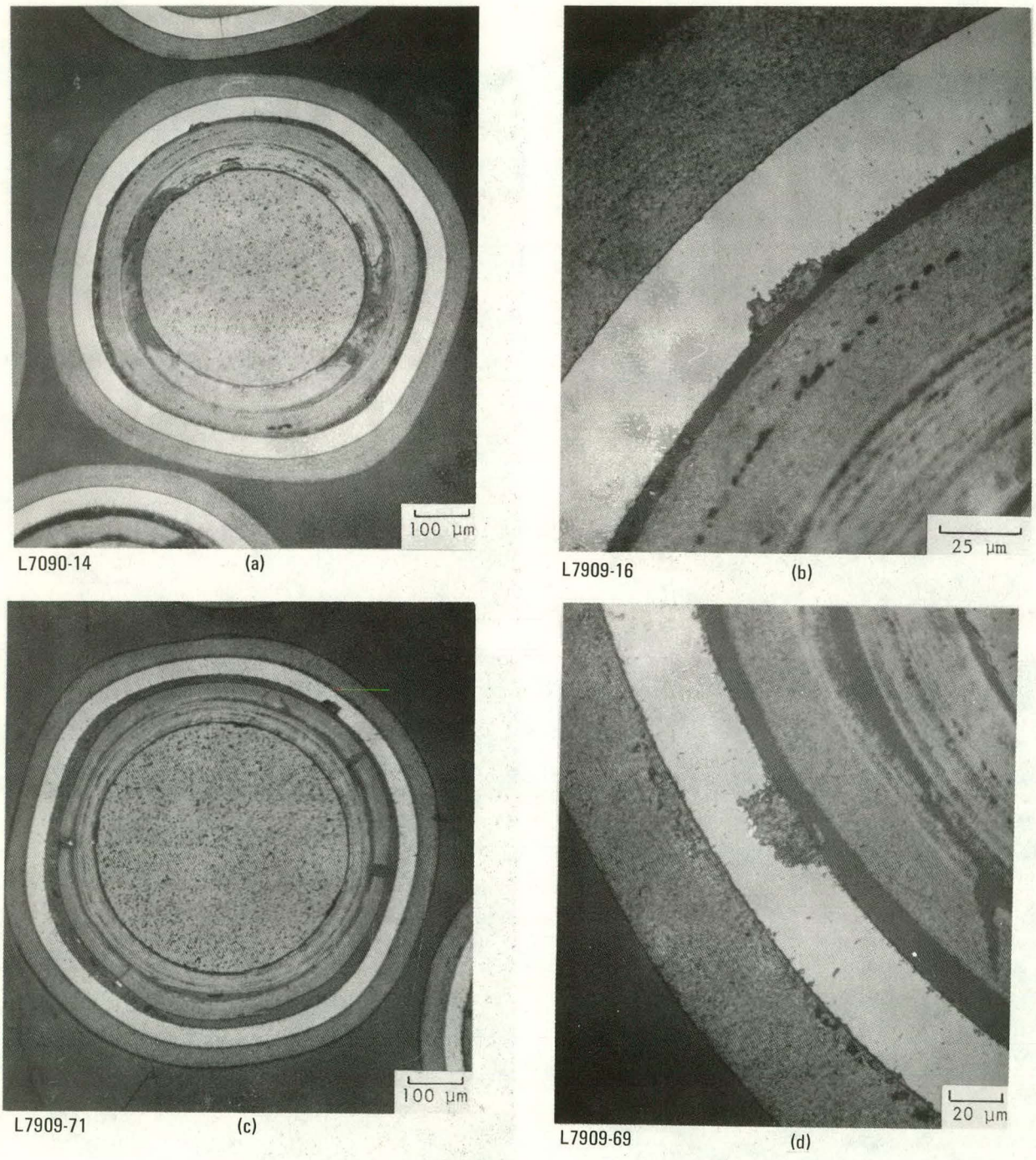

Fig. 5-8. Photomicrographs of two particles irradiated at 1240°C to a burn-up of 7.9% FIMA showing a localized attack of the SiC coating

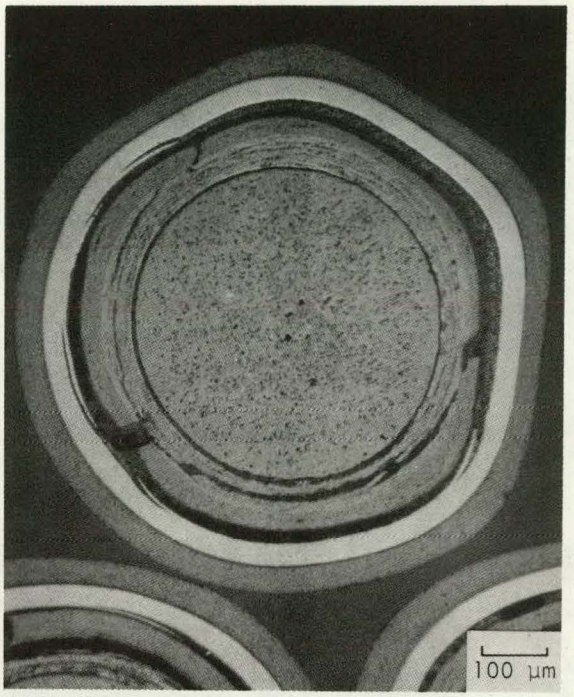

L7909-17

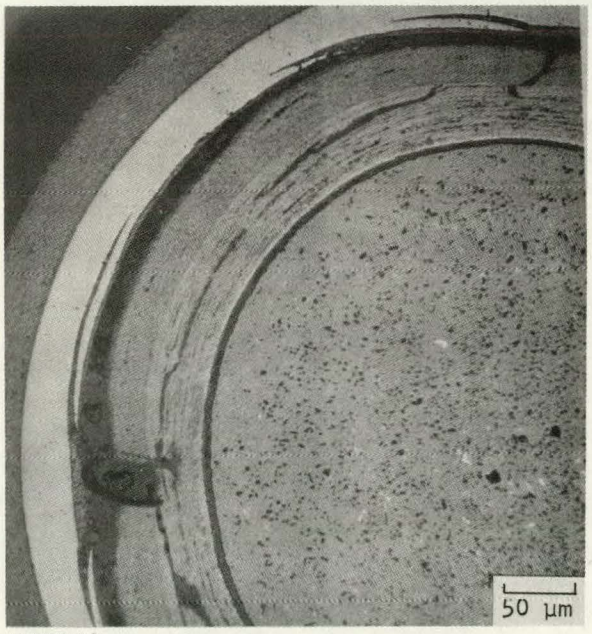

L7909-18

L7909-19

Fig. 5-9. Photomicrograph of fracturing of the SiC coating near the inner surface of particles irradiated at 1180°C to a fluence of 8.2×10^{25} n/m^2 (E > 29 f.J)$_{HTGR}$

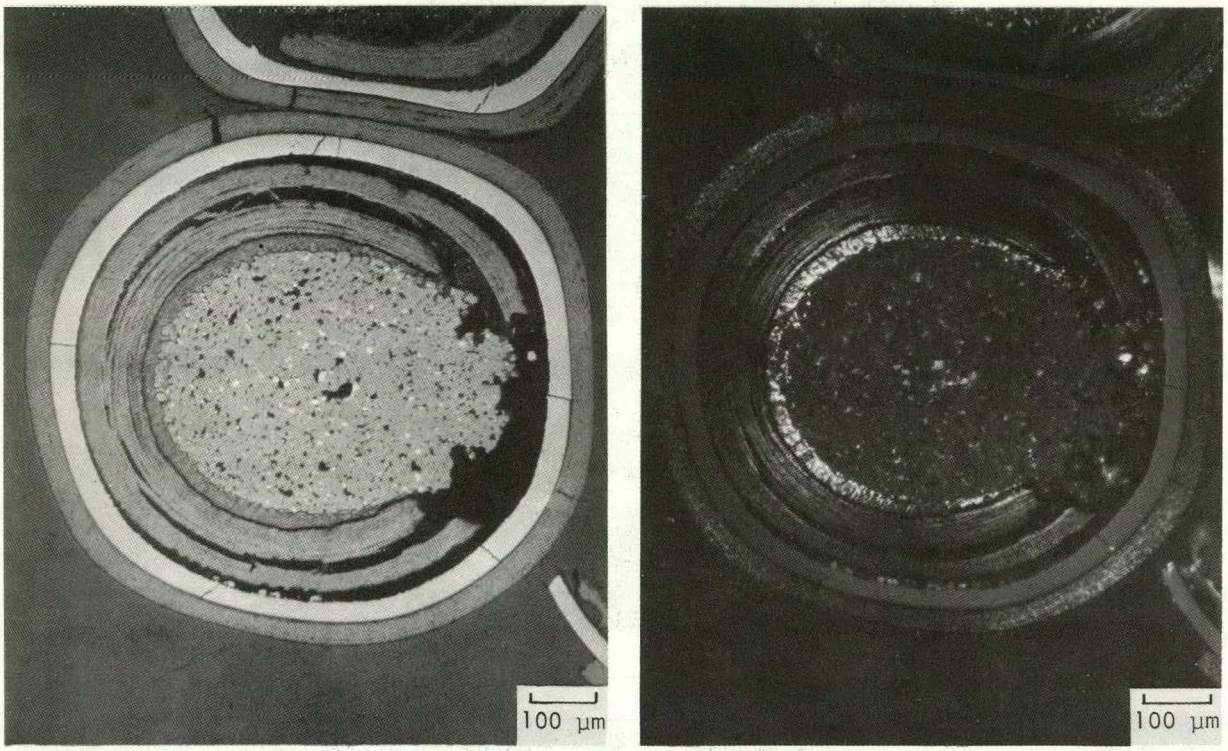

L7909-1 (a) L7909-2 (b)

Fig. 5-10. Photomicrographs of kernel migration of a particle irradiated at 1490°C to a burn-up of 10.5% FIMA: (a) bright field; (b) polarized light

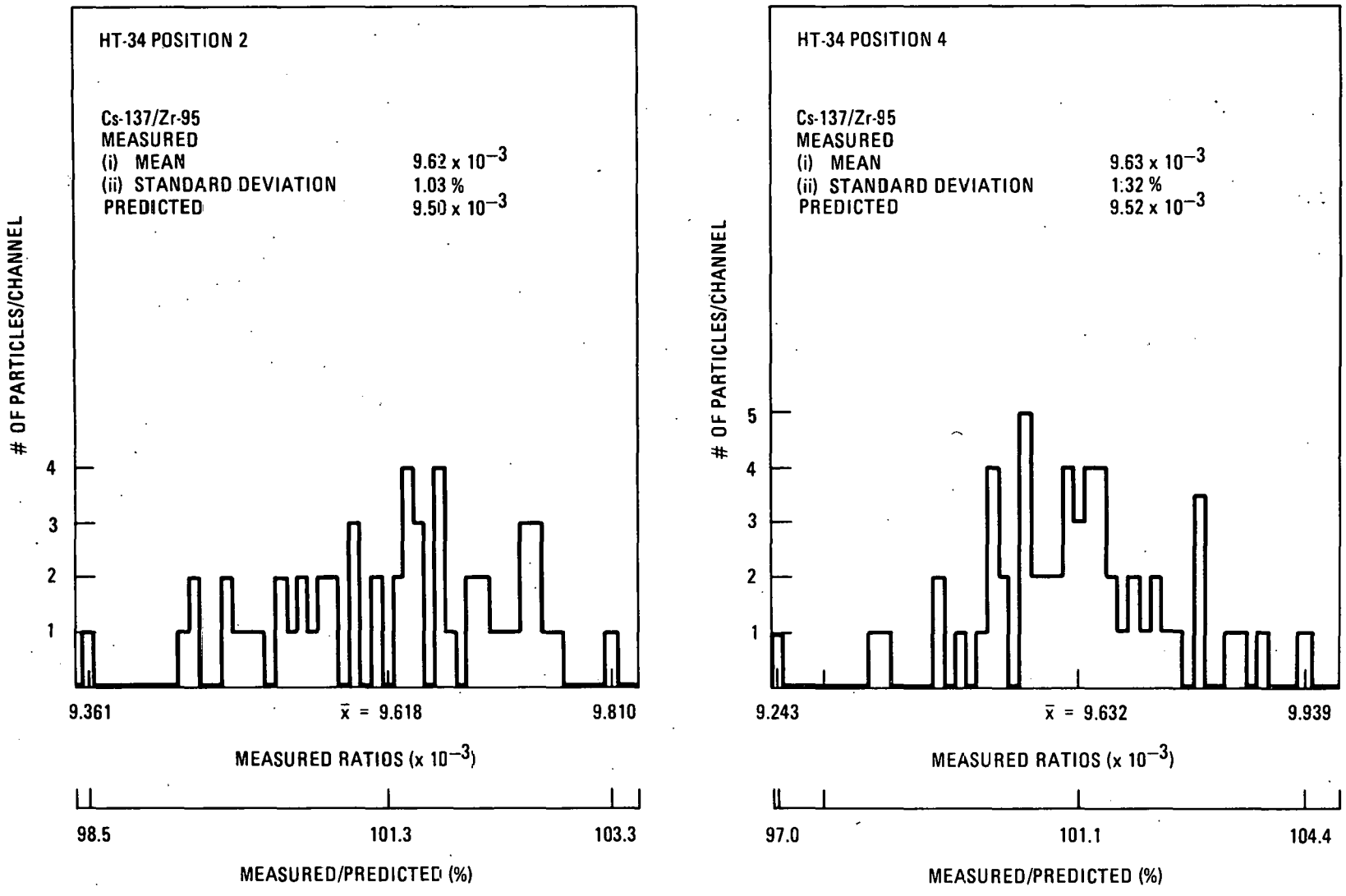

Fig. 5-11a. Histograms of the measured Cs-137/Zr-95 ratios. The measured/predicted Cs/Zr ratios are also given (NOTE: the scale is different for each sample).

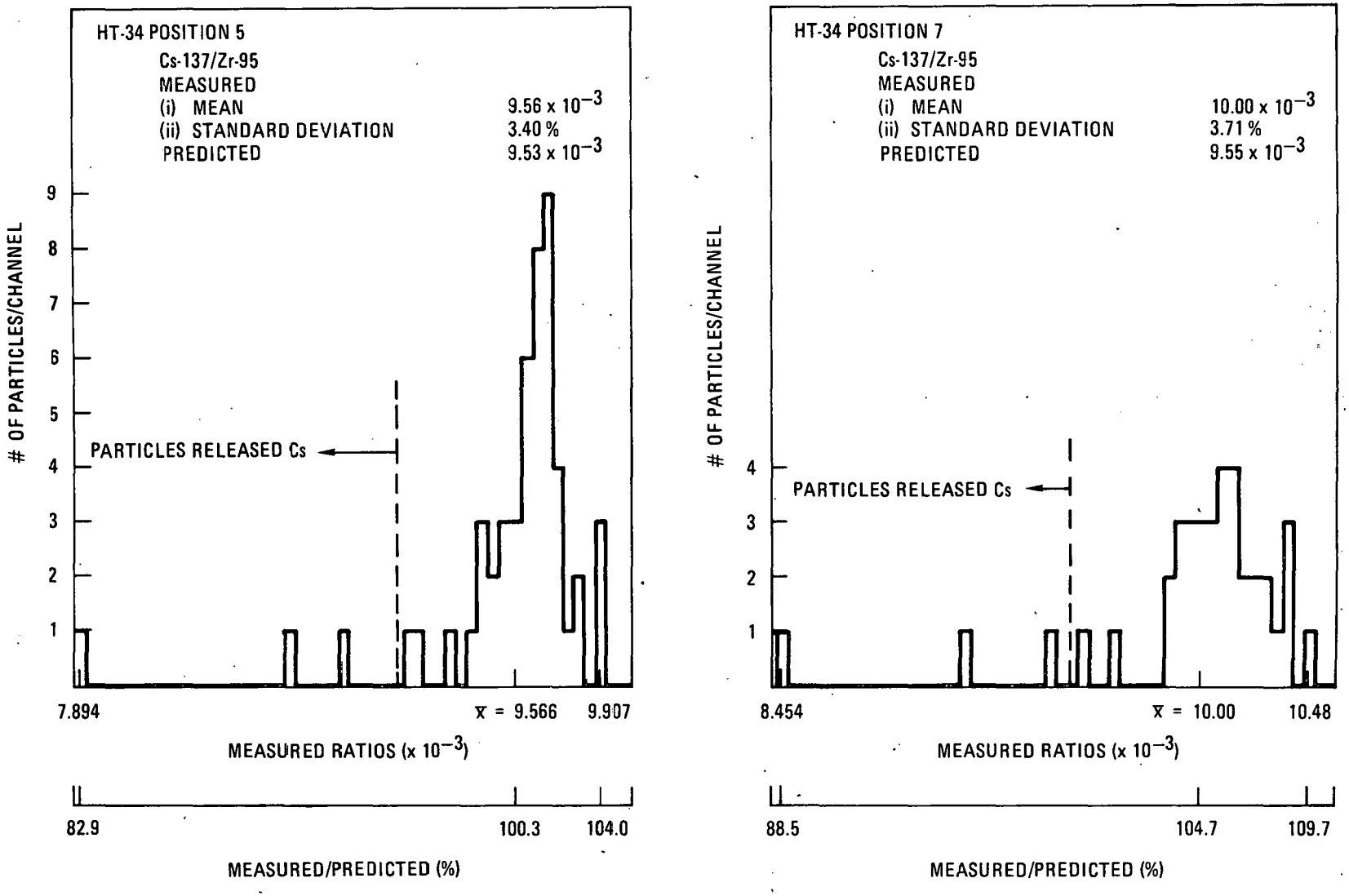

Fig. 5-11b. Histograms of Cs-137/Zr-95 ratios. The measured/predicted Cs/Zr ratios are also given. The figure indicates the particles that released Cs. (NOTE: the scale is different for each sample).

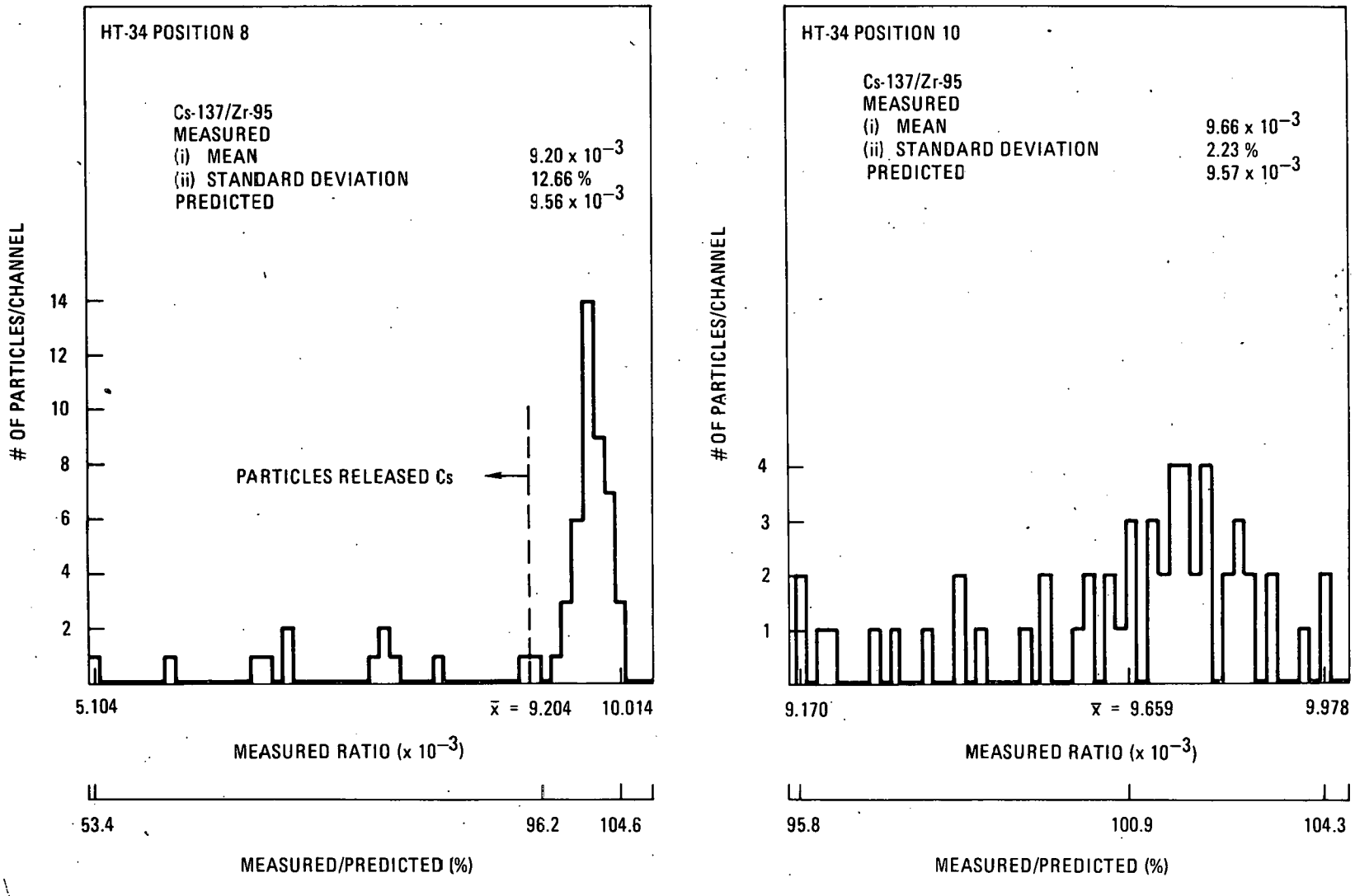

Fig. 5-11c. Histograms of Cs-137/Zr-95 ratios. The measured/predicted Cs/Zr ratios are also given. The figure indicates the particles that released Cs. (NOTE: the scale is different for each sample).

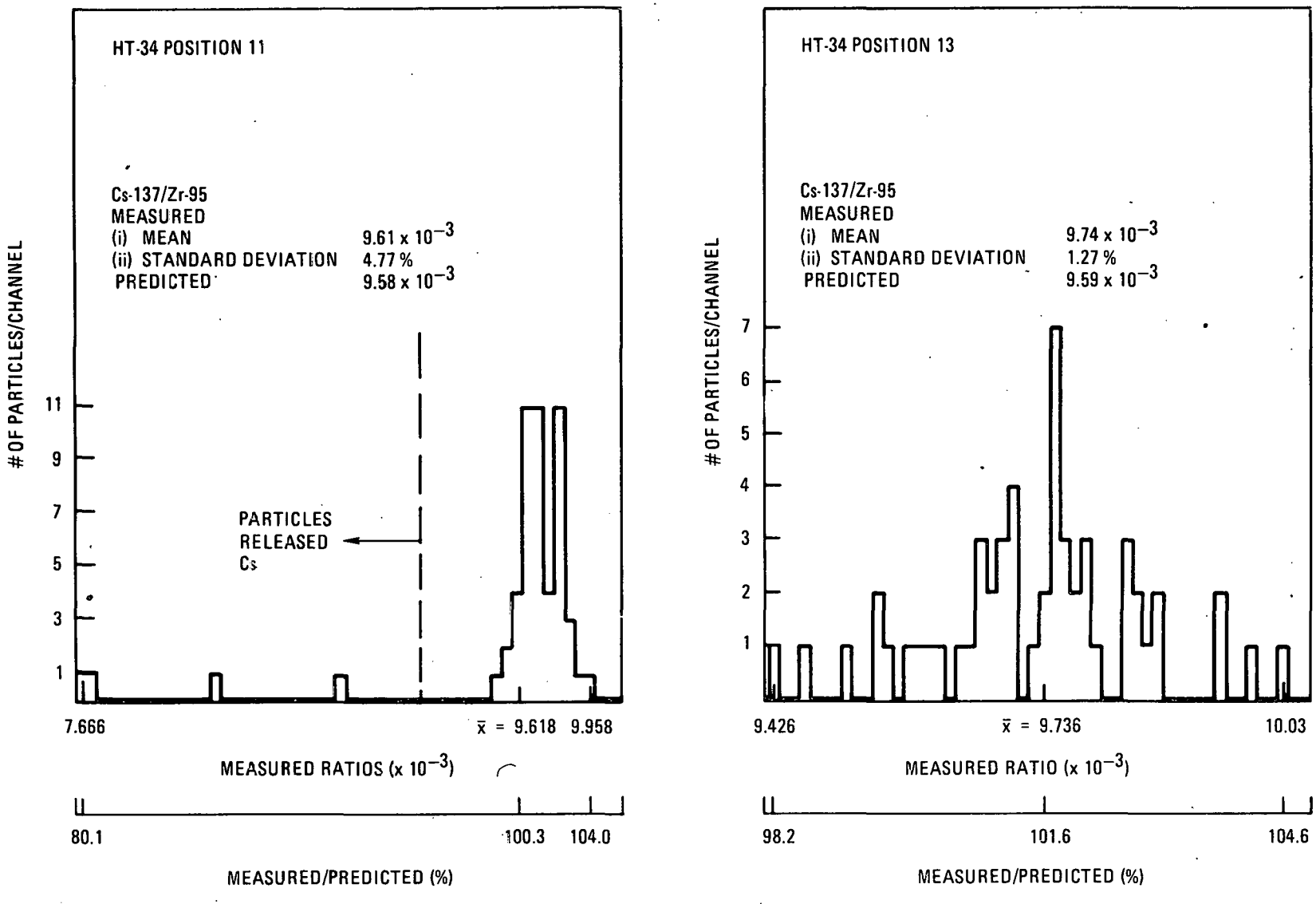

Fig. 5-11d. Histograms of Cs-137/Zr-95 ratios. The measured/predicted Cs/Zr ratios are also given. The figure indicates the particles that released Cs. (NOTE: the scale is different for each sample).

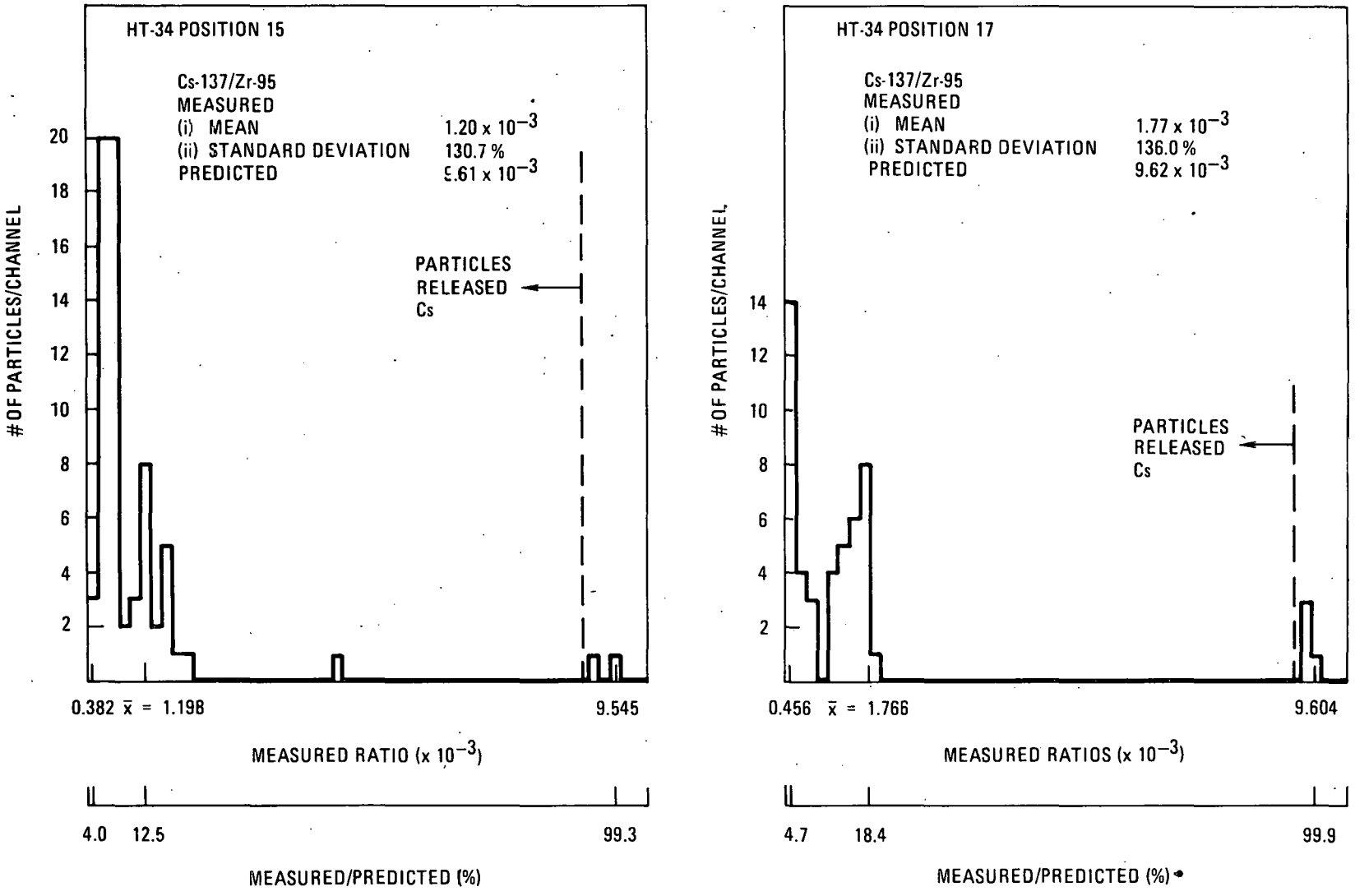

Fig. 5-11e. Histograms of Cs-137/Zr-95 ratios. The measured/predicted Cs/Zr ratios are also given. The figure indicates the particles that released Cs. (NOTE: the scale is different for each sample).

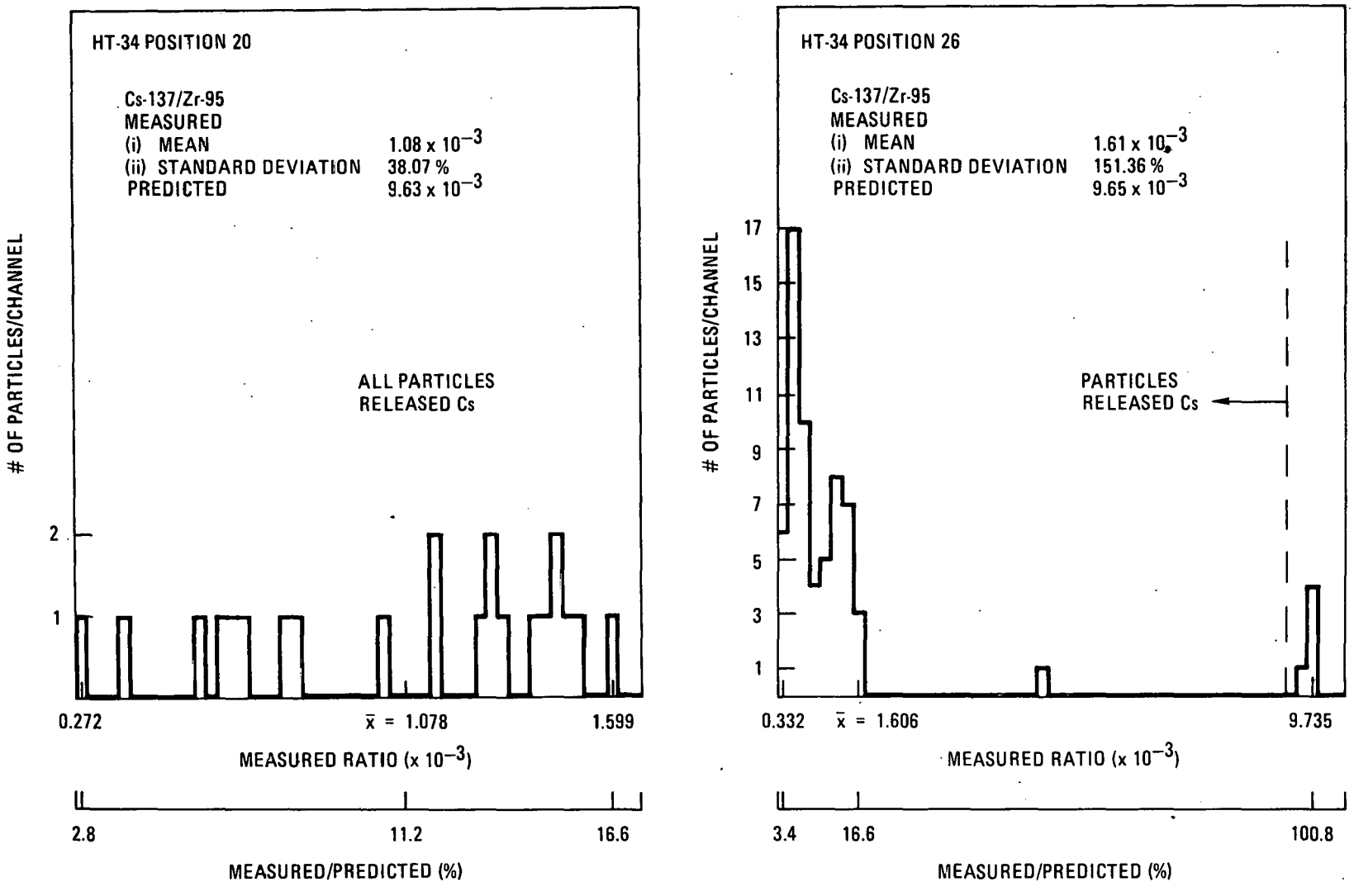

Fig. 5-11f. Histograms of Cs-137/Zr-95 ratios. The measured/predicted Cs/Zr ratios are also given. The figure indicates the particles that released Cs. (NOTE: the scale is different for each sample).

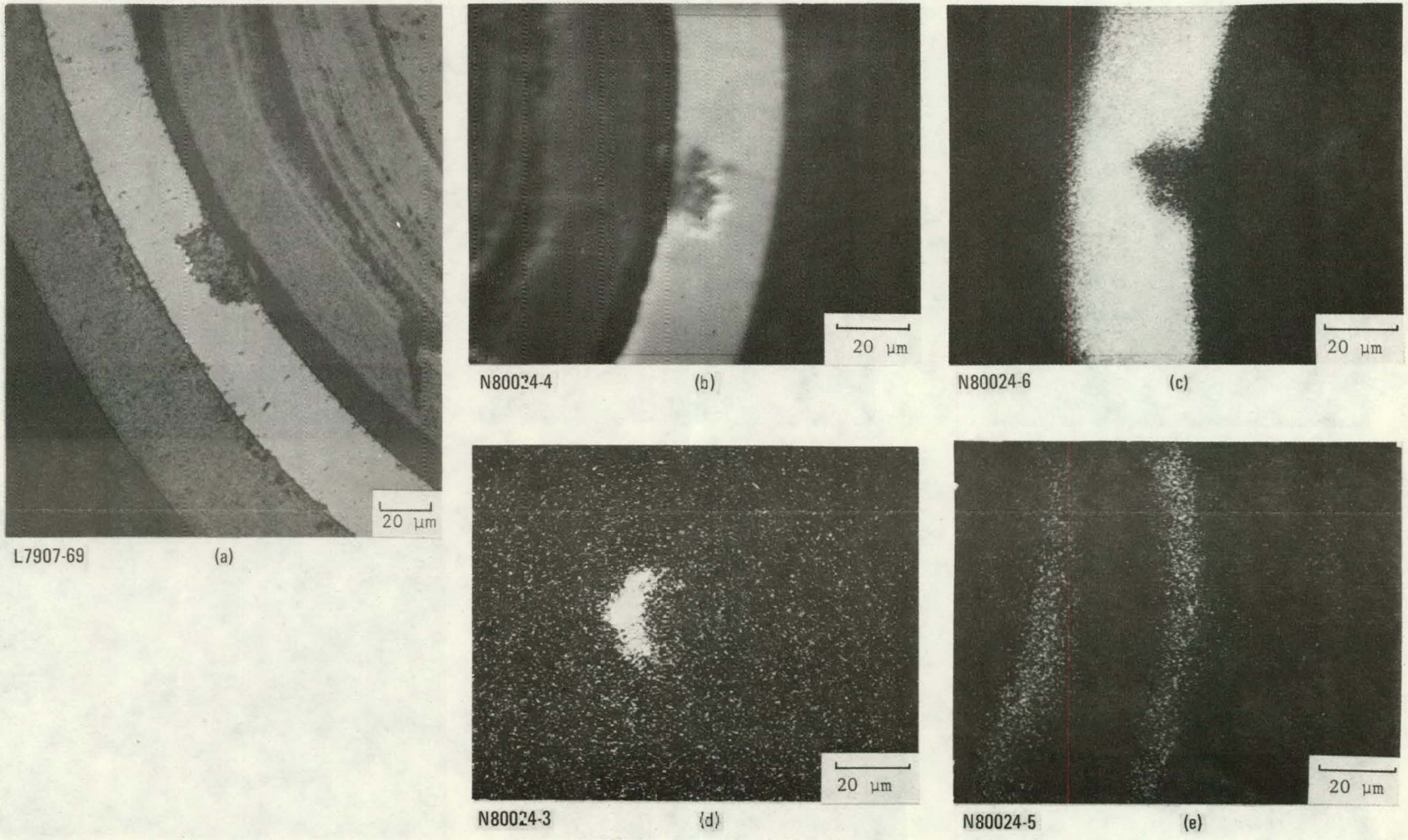

Fig. 5-12. Results of electron microprobe analysis of a SiC reaction zone of a particle (6252-14-0161-001) irradiated at 1240°C to a burnup of 7.6% FIMA and a fluence of 7.5×10^{25} n/m^2 $(E > 29\ fJ)_{HTGR}$ (a) Optical photomicrograph; (b) back-scattered electron image; (c) Si Kα; (d) Pd Lα; (e) Cl Kα

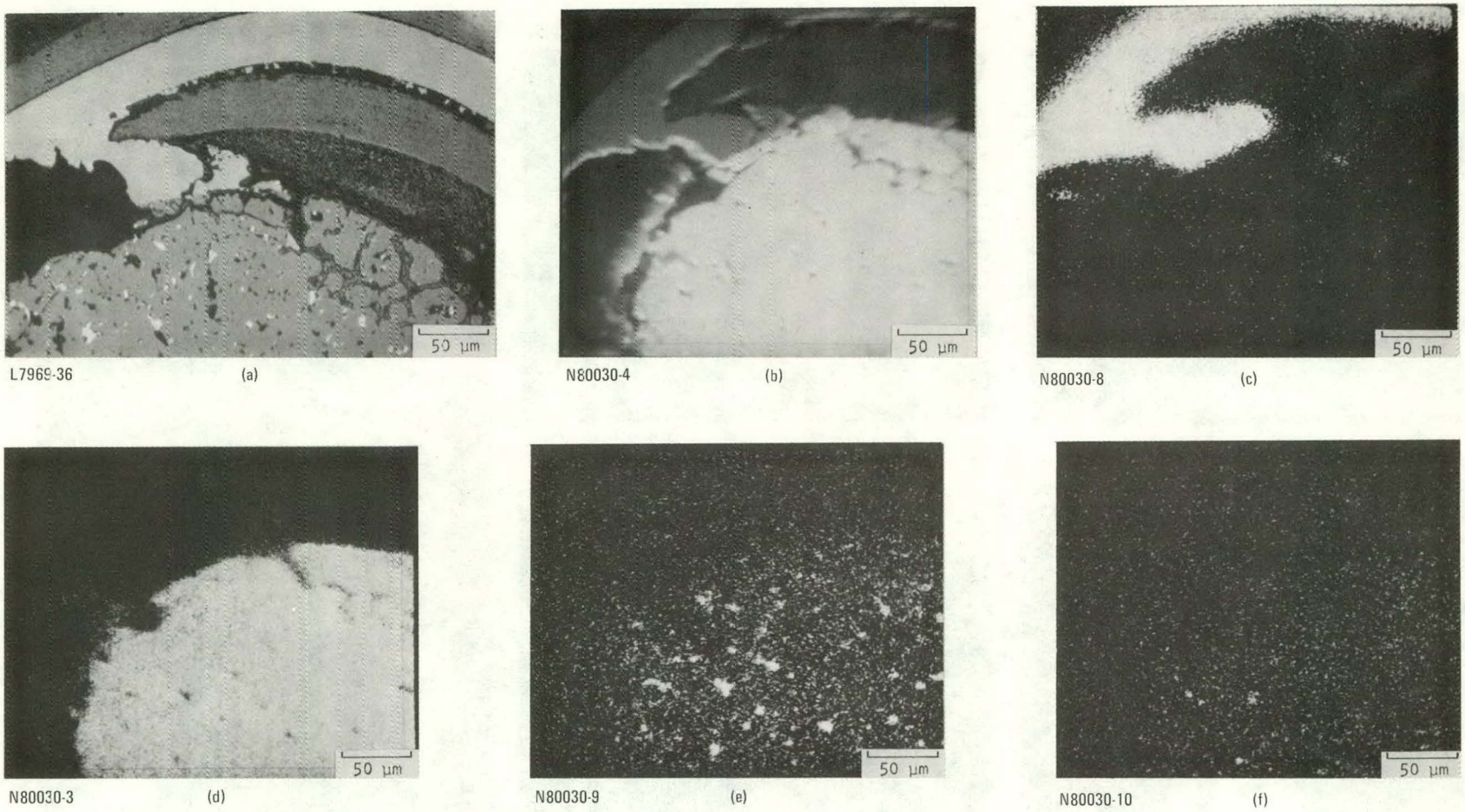

Fig. 5-13a. Results of electron microprobe examination of SiC corrosion of sample 17, irradiated at 1430°C to a burnup of 10.9% FIMA: (a) optical micrograph; (b) back-scattered electron image, (c) Si Kα; (d) Th Mα; (e) Mo Lα; (f) Ru Lα

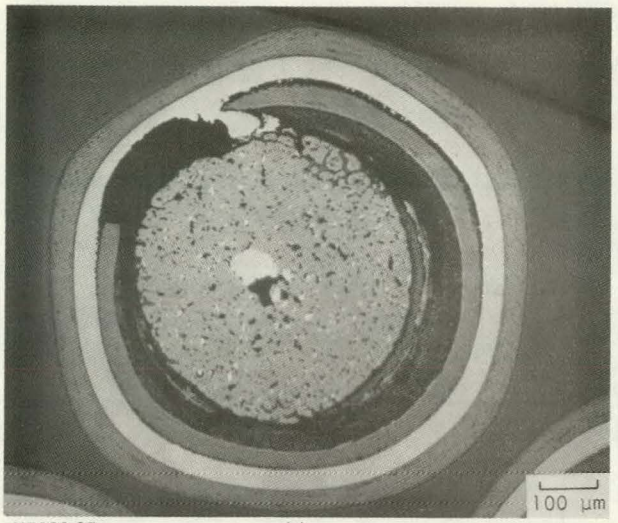

N7909-35 (a)

N80030-2 (b)

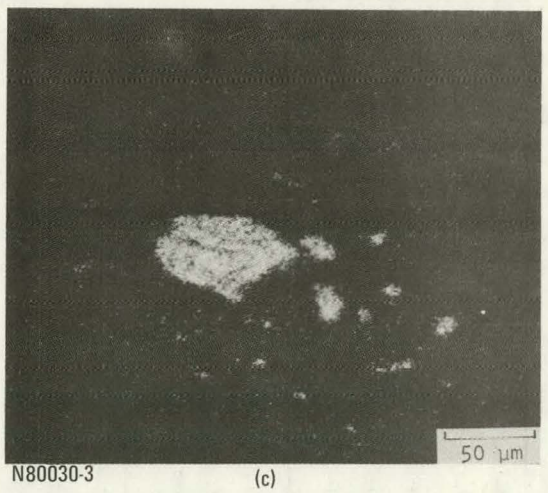

N80030-3 (c)

Fig. 5-13b. Results of electron microprobe of center of kernel of sample 17 irradiated at 1430°C to a burnup of 10.9% FIMA: (a) optical micrograph; (b) Mo Lα; (c) Ru Lα

TABLE 5-1

RESULTS OF VISUAL EXAMINATION

Capsule Position	Particle Batch Number (6252-)	Time-Averaged Temperature[a] (°C)	Fluence [x 10^{25} n/m^2 (E > 29 fJ)$_{HTGR}$]	Burnup (% FIMA)	Number of Particles Examined	OPyC Coating Failure (%)		Total Particle Failure (%)		Predicted Particle Failure (%)
						Mean	95% Confidence Limit P	Mean	95% Confidence Limit P	
Low Temperature Magazine										
2	20-0161-001	1180	5.1	5.1	56	0	$0 \leq P \leq 5.1$	0	$0 \leq P \leq 5.1$	0
4	07-0262-001	1180	5.8	5.7	57	0	$0 \leq P \leq 5.1$	0	$0 \leq P \leq 5.1$	0
5	14-0261-001	1210	6.1	6.0	56	8.9	$4.3 \leq P \leq 18$	0	$0 \leq P \leq 5.1$	59
7	14-0171-001	1230	6.7	6.7	56	0	$0 \leq P \leq 5.1$	0	$0 \leq P \leq 5.1$	51
8	13-0161-001	1220	7.0	7.0	57	0	$0 \leq P \leq 5.1$	0	$0 \leq P \leq 5.1$	0
10	14-0161-001	1240	7.5	7.6	57	1.8	$0.2 \leq P \leq 8.0$	0	$0 \leq P \leq 5.1$	0
11	15-0161-001	1250	7.7	7.9	57[b]	1.8	$0.2 \leq P \leq 8.0$	0	$0 \leq P \leq 5.1$	0
13	16-0161-001	1180	8.2	8.5	56	0	$0 \leq P \leq 5.1$	0	$0 \leq P \leq 5.1$	0
High Temperature Magazine										
15	20-0161-002	1430	9.2	10.5	30[d]	6.2[c]	$3.2 \leq P \leq 13$	6.2	$3.2 \leq P \leq 13$	0
17	07-0262-002	1430	9.4	10.9	81[d]	36[c]	$28 \leq P \leq 45$	36	$28 \leq P \leq 45$	94
18	14-0161-002	1440	9.5	11.2	81[d]	(e)	(e)	(e)	(e)	90
20	14-0271-001	1440	9.7	11.6	83[d]	71[c]	$57 \leq P \leq 87$	71	$57 \leq P \leq 87$	11
21	14-0181-001	1440	9.8	11.9	82[d]	78[c]	$64 \leq P \leq 94$	78	$64 \leq P \leq 94$	12
23	17-0161-001	1460	10.0	12.2	81[d]	(e)	(e)	(e)	(e)	9
24	15-0171-001	1450	10.1	12.4	81[d]	(e)	(e)	(e)	(e)	4
26	13-0171-001	1440	10.2	12.7	85[d]	19[c]	$13 \leq P \leq 27$	19	$13 \leq P \leq 27$	36

(a) Maximum surface temperature of particles
(b) Original sample size was 56
(c) OPyC coating failure was always observed with total particle failure
(d) Original sample sizes given because could not determine total number particles examined
(e) Could not determine due to very high coating failure (estimated to be >80%)

TABLE 5-2
RESULTS OF METALLOGRAPHIC EXAMINATION

Capsule Position	Particle Batch Number (6252-)	Time-Averaged Temperature (°C)		Fluence [$\times 10^{25}$ n/m^2 (E > 29 fJ)$_{HTGR}$]	Burnup (% FIMA)	Number of Observations								
								IPyC Coating		SiC Coating				
		Kernel	Surface			Total Sample	Kernel Migration	Failed	Debonded	Failed	Localized Attack	Porosity	Circumferential Fracture	OPyC Coating Failed
5	14-0261-001	1240	1210	6.1	6.0	16	0	9	10	0	0	0	0	0
10	14-0161-001	1280	1240	7.5	7.6	15	0	8	11	0	1[a]	8	2	0
11	15-0161-001	1300	1250	7.7	7.9	15	0	5	7	0	2[a]	13	1	0
13	16-0161-001	1230	1180	8.2	8.5	15	0	10	12	0	2[a]	12	6	0
15	20-0161-002	1490	1430	9.2	10.5	15	5	N.D.	N.D.	8	7[b]	0	0	2
17	07-0262-002	1490	1430	9.4	10.9	15	13	13	4	8	14[b]	0	0	1

[a] Penetration was: No. 10 - 18 μm; No. 11 - 9 μm (no measurement for other particles); and No. 13 - 10 and 9 μm.

[b] SiC attack had different cause and appearance than lower temperature samples.

THIS PAGE

WAS INTENTIONALLY

LEFT BLANK

TABLE 5-3
RESULTS OF γ-COATING[a] OF HT-34 SAMPLES

Capsule Position No.	No. of Particles Counted	Fission Product Activities (μCi/cm³ ThO_2)																					
		Zr-95 (724 KeV)				Cs-134 (605 KeV)				Cs-137 (662 KeV)				Ce-144 (134 KeV)				Pa-233 (312 KeV)				Ru-106 (512 KeV)			
		Measured				Measured				Measured				Measured				Measured				Measured			
		Mean (x 10^8)	Standard Deviation (%)	Predicted (x 10^8)	Difference[b] (%)	Mean (x 10^6)	Standard Deviation (%)	Predicted (x 10^6)	Difference[b] (%)	Mean (x 10^6)	Standard Deviation (%)	Predicted (x 10^6)	Difference[b] (%)	Mean (x 10^7)	Standard Deviation (%)	Predicted (x 10^7)	Difference[b] (%)	Mean (x 10^9)	Standard Deviation (%)	Predicted (x 10^9)	Difference[b] (%)	Mean (x 10^6)	Standard Deviation (%)	Predicted (x 10^6)	Difference[b] (%)
2	54	2.26	13	1.58	-30.1	2.33	13	2.07	-11.1	2.16	13	1.50	-30.6	3.98	13	3.68	-7.5	4.97	14	4.17	-16.1	ND	---	---	---
4	56	2.26	14	1.78	-21.2	2.49	14	2.40	-3.6	2.17	14	1.69	-22.1	4.03	14	4.15	-3.0	4.79	14	4.45	-7.1	ND	---	---	---
5	51	2.64	14	1.87	-29.2	2.96	15	2.56	-13.5	2.54	15	1.78	-29.9	4.71	14	4.39	-7.0	5.52	14	4.58	-17.0	ND	---	---	---
7	38	2.54	5.4	2.06	-18.9	3.21	6.5	2.86	-10.9	2.56	6.2	1.97	-23.0	4.56	4.7	4.86	6.6	4.98	5.6	4.83	-3.0	2.61	7.4	2.28	-12.6
8	56	2.65	4.5	2.15	-18.9	3.21	13	3.00	-6.5	2.44	13	2.06	-15.6	4.72	3.9	5.08	7.6	4.44	4.8	4.94	11.3	2.67	7.9	2.39	-10.5
10	53	2.97	20	2.34	-11.7	3.80	20	3.30	-13.2	2.87	20	2.24	-21.9	5.31	19	5.54	4.3	5.56	20	5.15	-7.4	3.22	20	2.62	-18.6
11	53	3.14	26	2.44	-22.3	4.03	18	3.44	-14.6	2.96	19	2.33	-21.3	5.58	27	5.78	3.6	5.70	25	5.25	-7.9	3.33	24	2.75	-17.4
13	55	3.17	3.4	2.61	-17.7	4.44	3.3	3.70	-16.7	3.10	3.4	2.50	-19.3	5.75	3.2	6.22	8.2	5.67	3.3	5.43	-4.2	3.40	5.5	2.97	-12.6
15	68	4.13	20	3.18	-23.0	0.28	301	4.48	1500	0.49	127	3.06	524	4.00	72	7.64	91.0	ND	---	---	ND	4.54	19	3.73	-17.8
17	49	4.13	2.5	3.32	-19.6	0.60	258	4.66	677	0.73	137	3.20	384	5.75	38	7.99	39.0	6.69	2.8	6.03	-9.9	ND	---	---	---
20	22	4.00	33	3.52	-12.0	0.08	78	4.92	6050	0.46	48	3.40	639	5.61	62	8.51	51.7	6.18	33	6.18	0	ND	---	---	---
26	66	4.50	15	3.83	-14.9	0.66	279	5.27	698	0.73	150	3.69	405	5.62	56	9.28	65.1	6.97	15	6.37	-8.6	ND	---	---	---

(a) Measured at ORNL in IMGA system

(b) % Difference = $\frac{\text{Predicted-measured}}{\text{Measured}} \times 100$

Note:
ND = Not determined

Blank

TABLE 5-4
FISSION PRODUCT RATIOS[a]

Position	Number of Particles	Cs-134/Zr-95				Cs-137/Zr-95				Cs-137/Ru-106				Cs-134/Cs-137				Ce-144/Zr-95			
		Measured				Measured				Measured				Measured				Measured			
		Mean	Standard Deviation (%)	Predicted Value	Ratio[b] (%)	Mean	Standard Deviation (%)	Predicted Value	Ratio[b] (%)	Mean	Standard Deviation (%)	Predicted Value	Ratio[b] (%)	Mean	Standard Deviation (%)	Predicted Value	Ratio[b] (%)	Mean	Standard Deviation (%)	Predicted Value	Ratio[b] (%)
		($\times 10^{-2}$)		($\times 10^{-2}$		($\times 10^{-3}$)		($\times 10^{-3}$)		($\times 10^{-1}$)		($\times 10^{-1}$)		($\times 10^{0}$)		($\times 10^{0}$)		($\times 10^{-1}$)		($\times 10^{-1}$)	
2	54	1.03	0.98	1.32	78.0	9.62	1.03	9.50	101.3	ND	--	--	--	1.07	1.24	1.39	77.0	1.77	1.05	2.32	76.3
4	56	1.10	1.23	1.35	81.5	9.63	1.32	9.52	101.1	ND	--	--	--	1.14	1.64	1.42	80.3	1.78	0.68	2.34	76.1
5	51	1.12	4.20	1.37	81.7	9.56	3.40	9.53	100.3	ND	--	--	--	1.17	1.79	1.43	81.8	1.78	1.17	2.35	75.7
7	38	1.26	3.86	1.39	90.6	10.00	3.71	9.55	104.7	9.86	6.23	8.64	114.1	1.25	2.49	1.46	85.6	1.79	0.94	2.35	74.0
8	56	1.21	12.14	1.40	86.4	9.20	12.66	9.56	96.2	9.12	13.58	8.60	106.2	1.32	7.28	1.46	90.4	1.78	1.27	2.36	75.1
10	53	1.28	2.58	1.41	90.8	9.66	2.23	9.57	100.9	8.93	5.82	8.53	104.7	1.32	1.45	1.47	89.8	ND	ND	2.37	ND
11	53	1.31	5.94	1.42	92.2	9.61	4.77	9.58	100.3	8.91	5.96	8.49	104.9	1.37	2.12	1.48	92.6	1.80	0.76	2.37	75.9
13	55	1.40	1.34	1.41	99.3	9.74	1.27	9.59	101.6	9.11	4.94	8.42	108.2	1.43	1.21	1.48	96.6	1.81	0.93	2.38	76.4
15	68	0.066	323	1.41	4.7	1.20	130	9.61	12.5	1.10	127	8.20	13.4	0.28	84.83	1.46	19.3	0.965	70.80	2.40	40.2
17	49	0.145	260	1.41	10.3	1.77	136	9.62	18.4	ND	--	--	--	0.32	122	1.46	22.3	1.39	38.5	2.41	57.7
20	22	0.0191	73.78	1.39	1.4	1.08	36.07	9.63	11.2	ND	--	--	--	0.17	65.30	1.45	11.7	1.33	51.40	2.42	55.0
26	66	0.143	284	1.38	10.5	1.61	151	9.65	16.7	ND	--	--	--	0.25	196	1.43	17.6	1.28	52.18	2.42	52.9

[a] Measured at ORNL in IMGA system

[b] $\text{Ratio} = \frac{\text{Measured}}{\text{Predicted}} \times 100$

TABLE 5-5
TRIGA FISSION GAS RELEASE DATA AND CALCULATED PARTICLE FAILURE

Capsule Position	Batch No. (6252-)	No. of Particles	EOL[a] Fuel Loadings (mg)		EOL[a] TRIGA Fission Gas Release (R/B)	r/b_f	No. of Particles Failed	Failure Fraction (%)
			U-233	U-235				
4	07-0262-001	56	0.26	0.06	4.4×10^{-5}	0.010	0	0
5	14-0261-001	50	0.26	0.07	4.3×10^{-5}	0.011	0	0
8	13-0161-001	56	0.24	0.07	3.2×10^{-4}	0.012	1	1.8
10	14-0161-001	56	0.24	0.08	7.3×10^{-5}	0.013	0	0
11	15-0161-001	56	0.23	0.08	2.0×10^{-4}	0.013	1	1.8
13	16-0161-001	52	0.23	0.09	7.2×10^{-5}	0.014	0	8

[a]End-of-Life

6. DISCUSSION

6.1. FISSION PRODUCT RELEASE

Fission product activities were measured in the particles of all the low-temperature and four high-temperature samples. The average measured and predicted activities (see Table 5-3) of each sample are plotted in Fig. 6-1. The activities were divided by the kernel volume to account for the differences in kernel sizes. The figure shows that the difference in measured and predicted values is relatively constant for the low-temperature samples. This difference is caused by uncertainties in the measured and predicted activities.

Zirconium is known to form a stable oxide. Therefore, in an oxide kernel, the Zr should remain in the kernel, as verified by the HT-34 results. The measured Zr activity was, on the average, 20% higher than the predicted value. This difference was relatively constant for both the low- and high-temperature samples. Figure 6-1 shows that Ru and Pa also remained in the kernel at both temperatures. However, the measured activities of Ce and Cs were significantly lower than the predicted values for the high-temperature samples. Therefore, Ce and Cs were released from the particles in those samples.

Various fission product ratios were calculated for the samples and are given in Table 5-4. Since Zr remained in the kernel even though the particle failed, this isotope could be compared to the more volatile isotopes to indicate fission product release and particle failure. Table 5-4 compares the measured fission product ratios, such as Cs/Zr, to the predicted ratios. The table shows that Cs and Ce were lost from the high-temperature samples. An average of 32% Ce was lost from the particles irradiated at ~1435°C based on comparing the low- and high-temperature Ce/Zr measured and predicted ratios.

The ratio of Cs-137 to Zr-95 was selected to evaluate in detail the particle failure of the capsule HT-34 samples. After studying the distributions of the Cs/Zr ratios (see Fig. 5-11), it was observed that the ratios were either relatively normally distributed or skewed to the lower Cs/Zr ratios. For example, sample 13 was normally distributed, and sample 11 was skewed. The conclusion was that some particles lost part of their Cs inventory. The question then arose as to how to determine the number of failed particles. It seemed logical that particles that had less than a certain measured Cs/Zr ratio were failed. The solution then was to find the lower limit of the Cs/Zr ratio of nonreleasing particles. To compare the 12 samples, the measured Cs/Zr ratios were normalized by dividing them by the predicted Cs/Zr. This new ratio will be written as (Cs/Zr)M/P, and is reported in Table 5-4.

The means and standard deviations of the (Cs/Zr)M/P ratio of the 1200°C samples were plotted in Fig. 6-2. The means of samples 2, 4, 10, and 13 were all about 101%, and the standard deviations were the smallest of the group. If there were no particle failures and predictions and the activity measurements were perfect, the ratio would be 100% for all samples. Samples 5, 8, and 11 had higher standard deviation and lower means because some particles had apparently released Cs. The ratio for sample 7 was exceptionally high for some unknown reason. Figure 5-13 shows that the Cs/Zr ratio of samples 2, 4, 10, and 13 had approximately normal distributions. The other four had skewed distributions. The assumption was then made that the particles from samples 2, 4, 10, and 13 had not released any Cs.

The next step was to determine the lower limit of (Cs/Zr)M/P for nonreleasing particles. Samples 2, 4, 10, and 13 were selected to be an internal standard. The mean and standard deviations of the total group of these particles were calculated to be 101.2% and 1.54% (of mean), respectively. For a large population of nonreleasing particles, $\geq$99.9% of the particles would have a ratio $\geq$95.8% at a 95% level of confidence, based on the internal standard.

The number of particles that released Cs-137 was then determined for the other samples. The (Cs/Zr)M/P values calculated for all the particles of each sample were compared to the lower limit of (Cs/Zr)M/P of nonreleasing particles (95.8%). An assumption was made that the mean of the nonreleasing group of particles of the samples that had some failed particles was the same (101.2%) as the internal standard. Since the mean ratio should ideally be 100%, all the (Cs/Zr)M/P ratios were then normalized to 100%. The lower limit of the (Cs/Zr)M/P of the nonreleasing particles was also normalized (94.6%). The range of (Cs/Zr)M/P ratios of each sample is plotted in Fig. 6-3. The number of particles above and below the normalized lower limit is given. The particles above the line were assumed to have retained all their Cs. The particles below the line lost part of their Cs inventory.

The results of the fission product failure analysis are summarized in Table 6-1. Six percent to 21% of the particles in four of the low-temperature samples released Cs. The SiC coating had failed in these particles. The SiC coating was designed to fail mechanically for samples 5 and 7 (thin buffer coatings). The SiC failure in samples 8 and 11 was not expected. The metallographic examination of sample 11 (sample 8 not examined) showed a fine porosity in the SiC coating. If the pores were interconnected, Cs may have migrated through the SiC coating in samples 8 and 11. Most of the OPyC coatings were visibly intact (examined at 20 x) on samples 7, 8, and 11 (see Table 6-1). Myers (Ref. 26) calculated that the Cs could not have diffused completely through an intact pyrocarbon coating in the time the samples were irradiated. Therefore, the Cs must have escaped through defects, possibly irradiation-induced microcracks, in the OPyC coating. The gas permeability of BISO ThO_2 particles irradiated in capsules P13R and P13S was partially attributed to microstructural cracking (Ref. 4). As-coated defects in the OPyC coating may have also caused the permeable coating. Since the OPyC failure was higher than the SiC coating failure for sample 5, the Cs may have escaped in particles with failed OPyC coatings. Sample 10, which was irradiated at approximately the same temperature as sample 11, apparently did not develop defects in the OPyC coating. The

metallographic examination indicated this sample also had porous SiC coatings, but no Cs was released from the particles.

The approach used to determine the particle failure appeared reasonable when the calculated lower limit (94.6%) for (Cs/Zr)M/P of nonreleasing particles was drawn on the histograms given in Fig. 5-11. For the high temperature samples (15, 17, 20, and 26) the obviously failed particles were well below the lower limit line, while a few particles were above the line. These few particles had not released any Cs. Looking at the distributions of samples 5 and 11, the point where the lower limit line divided the samples between releasing and nonreleasing particles seemed reasonable. The ratios of the failed particles were definitely separated from the ratios of the intact particles. There could be some argument that the number of failed particles determined for samples 7 and 8 may be overpredicted by one particle, because the Cs/Zr ratio of one of the failed particles is very close to the ratio of an intact particle.

Most particles in the high temperature samples released Cs. Although the SiC coating was failed, the OPyC coating had remained intact. Myers (Ref. 26) calculated that Cs could readily diffuse through the OPyC coating at the irradiation temperature of ~1450°C. The metallographic examination clearly showed the SiC coating failure was primarily caused by a chemical attack of the SiC rather than by a gas pressure buildup. Therefore, the Cs penetrated through the SiC coating and either diffused through the OPyC or migrated through defects in the OPyC coating.

The measured Cs retention by the particles was compared with predicted retention by the kernel. The predictions yielded a lower limit to the Cs retained by the particles. The true value of Cs retained by the particles would be given by the sum of (1) the Cs retained by the kernel and (2) the Cs retained by the coatings.

The calculations of the Cs retention by the kernel was based on a preliminary analysis of in-pile fission product release from the kernels of

intact particles (Ref. 27). The Cs retained by the kernel was obtained from the relation (Ref. 26):

$$fr = 1.0 - 2.95 \times 10^{-5} F^2 \sqrt{t}\, e^{-4680/T} \quad \text{for } fr > 0$$

where fr = fraction of Cs retained by the ThO_2 kernel
F = burnup (% FIMA)
t = time (s)
T = temperature (K)

The predicted values of Cs retention derived from the above equation are given in Fig. 6-3 and in Table 6-2. As shown in Fig. 6-3, they are consistent, in general, with the observed values. For all sample positions shown except 15 and 17, the mean value of the observed Cs retentions of the failed particles is approximately equal to or greater than the predicted ones; it will be recalled that the predicted values are only lower limits to the true values of Cs retention. For sample positions 5, 7, 8, and 20, where the observed mean and the predicted Cs retentions are similar, it is implied that all the Cs released from the kernel during the irradiation period escaped from the failed particle by the end of the irradiation.

For sample positions 15 and 17, less Cs was retained by the kernel than predicted. If the predictions of Cs retention are correct, as an analysis of the data of HT-33 (Ref. 16) indicate, this implies an additional contribution to Cs release in these cases. It is known that extensive kernel migration occurred in particles in these positions (see Fig. 5-10, for example), and it is possible that this phenomenon or associated processes are the cause of the increased fission product release from the kernel (Ref. 26). However, this requires a reexamination of the results in Fig. 3-6 for sample positions 20 and 26.

Since extensive kernel migration was observed in samples in positions 15 and 17 (see Table 5-2), similar results would be expected in positions 20 and 26. Unfortunately, such measurements were not made for the particles in

the latter positions. Nevertheless, it is reasonable to assume extensive kernel migration for the particles in sample positions 20 and 26 and to expect, therefore, predicted Cs retentions greater than observed. While the actual predictions of Cs retention are smaller than observed, the predictions are based on an approximation whose validity decreases as the fractional retention decreases. Consequently, if more precise equations were used, it is likely that the predicted Cs retentions for particles of sample positions 20 and 26 would be larger than shown in Fig. 6-3 and possibly larger than the mean of the observed values for these positions (Ref. 26).

6.2. CHEMICAL PERFORMANCE

The chemical performance of the TRISO ThO_2 particles was primarily evaluated by the metallographic examination of four 1200°C and two 1450°C samples. SiC coating reactions and kernel migration were observed. A total of 61 particles was examined.

The TRISO ThO_2 particles irradiated to 1200°C had no kernel migration as predicted. However, unexpected corrosion of the SiC coating was seen. The microstructure of the areas of corrosion took the form of either a localized attack or a fine porosity.

The localized chemical attack of the SiC coating was observed in 5 out of 46 particles. The maximum penetration of the SiC was 18 μm. Palladium was detected in the reaction zone by the electron microprobe examination. Also, Cl was measured along the inner surface of the SiC. Palladium attack has been observed several times in TRISO fissile particles (Ref. 28). Palladium attack in TRISO ThO_2 fuel has not been reported before. However, Pd attack was recently observed in the TRISO ThO_2 particles irradiated in capsule HRB-14 (Ref. 29) at approximately the same temperatures as HT-34.

The chemical attack of the SiC coating was unexpected, because the number of Pd atoms per particle was significantly less than HEU or LEU fissile particles. Table 6-3 gives the number of Pd atoms per particle for the

samples examined metallographically. SiC attack was observed in three 1200°C samples that had 5.6 to 6.4 x 10^{14} Pd atoms per particle formed during irradiation. SiC attack was observed in HRB-14 TRISO ThO_2 particles having 7 x 10^{14} Pd atoms per particle (Ref. 29); the results of both capsules are in good agreement. As a comparison of fissile and fertile particles, the UO_2 particles irradiated in capsule HRB-14 had 6.4 x 10^{15} Pd atoms per particle. Previous experimental observations have indicated that the Pd must concentrate in local regions near the SiC coating before SiC corrosion will occur (Ref. 30). The HT-34 results support this, because the attack only had occurred when the Pd had concentrated. If the Pd concentration could be prevented, the Pd attack of the SiC coating would be minimized (Ref. 30).

The current model for predicting changes in SiC thickness due to fission product attack was revised. The predicted HT-34 corrosion SiC thinning, based on the square root of time, is given in Ref. 31. A comparison of these data and the HT-34 corrosion measurements showed that the Pd penetration in the SiC coating was higher than the upper 90% confidence level of the referenced data. The data are shown in Fig. 6-4. The poor correlation could be attributed to the uncertainties of the measurements and the temperatures.

The other type of SiC corrosion at 1200°C was the porosity around the entire SiC coating. The small pores were located radially across the SiC coating, but were concentrated near the inner surface. The porosity was not dependent upon a thermal gradient. The cause of this corrosion is uncertain. Chlorine may have contributed to the corrosion, since it was measured by electron microprobe around the inner surface of the SiC. Brown and Faircloth (Ref. 32) observed similar porosity in TRISO low-enriched UO_2 irradiated at 1550°C to a burnup of 4% FIMA. Strontium was detected in the reaction zone. The corrosion seen in HT-34 may be batch dependent. TRISO ThO_2 particles were irradiated in capsule HT-33 under the same irradiation conditions as those of HT-34. The HT-33 samples were from different production coating runs, but were made to about the same design specifications as

the HT-34 samples. Two samples tested at 1200°C in HT-33 were examined and no SiC corrosion was observed (Ref. 16). Porosity was observed in a different batch tested at 1420°C in HT-33, but was not observed in two other batches tested at 1430°C in HT-34.

SiC porosity has also been observed in an irradiated particle sample heated in an out-of-pile thermal gradient experiment (Ref. 33). The sample was from a TRISO ThO_2 batch irradiated in capsule P13S. No porosity-type corrosion was seen in the SiC coating (Ref. 4) before heating. After the particles were heated for 2592 h at 1520°C, porosity had formed in the SiC coating.

Corrosion of the SiC coating was observed in the two samples irradiated at 1430°C. The corrosion apparently caused the SiC coating to fail in most particles. Similar corrosion was seen in three samples irradiated in capsules HT-31 and HT-33 (Ref. 16) at approximately the same temperatures. The corrosion occurred at the hot side of the particles. No fission products were detected in the reaction zone of the SiC coating. The SiC attack was most likely caused by either oxidation or a reaction with Cl. Thermodynamic predictions (Ref. 35) show that oxidation at the SiC coating would occur at the hot side of the particle. Corrosion was previously noted in TRISO UO_2 particles irradiated at 1250° and 1500°C and was hypothesized to be caused by oxidation (Ref. 36). However, a chemical reaction with Cl may have occurred instead. In a thermal-gradient annealing experiment at 1360° and 1440°C, SiC corrosion of unirradiated UC_2 particles had occurred at the hot side of the particles. The corrosion was attributed to Cl attack (Ref. 37). It should be noted that no Pd attack was observed in the HT-34 particles irradiated at 1430°C.

As expected, kernel migration had occurred. The maximum migration distance was measured to be 60 μm for sample 17. The kernel migration coefficient (KMC) was calculated to be 4.8×10^{-10} ($m^2 \times k/s$) at an average kernel temperature of 1490°C. This KMC value falls within the predicted range for the KMC at the 90% confidence level (Ref. 34).

6.3. MECHANICAL PERFORMANCE

The mechanical performance of the 1200°C samples was evaluated by characterizing the pressure vessel and OPyC coating failure. A summary of the failure of the TRISO ThO_2 particles irradiated in HT-34 is given in Table 6-1. The mechanical performance of the 1450°C samples will not be discussed because of the high SiC failure caused by chemical corrosion.

Visual and metallographic examinations and fission gas and fission product release measurements were used to evaluate coating failure for the HT-34 samples. None of the measurement methods may have given an accurate measure of the SiC coating failure, because the OPyC coating remained intact on most particles. The best indication of the SiC failure was determined by the Cs release measurements.

The most obvious result was that the pressure-vessel performance model over-predicted the failure of the two thin buffer coatings (samples 5 and 7). Figure 6-3 shows that 6 out of 89 particles (7%) were failed. For an infinite population, this failure would be $\leq$12% at 95% confidence. The predicted failure was ~55%. These results imply that there is considerable margin within the existing TRISO ThO_2 designs for increasing heavy metal fuel density.

As discussed in Section 3.1.1, the frequency of flaws was varied for samples 5 and 7. Increasing the flaw frequency from 9% to 29% did not increase the SiC failure, and therefore did not apparently affect the particle performance.

Although no pressure-vessel failure was predicted for the other six low-temperature samples, SiC failure was observed in two of the samples (see Table 6-1). However, the loss of integrity was apparently a chemical rather than a mechanical failure, as discussed in Section 6.1. The visual examination indicated zero pressure-vessel failure. It is concluded that no

pressure-vessel failure occurred in the particles; this is in good agreement with the model predictions.

The FGR measurement on sample 8 indicated that at least one particle failed, even though the OPyC coatings were all visibly intact. This result suggests that the OPyC coating had defects that allowed Kr to escape, which is consistent with the fission product release analysis discussed in Section 6.1.

The failed HT-34 particles, based on Cs release, were not visibly cracked, but rather were permeable to metallic and gaseous fission products. No data presently exist to predict the fission gas released from a permeable TRISO particle. Therefore, the FGR data cannot be used to determine accurately the particle failure fractions.

The OPyC coating failure was measured by a visual examination at 4x and 20x. Five samples had zero failure, and three had 1.8% to 8.9% failure. Batch 6252-15-0161-001 (sample 11) was the only sample having an OPyC coating that completely met the HTGR specification (Ref. 38). The OPyC failure was 1.8% for this batch. The OPyC failure of all other samples having ~800 μm diameters (candidate design for the FSV reactor) was <1.8%. These failures were less than the expected OPyC failure of 3% for HTGR particles (Ref. 9). The OPyC failure did not correlate with the OPyC properties of density, anisotropy, coating rate, microporosity, and active coating gas. The same results were observed for capsules HT-31 and HT-33 (Ref. 16). The lack of correlation is not surprising, because a narrow range of OPyC properties were tested and the sample sizes were small.

Capsule HT-34 was the first capsule to test TRISO particles that had H_2-diluted OPyC coatings. Samples 8, 10, 11, and 13 were reference-size particles. These four samples were compared to similar particles, except the OPyC was deposited using Ar dilution, irradiated at 1200°C in capsules HT-31 and HT-33. The amount of OPyC failure was similar for the two diluent

types. This indicates the similarity in irradiation performance of OPyC coatings deposited using H_2 or Ar diluent.

The effect of size on the OPyC coating performance (see Section 3.1.1) was evaluated. OPyC coating failure may increase with total diameter. Sample 2 had a total diameter of 862 μm and had no OPyC coating failure. The sample was irradiated to a fluence 5.1×10^{25} n/m^2 (E > 29 fJ) HTGR at a temperature of 1180°C. The increase in particle diameter from 800 to 862 μm did not cause OPyC coating failure at these irradiation conditions.

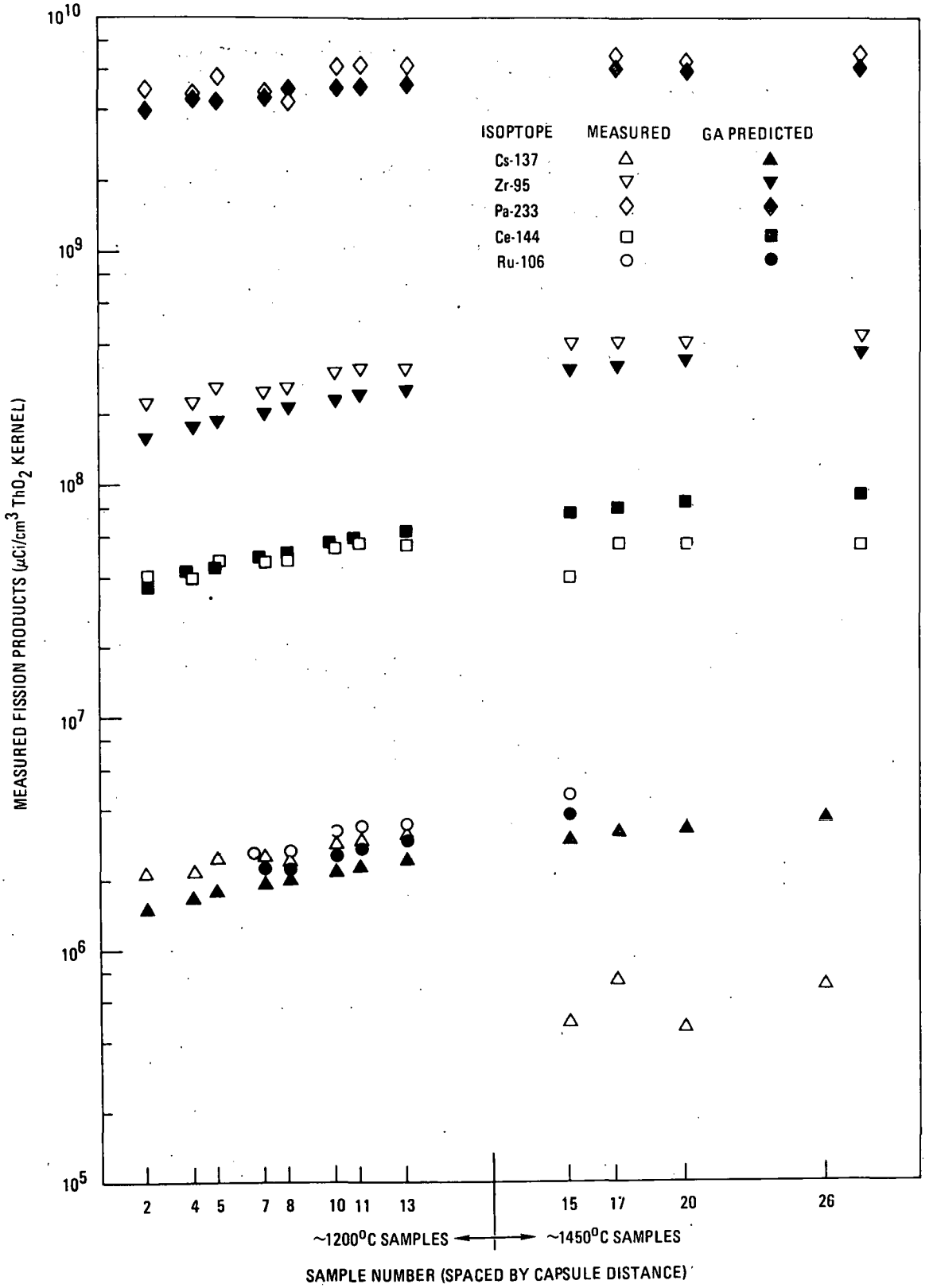

Fig. 6-1. Measured and predicted fission products of capsule HT-34 samples

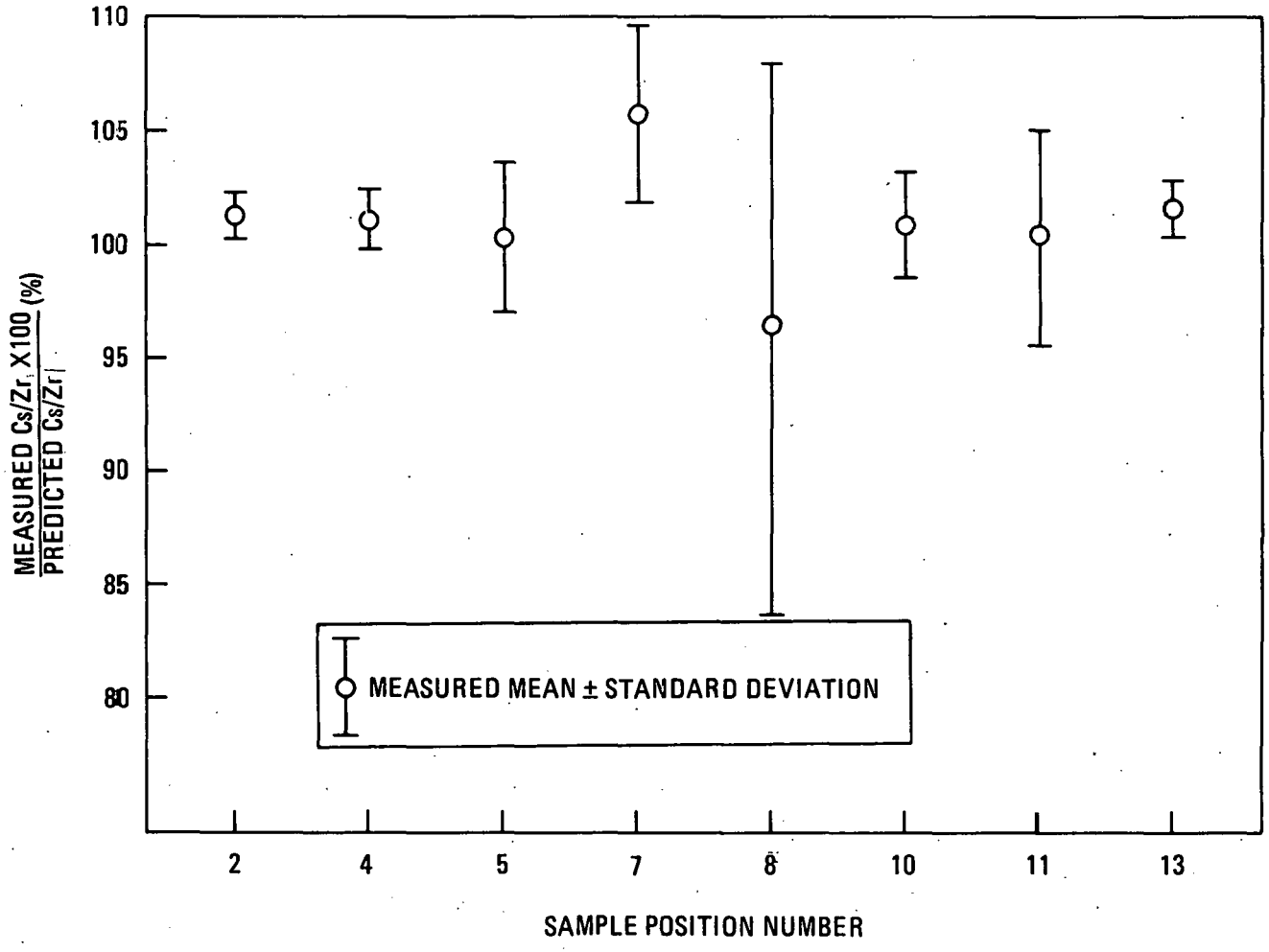

Fig. 6-2. Ratios of measured to predicted C-137/Zr-95 ratio of 1200°C samples

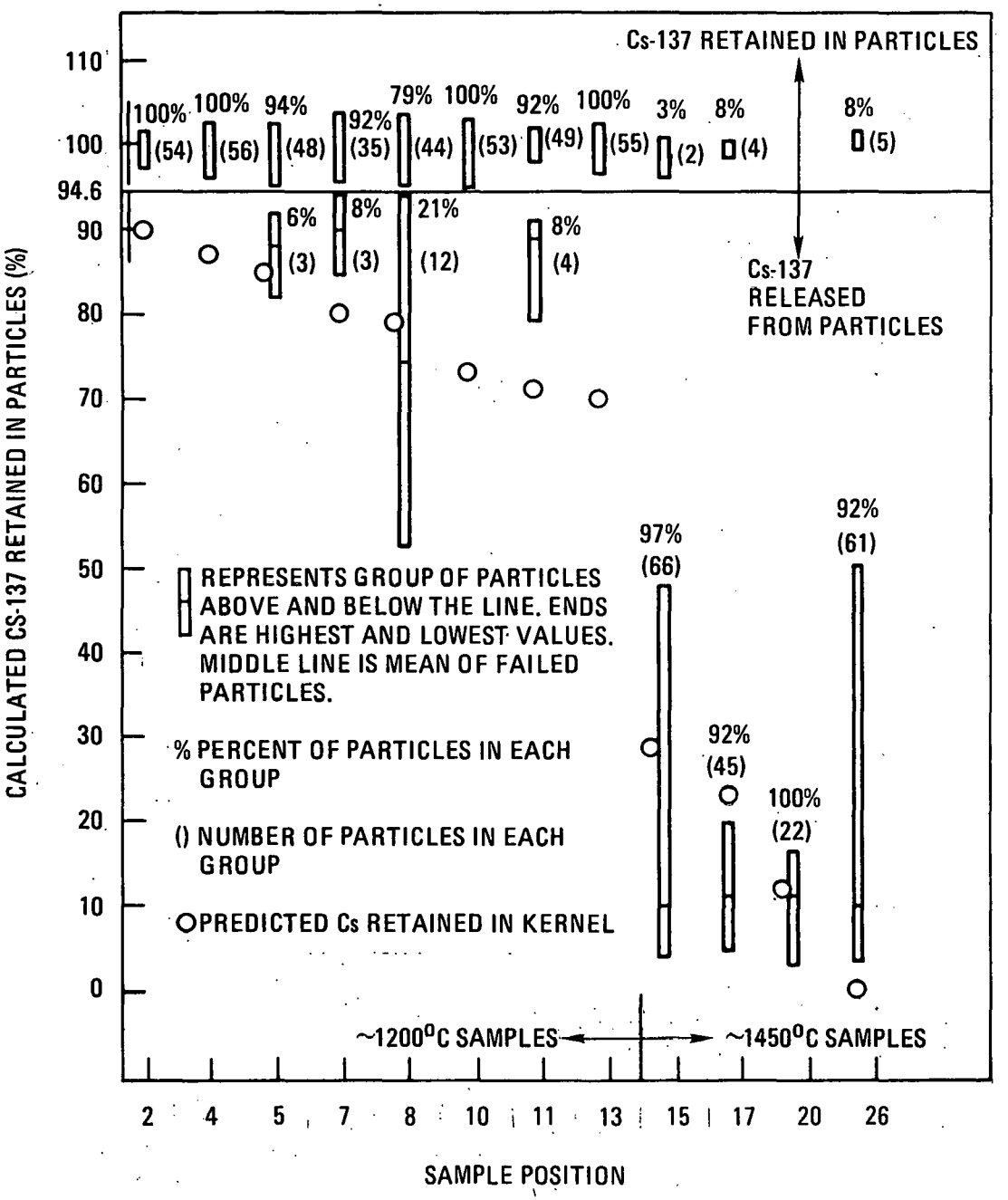

Fig. 6-3. Calculated amount of Cs-137 retained (measured Cs/Zr/predicted Cs/Zr) in particles from each sample

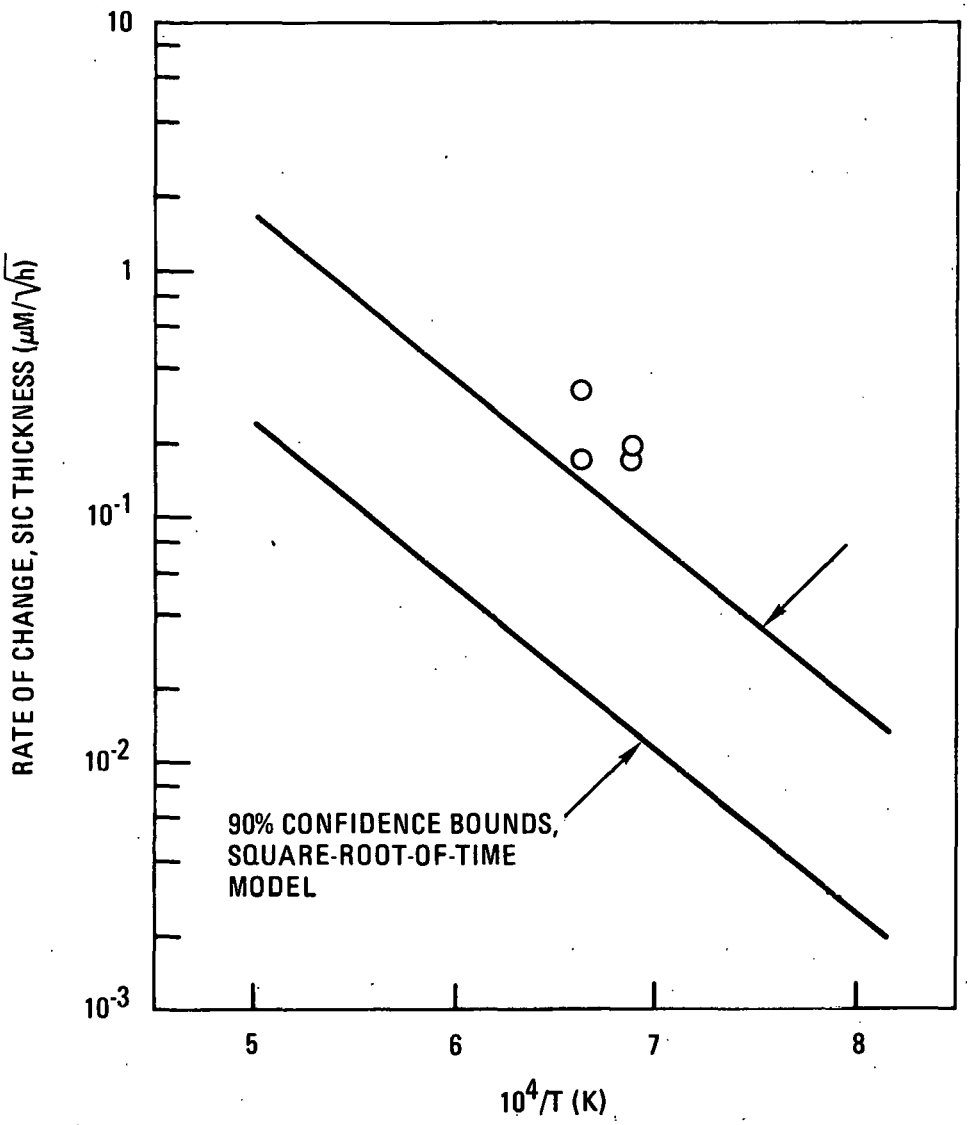

Fig. 6-4. Graph of SiC thinning versus temperature. The points given are the amount of SiC fission product attack measured on metallographic polished sections of HT-34 TRISO ThO_2 particles. The solid lines are the bounds of the square-root-of-time model for SiC thinning (Ref. 31).

TABLE 6-1
SUMMARY OF COATED PARTICLE FAILURE OF TRISO ThO_2 SAMPLES

Capsule Position	Particle Batch No. (6252-)	Coating Variables: Buffer Thickness (μm)	SiC Flaw Frequency (%)	OPyC Coating: Density (Mg/m^3)	OPyC Coating: BAF_o	OPyC Coating: OPyC Micro-porosity (mℓ/kg)	OPyC Coating: Coating Rate (μm/min)	Irradiation Conditions: Time-Averaged Temp. (°C)	Irradiation Conditions: Fluence [x 10^{25} n/m² (E > 29 fJ)$_{3TGR}$]	Irradiation Conditions: Burnup (% FIMA)	Predicted Particle Failure (%)	Visual Examination: OPyC Failure[a] (%)	Visual Examination: Total Particle Failure[a] (%)	Metallo-graphic Examination Total Particle Failure[a]	Failure Based on Kr Release[a,b] (%)	Failure Based on Release[a,c] (%)
Low Temperature Magazine																
2	20-0161-001	83	6	1.98	1.041	59	8.4	1180	5.1	5.1	0	0 (56)	0 (56)	ND	ND	0 (54)
4	07-0262-001	60	38	1.80	1.027	48	5.0	1180	5.8	5.7	0	0 (57)	0 (57)	ND	0 (56)	0 (56)
5	14-0261-001	27	29	1.97	1.040	54	7.1	1210	6.1	6.0	59	8.9 (55)	0 (56)	0 (16)	0 (16)	6 (51)
7	14-0171-001	35	9	1.97	1.041	57	7.1	1230	6.7	6.7	51	0 (56)	0 (56)	ND	ND	8 (38)
8	13-0161-001	57	16	1.79	1.031	57	8.3	1220	7.0	7.0	0	0 (57)	0 (57)	ND	1.8 (56)	21 (56)
10	14-0161-001	63	9	1.97	1.041	57	7.6	1240	7.5	7.6	0	1.8 (57)	0 (57)	0 (15)	0 (56)	0 (53)
11	15-0161-001	56	12	1.81	1.033	21	5.0	1250	7.7	7.9	0	1.8 (57)	0 (57)	0 (15)	1.8 (56)	8 (53)
13	16-0161-001	57	12	1.96	1.048	25	5.3	1180	8.2	8.5	0	0 (56)	0 (56)	0 (15)	0 (52)	0 (55)
High Temperature Magazine																
15	20-0161-002	82	6	1.98	1.041	59	8.0	1430	9.2	10.5	0	6.2 (83)	6.2 (80)	53 (15)	ND	97 (68)
17	07-0262-002	57	38	1.80	1.027	48	5.6	1430	9.4	10.9	94	36 (81)	36 (81)	53 (15)		92 (49)
18	14-0161-002	62	9	1.97	1.041	57	7.6	1440	9.5	11.2	90	(d)	(d)	ND		ND
20	14-0271-001	86	29	1.97	1.040	54	8.0	1440	9.7	11.6	11	71 (83)	71 (83)			100 (22)
21	14-0181-001	91	10	1.97	1.041	57	8.1	1440	9.8	11.9	12	78 (82)	78 (82)			ND
23	17-0161-001	80	6	1.95	1.049	28	5.0	1460	10.0	12.1	9	(d)	(d)			ND
24	15-0171-001	84	12	1.81	1.033	21	5.6	1450	10.1	12.4	4	(d)	(d)			ND
26	13-0171-001	79	16	1.79	1.031	57	8.5	1440	10.2	12.7	36	19 (85)	19 (85)			92 (66)

[a] Numbers in parentheses are numbers of particles measured.

[b] Measured using TRIGA reactor.

[c] Measured using ORNL IMGA system.

[d] Could not determine due to very high coating failure (>80%).

NOTE: ND = Not determined

TABLE 6-2
COMPARISON OF PREDICTED AND MEASURED Cs RETAINED IN FAILED TRISO ThO_2 PARTICLES IN CAPSULE HT-34

Sample Position	Time-Averaged[a] Kernel Temperature (°C)	Burnup (% FIMA)	Cs Retained (%)	
			Measured[b]	Predicted[c]
5	1240	6.0	88	85
7	1270	6.7	90	80
8	1260	7.0	74	79
11	1300	7.9	84	71
15	1490	10.5	10	29
17	1490	10.9	11	23
20	1500	11.6	11	12
26	1500	12.7	10	0

[a]Time of irradiation was 9.67×10^6 sec
[b]Average of failed particles (see Fig. 6-3)
[c]Predicted Cs retained from ThO_2 kernel

TABLE 6-3
COMPARISON OF SiC ATTACK AND Pd PER PARTICLE OF TRISO ThO_2 PARTICLES

Irradiation Conditions[a]			Number of Pd Atoms per Particle x 10^{14}	Maximum Pd Penetration[b] in SiC (μm)
Sample No.	Surface Temperatures (°C)	Burnup (% FIMA)		
5	1210	6.1	4.6	0
10	1240	7.5	5.6	18
11	1250	7.7	5.9	9
13	1280	8.2	6.4	10
15	1430	9.2	7.8	0
17	1430	9.4	8.1	0

(a) Total irradiation time 2686 hours

(b) Measured on metallographic polished section

7. SUMMARY AND CONCLUSIONS

The summary and conclusions of the evaluation of TRISO coated 450 μm-ThO_2 particles irradiated in capsule HT-34 are the following:

1. The particle performance model over predicted the pressure-vessel failure for the two 30-μm-thick-buffer samples irradiated at 1200°C to a burnup of 6.7% FIMA. The results showed that the model predictions were conservative. The predicted and observed pressure-vessel failure of the other 1200°C samples was zero.

2. The OPyC coating failure of the ~800 μm-diameter particles (candidate design for FSV) was <1.8% for the samples irradiated at ~1200°C to a fluence of 5.8 to 8.2 x 10^{25} n/m^2 $(E > 29\ fJ)_{HTGR}$ and was less than the expected failure (3%) for HTGR particles.

3. The H_2-diluted OPyC coatings had irradiation performance similar to the Ar-diluted coatings at 1200°C.

4. The variation of flaw frequency in the SiC coating did not apparently have any effect on pressure-vessel failure.

5. Two types of chemical attack of the SiC coating occurred in the 1200°C samples. Localized attack penetrated the SiC to a maximum of 18 μm and was caused by Pd. The other type of attack was in the form of a fine porosity around the circumference of the SiC. The pores were observed across the entire SiC thickness, but were concentrated on the inner surface. The corrosion may have been caused by Cl or fission products.

6. The SiC coating of the 1450°C samples was locally attacked at the hot side of the particle. The corrosion was most likely due to oxidation or Cl attack. In most particles, the attack failed the SiC coating.

7. The kernel migration was measured to be a maximum of 60 μm in particles irradiated at 1430°C to a burnup of 10.5% FIMA. This migration distance was in good agreement with prediction.

8. In half of the 1200°C samples, 6% to 29% of the particles released Cs. Porosity in the SiC coating and as-coated or irradiation-induced defects in the OPyC coating apparently caused the release of Cs.

9. Almost all of the particles irradiated at ~1450°C released Cs, because the SiC coating had chemically corroded.

10. The observed amount of Cs retained by failed particles was compared to the predicted Cs retained in the ThO_2 kernels. At ~1200°C, there was good agreement. At 1450°C, the agreement was fair. It was speculated that kernel migration may have caused an increase in Cs release in the 1450°C samples.

8. ACKNOWLEDGMENTS

The authors wish to acknowledge the following GA personnel:

P. R. Macy and E. T. Kuzuma for the preparation of the capsule samples and reduction of the preirradiation quality-control data; R. P. Vanek and R. O. Whipple for manufacturing the fuel; M. D. Cronin for calculating pressure vessel model studies; M. D. Caddell for engineering calculations and data reduction of the postirradiation data; W. E. Simpson for the hot cell metallography; B. Myers for help in the fission product analysis; O. M. Stansfield, W. J. Scheffel, and C. L. Smith for technical advice; R. Portwood for editing this document; and the Technical Typing staff for their most efficient and expert preparation of this document.

We also express our gratitude to all the personnel at Oak Ridge National Laboratory who assisted throughout the testing of the fuel in capsule HT-34. In particular, we acknowledge the following people: K. R. Thoms for planning of the capsule operation, in-reactor operation, and operating history analysis; M. J. Kania and A. M. Howard for thermal analysis; E. L. Ryan and the staff of the High Radiation Experiment Laboratory for capsule disassembly and visual examination; E. L. Long for his invaluable help in coordination of the entire irradiation experiment and for his technical advice; T. N. Tiegs for gamma counting the GA samples using IMGA, his patience and expertise in interpreting and evaluating the gamma scan data, and coordination of the electron microprobe examination and evaluating the microprobe results; and T. J. Hansen for the electron microprobe examination.

9. REFERENCES

1. Kovacs, W. J., et al., "Preirradiation Report of TRISO and BISO-Coated ThO_2 Particles for Irradiation in Capsules HT-31 and HT-33," ERDA Report GA-A13923, General Atomic Company, November 1976.
2. Long, E. L., et al., Irradiation Performance of HTGR BISO Fertile Particles in HFIR Experiments HT-17, -18, and -19," DOE Report ORNL/TM-6414, Oak Ridge National Laboratory, November 1978.
3. Scott, C. B., and D. P. Harmon, "Postirradiation Examination of Capsule F-30," ERDA Report GA-A13208, General Atomic Company, April 1975.
4. Scott, C. B., et al., "Postirradiation Examination of Capsules P13R and P13S," ERDA Report GA-A13827, General Atomic Company, October 1976.
5. Whipple, R. O., "Batch Size Vs. Coating Properties in the 24-Cn Dry Coater-I," General Atomic Company unpublished data, May 31, 1977.
6. "FSV Fuel Specification," General Atomic Company unpublished data.
7. Miller, C. M., "Preirradiation Characterization of FSV Fuel Test Elements FTE-1 Through FTE-8," General Atomic Company unpublished data, May 1, 1980.
8. Harmon, D. P., and C. B. Scott, "Development and Irradiation Performance of LHTGR Fuel," ERDA Report GA-A13173, General Atomic Company, October 1975.
9. Kovaks, W. J., et al., "Technical Support Document for Issue C of the HTGR Fuel Product Specification," General Atomic Company unpublished data, August 1979.
10. Kaae, J. L., et al., "Improvements in the Performance of Nuclear Fuel Particles Offered by Silicon-Alloyed Carbon Coatings," Nucl. Technol., 35, 536 (1977).
11. "FMB-3 Fuel Specification for Irradiation Experiments," General Atomic Company, unpublished data.

12. "HTGR Fuels and Core Development Program. Quarterly Progress Report for the Period Ending February 28, 1978," DOE Report GA-A14863, General Atomic Company, March 1978.

13. Kaae, J. L., "Microstructures of Isotropic Pyrolytic Carbons," ERDA Report GA-A12892, General Atomic Company, March 1974.

14. Homan, F. J., and P. R. Kasten, "Gas-Cooled Reactor Programs High-Temperature Gas-Cooled Base-Technology Program. Annual Progress Report for Period Ending December 31, 1979," DOE Report ORNL-5643, Oak Ridge National Laboratory, July 1980.

15. Crockett, T. B., General Atomic Company, unpublished data, September 11, 1979.

16. Sedlak, B. J., "Postirradiation Examination Report of TRISO and BISO ThO_2 Particles Irradiated in Capsules HT-31 and HT-33," DOE Report GA-15544, General Atomic Company, January 1980.

17. "HTGR Base Program - Monthly Progress Report for May," Oak Ridge National Laboratory, unpublished data, June 1978.

18. Kania, M. J., "HTCAP - A Fortran IV Program for Calculating Coating Particle Operating Temperatures in HFIR Target Irradiation Experiments," ERDA Report ORNL/TM-5332, Oak Ridge National Laboratory, May 1976.

19. Long, E. L., Oak Ridge National Laboratory, private communication, September 6, 1978.

20. Caddell, M. D., General Atomic Company, unpublished data, October 18, 1979.

21. McElmury, S. S., and O. M. Stansfield, "An Analysis of the Effect of Buffer-IPyC Coating Separation on the Temperature Distribution in TRISO UC_2 Fuel Particles," ERDA Report GA-A13500, General Atomic Company, December 1, 1975.

22. Valentine, K. H., and M. J. Kania, "IMGA Operating Manual," DOE Report ORNL/TM-6576, Oak Ridge National Laboratory, August 1979.

23. Anderson, E. E., et al., "An In-Core Furnace for the High-Temperature Irradiation Testing of Reactor Fuels," Nucl. Technol., 11, 259 (1971).

24. Lofing, D. R., et al., "The Use of Gamma-Ray Spectroscopy in the Study of Fission-Product Release From Nuclear Fuels," General Atomic Division of General Dynamics Report GA-4615, General Atomic Company, October 8, 1963.

25. "HTGR Generic Technology Program Fuels and Core Development. Quarterly Progress Report for the Period Ending August 31, 1978," ERDA Report GA-A15093, General Atomic Company, September 1978.

26. Myers, B. F., General Atomic Company unpublished data, July 7, 1980.

27. "HTGR Fuel Development Department Technical Status Report for the Quarter Ending September 30, 1979," General Atomic Company unpublished data, October 31, 1979.

28. Homan, F., et al., "Low-Enriched Fuel Particle Performance Review," DOE Report GA-A14759, General Atomic Company, August 1978.

29. Young, C. A., "Pre- and Postirradiation Evaluation of Fuel in Capsule HRB-14," DOE Report GA-A15969, General Atomic Company, to be published.

30. Smith, C. L., General Atomic Company unpublished data, September 4, 1979.

31. "HTGR Fuel Development Department Technical Status Report for the Quarter Ending June 30, 1980," General Atomic Company unpublished data, August 1980.

32. Brown, P. E., and R. L. Faircloth, "Metal Fission Product Behavior in High-Temperature Reactors - UO_2 Coated Particle Fuel," J. Nucl. Mater., 59, 29 (1976).

33. Foster, R. E., General Atomic Company unpublished data, January 24, 1980.

34. Stansfield, O. M., et al., "Performance of ThO_2 In HTGR Fuel Particles," DOE Report GA-A14745, General Atomic Company, March 1978.

35. Flowers, R. H., and G. W. Horsley, "The Influence of Oxide Kernels on the Manufacture and Performance of Coated Particle Fuel," Atomic Energy Research Establishment (U.K.) Report R5959, 1968.

36. Homan, F. J., and E. L. Long, "Irradiation Performance of HTGR Recycle Fissile Fuel," ERDA Report ORNL/TM-5502, Oak Ridge National Laboratory, August 1976.

37. Grubmeir, H., et al., "Silicon Carbide Corrosion in High-Temperature Gas-Cooled Reactor Fuel Particles," Nucl. Technol., 35, 413 (1977).

38. "HTGR Product Specification, Issue C," General Atomic Company unpublished data, August 1979.